Electrochemistry of biomimetic membranes

4

Electrochemistry of Biomimetic Membranes

Rolando Guidelli and Lucia Becucci

Dept. of Chemistry, Florence University, Via della Lastruccia 3
50019 Sesto Fiorentino, Firenze, Italy

I. INTRODUCTION

Biological membranes are by far the most important electrified interfaces in living systems. They consist of a bimolecular layer of lipids (the lipid bilayer) incorporating proteins. Lipid molecules are *amphiphilic*, i.e., consist of a hydrophobic section (the hydrocarbon tail) and a hydrophilic section (the polar head). In biological membranes the two lipid monolayers are oriented with the hydrocarbon tails directed toward each other and the polar heads turned toward the aqueous solutions that bath the two sides of the membrane. The resulting lipid bilayer is a matrix that incorporates different proteins performing a variety of functions. Biomembranes form a highly selective barrier between the inside and the outside of living cells. They are highly insulating to inorganic ions, and large electrochemical potentials can be maintained across them. The permeability and structural properties of biological membranes are sensitive to the chemical nature of the membrane

Modern Aspects of Electrochemistry, Number 53, edited by Noam Eliaz, Springer, New York, 2011.

components and to events that occur at the interface or within the bilayer. For example, biomembranes provide the environmental matrix for proteins that specifically transport certain ions and other molecules, for receptor proteins and for signal transduction molecules. The lipid and protein portions of biomembranes are also sensitive to the presence of lipophilic perturbants. Anaesthetics, for example, readily partition into lipid membranes, altering their electrical and permeability characteristics, thus providing an indicator for these agents. The various responses observed in biomembranes are concentration-dependent, usually very rapid and reversible, and frequently voltage-dependent.

II. THE BIOMIMETIC MEMBRANES: SCOPE AND REQUIREMENTS

In view of the complexity and diversity of the functions performed by the different proteins embedded in a biomembrane (the integral proteins), it has been found convenient to incorporate single integral proteins or smaller lipophilic biomolecules into experimental models of biological membranes, so as to isolate and investigate their functions. This serves to reduce complex membrane processes to well-defined interactions between selected proteins, lipids and ligands. There is great potential for application of experimental models of biomembranes (the so-called biomimetic membranes) for the elucidation of structure-function relationships of many biologically important membrane proteins. These proteins are the key factors in cell metabolism, e.g., in cell-cell interactions, signal transduction, and transport of ions and nutrients. Thanks to this important function, membrane proteins are a preferred target for pharmaceuticals, with about 60% of consumed drugs addressing them. Biomimetic membranes are also useful for the investigation of phase stability (e.g., lipid-lipid phase separation, lipid raft formation, lateral diffusion), protein-membrane interactions (e.g., receptor clustering and co-localization), and membrane-membrane processes such as fusion, electroporation and intercellular recognitions. They are also relevant to the design of membrane-based biosensors and devices, and to analytical platforms for assaying membrane-based processes.

With only a few exceptions, biomimetic membranes consist of a more or less complex architecture that includes a lipid bilayer. In order of increasing complexity, they can be classified into: black lipid membranes (BLMs), solid-supported bilayer lipid membranes (sBLMs), tethered bilayer lipid membranes (tBLMs), polymer-cushioned bilayer lipid membranes (pBLMs), S-layer stabilized bilayer lipid membranes (ssBLMs), and protein-tethered bilayer lipid membranes (ptBLMs). Mercury-supported lipid monolayers and alkanethiol/lipid *hybrid bilayers* are particular biomimetic membranes that contain a single lipid monolayer.

The possibility of self-assembling monolayers and bilayers on metals with formation of rugged functionalized electrodes has stimulated a research aiming at exploiting self-assembly for the realization of biomembrane models capable of incorporating integral proteins in a functionally active state. To achieve this goal, biomembrane models consisting of lipid bilayers should meet a number of requirements:

(i) they should be robust enough for long-term stability, and be easily and reproducibly prepared;
(ii) they should have the lipid bilayer in the liquid crystalline state, and such as to allow lateral mobility;
(iii) they should have water (or, at least, a highly hydrated hydrophilic region) on both sides of the lipid bilayer;
(iv) they should be sufficiently free from pinholes and other defects that might provide preferential pathways for electron and ion transport across the lipid bilayer.

Requirements (ii) and (iii) are necessary for the incorporation of integral proteins into the lipid bilayer in a functionally active state. In fact, integral proteins have a hydrophobic domain buried inside the biomimetic membrane, which must be sufficiently fluid to accommodate this domain. Often, they also have hydrophilic domains protruding by over 6 nm outside the lipid bilayer. To avoid their denaturation and to promote their function, incorporation of integral proteins into biomimetic membranes must ensure that their extramembrane hydrophilic domains are accommodated in a hydrophilic medium on both sides of the lipid bilayer. Moreover, the transport of hydrophilic ions across a solid-supported lipid bilayer via ion channels or ion pumps is only possible if an aqueous or hydrophilic layer is interposed between the bilayer and the sup-

port. Requirement (iv) is needed to make the biomembrane model sufficiently blocking as to characterize ion channel or ion pump activity by electrochemical means without the disturbing presence of stray currents due to defects.

Apart from lipid molecules, the molecules that are most commonly employed for the fabrication of biomimetic membranes are *hydrophilic spacers* and *thiolipids*. Hydrophilic spacers consist of a hydrophilic chain (e.g., a polyethyleneoxy or oligopeptide chain) terminated at one end with an anchor group for tethering to a support and, at the other end, with a hydrophilic functional group (e.g., a hydroxyl group). Sulfhydryl or disulfide groups are employed as anchor groups for tethering to metals such as gold, silver or mercury (see Fig. 1B); methyl-, methyloxy- or chloride-substituted silane groups are used for tethering to glass, quartz, silica or mica. The latter supports are nonconducting and cannot be investigated by electrochemical techniques. Hydrophilic spacers serve to separate the lipid bilayer from a solid support, to compensate for surface roughness effects, to prevent any incorporated peptides or proteins from touching the support surface (thus avoiding loss of their functionality due to denaturation), and to provide an ionic reservoir underneath the lipid bilayer.

Thiolipids differ from hydrophilic spacers in that the hydrophilic chain is covalently linked to one or, more frequently, two alkyl chains at the opposite end with respect to the anchor group, as shown in Fig. 1A. The alkyl chains simulate the hydrocarbon tails of a lipid molecule and provide one half of the lipid bilayer to the biomimetic membrane. When tethered to a support, hydrophilic spacers expose to the bulk aqueous phase a hydrophilic surface, while thiolipids expose a hydrophobic surface. Clearly, lipid bilayers formed on top of hydrophilic spacers are noncovalently linked to them and can be regarded as *freely suspended*. Conversely, lipid monolayers assembled on top of thiolipid monolayers form lipid bilayers that are tethered to the support.

Before discussing advantages and disadvantages of these systems, we will describe in detail the electrochemical technique that is commonly employed for their investigation, namely electrochemical impedance spectroscopy (EIS), as well as some fabrication methodologies. In fact, our attention will be mainly focused on those biomimetic membranes that are amenable to investigation by electrochemical methods. Biomimetic membranes that are in-

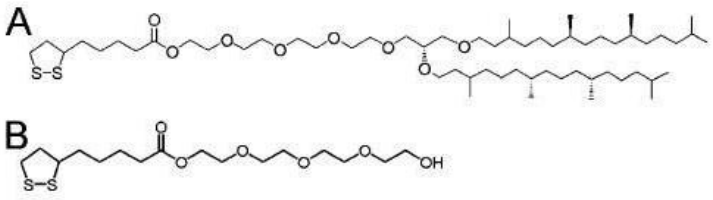

Figure 1. (A) Structure of a widely adopted thiolipid, called DPTL.[1] It consists of a tetraethyleneoxy chain terminated at one end with a lipoic acid residue and covalently linked at the other end to two phytanyl chains. (B) Structure of the corresponding hydrophilic spacer (TEGL), in which the two phytanyl chains are replaced by a hydroxyl group.

vestigated exclusively by non-electrochemical surface sensitive techniques, such as those formed on insulating supports (e.g., glass, mica, quartz, silica, etc.), will be considered only briefly.

III. ELECTROCHEMICAL IMPEDANCE SPECTROSCOPY

Many membrane proteins are *electrogenic*, i.e., translocate a net charge across the membrane. Consequently, it is possible to monitor their function directly by measuring the current flowing along an external electrical circuit upon their activation. Analogously, their deactivation by some antagonist can be monitored by a drop in current. The techniques of choice for these measurements are EIS and potential-step chronoamperometry or chronocoulometry, because the limited volume of the ionic reservoir created by a hydrophilic spacer in solid-supported biomimetic membranes cannot sustain a steady-state current.

Electrochemical impedance spectroscopy applies an a.c. voltage of given frequency to the system under study and measures the resulting current that flows with the same frequency. Both the amplitude of the a.c. current and its phase shift with respect to the a.c. voltage are measured. The frequency is normally varied gradually from 10^{-3} to 10^{5} Hz. To interpret measured impedance spectra, it is necessary to compare them with the electrical response of an equivalent circuit simulating the system under investigation. As a

rule, an equivalent circuit is assembled from resistors and capacitors, representing the electrically dominant components of biomimetic membranes. In general, a metal-supported self-assembled mono- or multilayer can be regarded as consisting of a series of slabs with different dielectric properties. When ions flow across each slab, they give rise to an ionic current $\boldsymbol{J}_{\text{ion}} = \sigma\boldsymbol{E}$, where $\boldsymbol{E}$ is the electric field and σ is the conductivity. Ions may also accumulate at the boundary between contiguous dielectric slabs, causing a discontinuity in the electric displacement vector $\boldsymbol{D} = \varepsilon\boldsymbol{E}$, where ε is the dielectric constant. Under a.c. conditions, the accumulation of ions at the boundary of the dielectric slabs varies in time, and so does the electric displacement vector, giving rise to a capacitive current $\boldsymbol{J}_{\text{c}} = \text{d}\boldsymbol{D}/\text{d}t$. The total current is, therefore, given by the sum of the ionic current and of the capacitive current. In this respect, each dielectric slab can be simulated by a parallel combination of a resistance, accounting for the ionic current, and of a capacitance, accounting for the capacitive current, namely by an *RC mesh*. Accordingly, the impedance spectrum of a self-assembled layer can be simulated by a series of RC meshes. It should be noted that lateral heterogeneities, such as defects or microdomains, cannot be accounted for by simulating them by RC meshes in parallel with each other. In fact, in view of Kirchhoff's laws for the combination of circuit elements, the parallel connection of RC meshes is reduced again to a single RC mesh, with averaged values for the resistance and the capacitance.

Application of an a.c. voltage of amplitude v and frequency f to a pure resistor of resistance R yields a current of equal frequency f and of amplitude v/R, in phase with the voltage. Conversely, application of the a.c. voltage to a pure capacitor of capacitance C yields a current of frequency f and amplitude $2\pi fC$, out of phase by $-\pi/2$ with respect to the voltage, i.e., in quadrature with it. This state of affairs can be expressed by stating that the admittance Y of a resistance element equals $1/R$, while that of a capacitance element equals $-\text{i}\omega C$, where $\omega = 2\pi f$ is the angular frequency and i is the imaginary unit. More generally, in an equivalent circuit consisting of resistances and capacitances, Y is a complex quantity, and the impedance Z is equal to $1/Y$, by definition. Hence, Z equals R for a resistance element, and $\text{i}/\omega C$ for a capacitance element. In analogy with the resistance in d.c. measurements, the overall im-

pedance of two circuit elements in series is equal to the sum of the impedances of the single circuit elements. Conversely, the overall impedance of two circuit elements in parallel is such that its reciprocal is equal to the sum of the reciprocals of the single circuit elements. Consequently, if two circuit elements have appreciably different impedances, their overall impedance is controlled by the circuit element of higher impedance if they are in series and by the circuit element of lower impedance if they are in parallel.

Bearing this in mind, let us consider a biomimetic membrane consisting of a thiolipid tethered to an electrode surface, with a lipid monolayer on top of it. As a first approximation, this tethered bilayer lipid membrane (tBLM) can be regarded as consisting of three adjacent slabs: the hydrophilic spacer moiety, the lipid bilayer moiety, and the aqueous solution bathing the lipid bilayer. A simple equivalent circuit commonly employed to interpret the impedance spectrum of a tBLM is shown in Fig. 2; R_Ω is the resistance of the aqueous electrolyte, R_m and C_m are the resistance and capacitance of the lipid bilayer, and C_s is the capacitance of the hydrophilic spacer. As an example, we will consider a tBLM that makes use of a convenient and widely used thiolipid called DPTL, first employed by Schiller et al.[1] (see Fig. 1A). It consists of a tetraethyleneoxy hydrophilic chain covalently linked at one end to a lipoic acid residue, for anchoring to the metal via a disulfide group, and bound at the other end via ether linkages to two phytanyl chains. Figure 2 shows the impedance spectrum of a tBLM consisting of a DPTL monolayer anchored to a mercury electrode, with a diphytanoylphosphatidylcholine (DPhyPC) monolayer on top of it. This tBLM incorporates gramicidin, a linear neutral pentadecapeptide that spans lipid bilayers by forming a N-terminus-to-N-terminus dimer.[2] The elements of the equivalent circuit are influenced by the movement of K^+ ions across the lipid bilayer, induced by the gramicidin channel. The spectrum is displayed on a Bode plot, namely a plot of $\log|Z|$ and phase angle ϕ against $\log f$, where $|Z|$ is the magnitude of the impedance.

As already stated, the impedance of circuit elements in series is determined by the element with the highest impedance; conversely, the impedance of circuit elements in parallel is determined by the element with the lowest impedance. Therefore, at the highest frequencies, $f=\omega/2\pi$, the overall impedance $|Z|$ is determined by the resistance R_Ω, because the impedance of the C_s element,

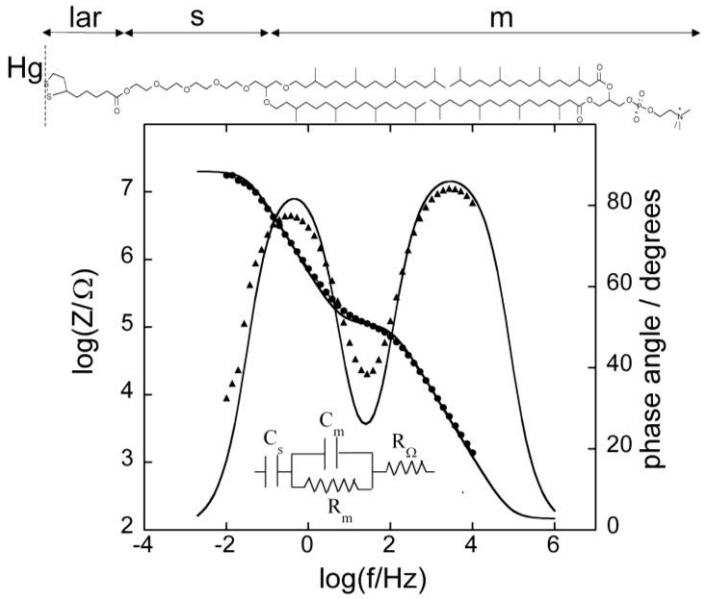

Figure 2. Plot of log|*Z*| (solid circles) and ϕ (solid triangles) against log *f* (Bode plot) for a mercury-supported DPTL|DPhyPC bilayer incorporating gramicidin from its 1×10^{-7} M solution in aqueous 0.1 M KCl at –0.600 V vs. Ag|AgCl(0.1M KCl).[2] The solid curve is the best fit of the equivalent circuit shown in the figure to the impedance spectrum, with C_s=0.25 μF, R_m=106 kΩ, C_m=14 nF, and R_Ω=146 Ω. Drop area = 2.2×10^{-2} cm^2. Top: structure of DPTL in tail-to-tail contact with a DPhyPC lipid molecule. The double-headed arrows mark the lipoic acid residue (lar), spacer (s) and lipid bilayer (m) sections of the tBLM.

$1/(\omega C_s)$, is $<<R_\Omega$; the same is true for the impedance of the R_mC_m mesh, which is determined by the lowest of the impedances of these two elements in parallel, i.e., $1/(\omega C_m)$. At the highest frequencies, |*Z*| is therefore controlled by R_Ω, which is independent of frequency and is characterized by a phase angle ϕ=0. With decreasing frequency, $1/(\omega C_m)$ becomes greater than R_Ω, while still remaining lower than R_m, and it is also > $1/(\omega C_s)$, because C_s is > C_m. Hence, |*Z*| coincides with $1/(\omega C_m)$, and the log|*Z*| vs. log *f* plot has a slope equal to –1, while the phase angle tends to 90°. With a further decrease in frequency, $1/(\omega C_m)$ becomes comparable with and ultimately less than R_m, and the Bode plot tends to become

independent of frequency, which would correspond to complete control by R_m. At the same time, ϕ decreases tending to zero. However, before this can occur, a further decrease in frequency makes $1/(\omega C_s) >> R_m$, causing $|Z|$ to coincide with $1/(\omega C_s)$. Hence, the slope of the Bode plot becomes once again equal to –1 and ϕ tends to 90°. The solid curve in Fig. 2 is the best fit of the $C_s(R_mC_m)R_\Omega$ equivalent circuit to the experimental plot. This Bode plot is rather featureless. A Bode plot richer in features is obtained by incorporating in the same tBLM the ion carrier valinomycin, a hydrophobic depsipeptide that cages a desolvated potassium ion shuttling it across the lipid bilayer.[3] In this case, the ϕ vs. log f plot exhibits an additional hump, as shown in Fig. 3. We will show in what follows that valinomycin allows an additional dielectric slab of the tBLM to be disclosed.

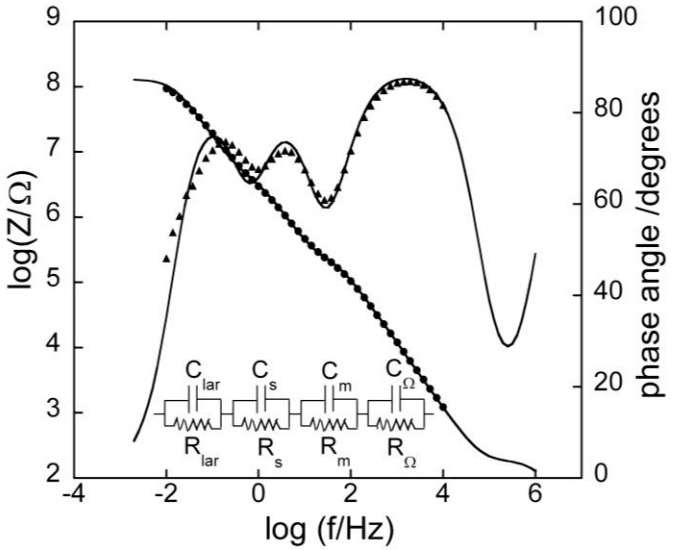

Figure 3. Plot of log|Z| (solid circles) and ϕ (solid triangles) against log f (Bode plot) for a mercury-supported DPTL|DPhyPC bilayer incorporating valinomycin from its 1.5×10^{-7} M solution in aqueous 0.1 M KCl at –0.375 V vs. Ag|AgCl(0.1M KCl).[3] The solid curve is the best fit of the equivalent circuit shown in the figure to the impedance spectrum, with C_{lar}=92 nF, R_{lar}=0.126 GΩ, C_s=20 nF, R_s=0.155 MΩ, C_m=73 nF, R_m=2.2 MΩ, C_Ω=0.95 nF, R_Ω=170 Ω. Drop area= 2.2×10^{-2} cm^2.

Impedance spectra can also be displayed on other types of plots. To justify their use, we must consider that the impedance Z of a single RC mesh is given by:

$$Z^{-1} = R^{-1} - \mathrm{i}\omega C \tag{1}$$

Writing $Z \equiv Z' + \mathrm{i}Z''$, where Z' and Z'' are the in-phase and quadrature components of the impedance Z, and rearranging terms, we obtain:

$$Z' = R/\left(1+\omega^2 R^2 C^2\right) \tag{2a}$$

$$Z'' = Z'\,\omega RC \tag{2b}$$

Eliminating ωRC from Eqs. (2a) and (2b) we get:

$$Z''^2 + Z'^2 - RZ' = 0 \rightarrow \left(Z' - R/2\right)^2 + Z''^2 = (R/2)^2 \tag{3}$$

Equation (3) yields a semicircle of diameter R and center of coordinates (R/2,0) on a Z'' vs. Z' plot, called Nyquist plot. Noting that the maximum of this semicircle is characterized by the equality of Z' and Z'', from Eq. (2b) it follows that the angular frequency ω at this maximum equals the reciprocal of the time constant RC of the mesh. In the presence of a series of RC meshes, their time constants may be close enough to cause the corresponding semicircles to overlap partially. In this case, if the mesh of highest time constant has also the highest resistance, R_1, as is often the case, then the Nyquist plot of the whole impedance spectrum exhibits a single well-formed semicircle, R_1 in diameter. The semicircles of the remaining meshes are compressed in a very narrow area close to the origin of the Z'' vs. Z' plot, and can be visualized only by enlarging this area. Therefore, the Nyquist plot of the whole spectrum can be conveniently employed if one is interested in pointing out the resistance R_1 of the dielectric slab of highest resistance. This is apparent in Fig. 4, which shows the Nyquist plot for the tBLM incorporating valinomycin, whose Bode plot is reported in Fig. 3. The whole Nyquist plot displays a single semicircle. However, the enlargement of the initial portion of the plot in the inset

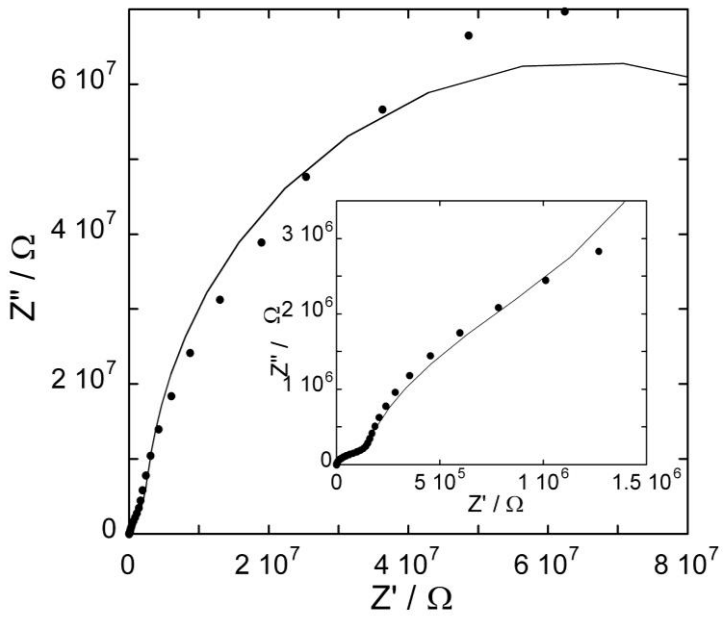

Figure 4. Plot of *Z*' against *Z*' (Nyquist plot) for the same tBLM as in Fig. 3. The solid curve is the best fit of the equivalent circuit shown in Fig. 3 to the impedance spectrum, obtained by using the same *R* and *C* values. The semicircle in the figure corresponds to the RC mesh of highest time constant and highest resistance, ascribable to the lipoic acid residue. The inset shows an enlargement of the initial portion of the Nyquist plot.

of Fig. 4 reveals the presence of two additional partially fused semicircles.

The solid curve in Fig. 4 is the best fit of the equivalent circuit shown in Fig. 3 to the impedance spectrum. This equivalent circuit consists of a series of four RC meshes, simulating the lipoic acid residue, the tetraethyleneoxy hydrophilic spacer, the lipid bilayer and the aqueous phase bathing the lipid bilayer (see the structure on top of Fig. 2). Note that, in the present case, the combination (lipoic acid residue + hydrophilic spacer) is no longer simulated by a pure capacitance, and the aqueous phase is no longer simulated

by a pure resistance. In fact, even though the lipoic acid residue is the dielectric slab in direct contact with the metal, we cannot exclude a slight ionic flux across it and a resulting high (but not an infinitely high) resistance. Analogously, even though the capacitance of the aqueous phase interposed between the lipid bilayer and the auxiliary electrode is very low, it is not infinitely low, and its inclusion improves the fit.

To better visualize all semicircles, we have found it convenient to represent impedance spectra on a ωZ' vs. ωZ'' plot.[3] Henceforth, this plot will be briefly referred to as an *M plot*, since ωZ' and ωZ'' are the components of the modulus function M. A single RC mesh yields a semicircle even in this plot. Thus, if we multiply both members of Eq. (3) by ω^2 and we combine the resulting equation with Eq. (2b), after simple passages we obtain:

$$\omega^2 Z''^2+\omega^2 Z'^2-\omega Z''/C=0\rightarrow\left(\omega Z''-\frac{1}{2C}\right)^2+(\omega Z')^2=\left(\frac{1}{2C}\right)^2 \quad (4)$$

This is the equation of a semicircle of diameter C^{-1} and center of coordinates $(2/C,0)$ on a ωZ' vs. ωZ'' plot. Moreover, ω at the maximum of the semicircle is again equal to the reciprocal of the time constant RC of the mesh. While ω decreases along the positive direction of the abscissas on a Z'' vs. Z' plot, it increases on a M plot. Therefore, for a series of RC meshes, the last semicircle on the M plot is characterized by the lowest time constant. This is, unavoidably, the semicircle simulating the solution that baths the self-assembled film, due to its very low capacitance. Figure 5 shows the M plot relative to the same impedance spectrum that yields the Bode plot in Fig. 3 and the Nyquist plot in Fig. 4. The solid curve is the best fit of the equivalent circuit in Fig. 3, consisting of four RC meshes in series. Proceeding along the positive direction of the abscissas, the dashed curves express the contribution to ωZ' from each of the four different RC meshes, namely the quantity $\omega g_i/(g_i^2+\omega^2 C_i^2)$, where $g_i=1/R_i$ and C_i are the conductance and capacitance of the i-th mesh. The deviations of the dashed curves from a pure semicircle measure the extent of their overlapping with the neighboring semicircles. The four semicircles overlap only to a moderate extent, thus allowing their straightforward

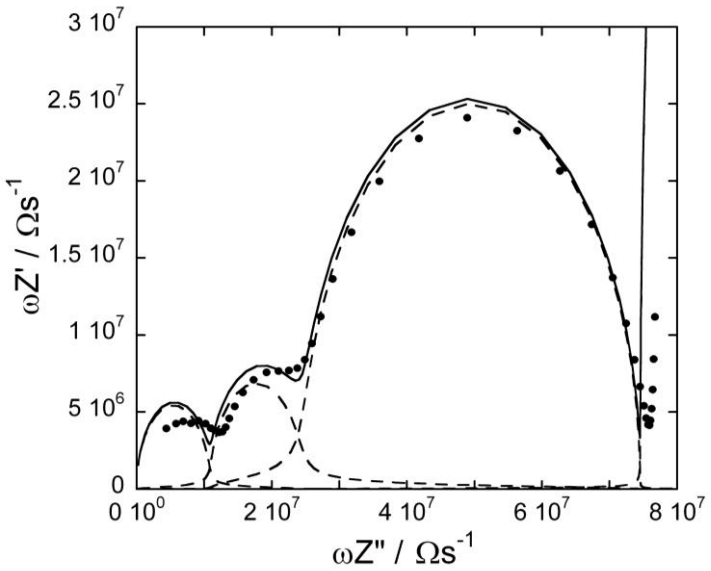

Figure 5. Plot of $\omega Z'$ against $\omega Z''$ (M plot) for the same tBLM as in Fig. 3. The solid curve is the best fit of the equivalent circuit shown in Fig. 3 to the impedance spectrum, using the same R and C values. The dashed curves are the contributions to $\omega Z'$ from the different RC meshes; proceeding along the positive direction of the abscissas, these curves are ascribed to the lipoic acid residue, the tetraethyleneoxy moiety, the lipid bilayer moiety, and the aqueous solution bathing the tBLM.[3]

deconvolution. This is due to an appreciable difference between the time constants of the four RC meshes, which are evenly distributed over a frequency range covering seven orders of magnitude. The capacitance of the solution interposed between the working and the counter electrode is of the order of 1 nF cm^{-2}. If it is disregarded by simulating the aqueous phase by a pure resistance, the contribution of the solution to the M plot is represented by a vertical straight line. As a matter of fact, the radius of the semicircle simulating the solution is not infinitely large, and its curvature is often clearly visible. The RC mesh of the aqueous solution does not depend on the architecture of the tBLM. Hence, the corresponding semicircle can be excluded, at least partially, from the M plot in order to better visualize the contribution from the other

meshes. The M plot permits the agreement between an experimental impedance spectrum and the corresponding fit to a series of RC meshes to be verified in detail. In this respect, it differs from the Bode plot, which is often almost featureless.

A plot that has been frequently adopted in the literature to display an impedance spectrum richer in features than the Bode plot is the Y'/ω vs. Y''/ω plot, sometimes called Cole-Cole plot.[4-6] Here Y' and Y'' are the in-phase and quadrature component of the electrode admittance. However, this plot yields a semicircle for a series combination of a resistance and a capacitance, and not for their parallel combination. Thus, the impedance Z of a RC series is given by:

$$Z = R + \mathrm{i}/(\omega C) \tag{5}$$

Noting that $Y \equiv Y' - \mathrm{i}Y'' = 1/Z$, rearrangement of Eq. (5) yields:

$$Y''/\omega = C/\left(\omega^2 R^2 C^2 + 1\right) \tag{6a}$$

$$Y'/\omega = \omega RC\left(Y''/\omega\right) \tag{6b}$$

Eliminating ωRC from Eqs. (6a) and (6b) we get:

$$\left(\frac{Y''}{\omega}\right)^2 + \left(\frac{Y'}{\omega}\right)^2 - C\left(\frac{Y''}{\omega}\right) = 0 \rightarrow \left(\frac{Y''}{\omega} - \frac{C}{2}\right)^2 + \left(\frac{Y'}{\omega}\right)^2 = \left(\frac{C}{2}\right)^2 \tag{7}$$

On a Cole-Cole plot, this equation yields a semicircle of diameter C and center of coordinates (C/2,0). Here too, from Eq. (6b) it follows that ω at the maximum of the semicircle equals $1/RC$. Strictly speaking, a Cole-Cole plot is not suitable for verifying the fitting of a series of RC meshes to an experimental impedance spectrum. Thus, the admittance of a single RC mesh is given by:

$$\begin{gathered} Y = R^{-1} - \mathrm{i}\omega C \rightarrow Y'/\omega = (\omega R)^{-1} \\ Y''/\omega = C \end{gathered} \tag{8}$$

For a RC mesh to yield a semicircle on a Cole-Cole plot, an equation analogous to Eq. (7) should be satisfied:

$$\left(\frac{Y''}{\omega}-x\right)^2+\left(\frac{Y'}{\omega}\right)^2=x^2 \rightarrow (C-x)^2+\left(\frac{1}{\omega R}\right)^2=x^2 \qquad (9)$$

where x is the radius of the semicircle on this plot. Solving this equation yields:

$$x=\frac{C}{2}\left(1+\frac{1}{\omega^2R^2C^2}\right) \qquad (10)$$

Consequently, the Cole-Cole plot for a single RC mesh yields a semicircle of diameter C only for ω values high enough to make $\omega^2R^2C^2 >> 1$. Figure 6 shows the Cole-Cole plot for the same impedance spectrum displayed on the Bode, Nyquist and M plots in

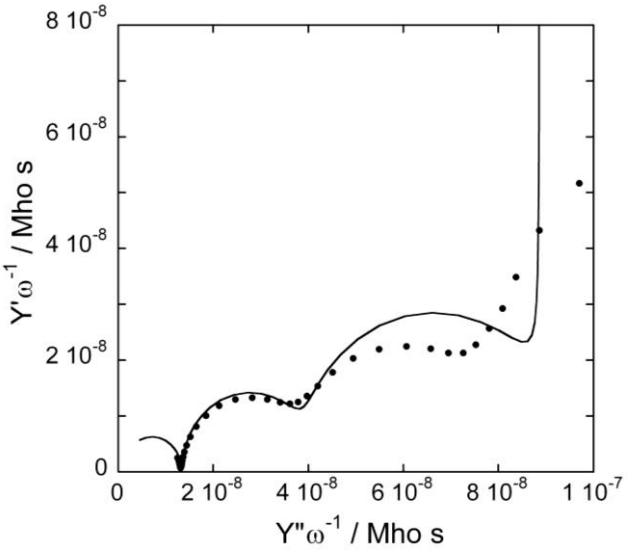

Figure 6. Plot of Y'/ω against Y''/ω (Cole-Cole plot) for the same tBLM as in Fig. 3. The solid curve is the best fit of the equivalent circuit shown in Fig. 3 to the impedance spectrum, using the same R and C values.

Figs. 3, 4 and 5. In a Cole-Cole plot, ω decreases along the positive direction of the Y''/ω axis. It is apparent that the fitting of a series of four RC meshes to the experimental spectrum shows appreciable deviations at the lower frequencies when the spectrum is displayed on a Cole-Cole plot.

An equivalent circuit consisting of a series of RC meshes with relatively close time constants yields calculated semicircles on Nyquist, M or Cole-Cole plots that overlap to an appreciable extent. Such an overlapping resembles a single depressed semicircular arc, namely an arc whose center lies below the horizontal axis. These arcs are often fitted to an equivalent circuit consisting of a parallel combination of a resistance R and of a *constant phase element* (CPE), whose empirical impedance function has the form: $Z_{CPE}=-(i\omega)^{-\alpha}/A$.[7] The hybrid CPE reduces to a pure capacitive impedance, $i/\omega A$, for $\alpha=1$, and finds its justification in a continuous distribution of time constants around a mean. The impedance of this parallel combination, called ZARC, is given by:

$$Z_{ZARC}^{-1} = R^{-1} - (i\omega)^{\alpha} A \rightarrow Z_{ZARC} = \frac{R}{1-(i\omega)^{\alpha} RA} \qquad (11)$$

For $\alpha = 1$, this expression reduces to the impedance of a RC mesh, and A coincides with the capacitance.

The use of ZARC elements for the fitting to impedance spectra of films deposited on satisfactorily smooth supports, such as mercury, seems redundant and difficult to relate to the structure of the film. In this case, a more significant approach is the following. The experimental spectra are fitted by an equivalent circuit consisting of a progressively increasing number of RC meshes in series.[8] The quality of the fitting is conveniently monitored on a M plot. Fitting errors less than 10% for the R and C values of the different RC meshes can be regarded as acceptable. When the addition of a further RC mesh does not determine a detectable improvement in the agreement between experimental and calculated M plots, the fitting error for the added RC mesh is normally found to be close to 100%. The last added RC mesh is, therefore, discarded from the fitting.

IV. FORMATION OF LIPID FILMS IN BIOMIMETIC MEMBRANES

Methodologies for the fabrication of biomimetic membranes vary somewhat from one biomimetic membrane to another. However, a number of experimental procedures for the formation of lipid monolayers and bilayers on solid supports are common to several biomimetic membranes. The most popular procedures are vesicle fusion, Langmuir-Blodgett and Langmuir-Schaefer transfers, and rapid solvent exchange. The formation of lipid monolayers and bilayers on gold and silver substrates is commonly monitored by surface plasmon resonance (SPR). Therefore, a brief description of this surface-sensitive technique seems appropriate.

1. Surface Plasmon Resonance

Surface plasmons are collective electronic oscillations in a metal layer, about 50 nm in thickness, excited by photons from a laser beam.[9] The beam is reflected by the back surface of the metal layer, while its front surface supports a dielectric film (e.g., a lipid bilayer), usually in contact with an aqueous solution. The evanescent electromagnetic field thereby generated in the metal layer can couple with the electronic motions in the dielectric film. The intensity of the electromagnetic field associated with surface plasmons has its maximum at the metal/(dielectric film) surface and decays exponentially into the space perpendicular to it, extending into the metal and the dielectric. This makes SPR a surface-sensitive technique particularly suitable for the measurement of the optical thickness of ultrathin films adsorbed on metals. As a rule, the incident angle of the laser beam is varied with respect to the back surface of the metal layer, and the reflected light intensity is measured. At a certain angle of incidence there exists a resonance condition for the excitation of surface plasmons, which causes the energy of the incident laser light to be absorbed by the surface plasmon modes and the reflectivity to attain a minimum (see Fig. 7).

The angular position of the minimum of the SPR reflectivity curves (i.e., the curves of reflectivity versus incident angle; see Fig. 7b) is critically dependent on the thickness of the layer adsorbed on the support surface. When macromolecules assemble into a

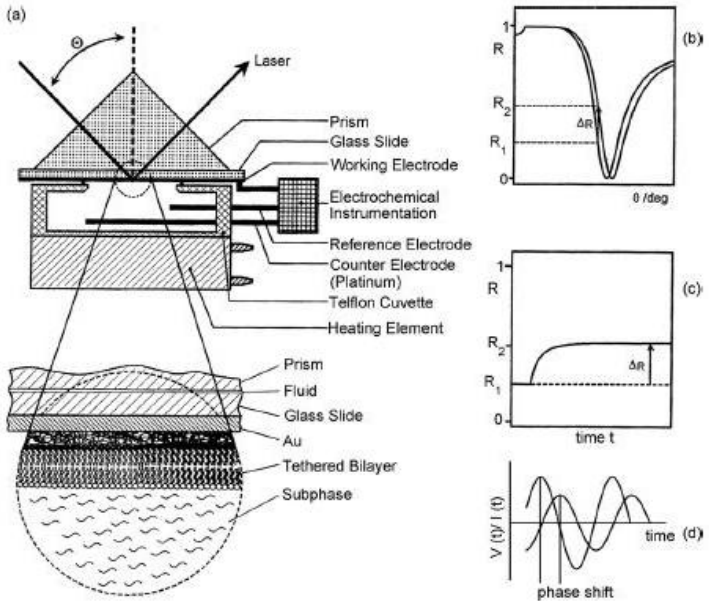

Figure 7. (a) Experimental set-up for surface plasmon resonance measurements, combined with an EIS module for simultaneous SPR and electrochemical measurements on tBLMs. The enlargement shows the solid/solution interface with the thin Au layer used for surface plasmon excitation, and the tethered lipid bilayer in contact with the aqueous phase; (b) typical SPR reflectivity curves before and after the formation of the distal lipid monolayer (on top of the self-assembled proximal tethered lipid monolayer) by vesicle fusion; (c) kinetics of the fusion process recorded by monitoring the change of reflectivity at a fixed angle of incidence as a function of time; (d) time dependence of the small-amplitude a.c. voltage used in EIS measurements and of the resulting a.c. current of equal frequency and different phase angle. (Reprinted from Ref.[9b] with kind permission from Elsevier.)

dielectric layer at the metal surface, the reflectivity minimum is shifted to a higher angle. Physical layer thicknesses can be calculated by quantitative modeling of the reflectivity curves using Fresnel's equations. This requires knowledge of the refractive index *n* and of the film thickness *d* of each dielectric slab of the multilayer system under investigation. The exact refractive index of the compound forming a layer on the metal surface is unknown; however, reasonable approximations for refractive indices are n=1.45 for proteins and n=1.5 for lipids. Once the refractive indices are established, the layer thickness can be extracted from a comparison between experimental and calculated reflectivity curves. By monitoring the reflectivity at a particular fixed angle of incidence close to resonance, the kinetics of adsorption at the interface can be monitored (see Fig. 7c). The reflectivity at the fixed angle increases in time from its value prior to the adsorption of the molecules, attaining a maximum limiting value when the adsorption process terminates.

At resonance, the interfacial evanescent field is enhanced by a factor of 16 (for a gold/water interface at λ = 633 nm) relative to the incoming light. Its strength is maximal at the metal surface, and decays exponentially normal to the surface with a penetration depth of 150 nm. Surface plasmon fluorescence spectroscopy (SPFS) exploits this large field enhancement to excite fluorophores located within the evanescent field.[10] This feature distinguishes SPFS from total internal reflection fluorescence (TIRF) microscopy, which basically utilizes the same optical excitation geometry but operates without a metal surface and thus with much lower field enhancement. Nonradiative energy transfer (quenching) from the excited fluorophore to a planar gold surface decays with the third power of the distance. In practice, the fluorescence intensity of the fluorophore increases gradually with increasing distance of the fluorophore from the gold layer, until it remains completely unquenched at a distance of about 30 nm.[11] Simultaneous SPR and SPFS analysis allows an estimate of both the thickness of a film and its separation from the substrate surface. Thus, when a lipid bilayer is formed on a gold support by vesicle fusion, this combined analysis may distinguish unambiguously whether vesicles or planar lipid films are adsorbed on the support surface.

Both SPR and EIS allow an evaluation of film thickness, based on a reasonable estimate of the refractive index of the film

in the case of SPR, or of its dielectric constant in the case of EIS. However, it must be borne in mind that the two techniques are sensitive to different features of a film.

2. Vesicle Fusion

Vesicles (or, more precisely, unilamellar vesicles) are spherical lipid bilayers that enclose an aqueous solution. To obtain vesicles, lipids are usually dissolved in an organic solvent. The solvent is then evaporated using a nitrogen stream or vacuum, so that a thin lipid film is produced on the glass surface of a vial. The lipid film is hydrated with an aqueous solution, whose temperature should be above the gel to liquid-crystalline transition temperature of the lipid with the highest transition temperature in the mixture. Giant unilamellar vesicles (GUVs) have a diameter ranging from 1 to 300 μm. They are usually produced by an electroformation approach. Multilamellar vesicles (MLVs) are quickly generated by the general protocol described above. Starting from MLVs, large unilamellar vesicles (LUVs, 100 to 1000 nm in diameter) with a narrow size distribution around a desired value are produced by freeze-thaw cycling the vesicles, followed by extrusion; this consists in pressing the vesicle suspension repeatedly through a membrane of defined pore size. Small unilamellar vesicles (SUVs, 20 to 50 nm in diameter) are prepared by extrusion through membranes with smaller pore size (about 30 nm) or by supplying ultrasound energy to the MLV suspension by using an ultrasonic bath or an ultrasonic probe (sonication).

The procedure for vesicle fusion consists of adsorbing and fusing SUVs on a suitable substrate from their aqueous dispersion. If the substrate is hydrophilic, vesicle fusion gives rise to a lipid bilayer by rupture of the vesicles and their *unrolling* and spreading onto the substrate. Conversely, if the substrate is hydrophobic, a lipid monolayer with the hydrocarbon tails directed toward the substrate is formed by rupture of the vesicles, splitting of the vesicular membrane into its two monomolecular leaflets and their spreading[12], as shown schematically in Fig. 8. This is confirmed by the different thickness change following vesicle fusion on a hydrophobic substrate (2–2.5 nm) with respect to a hydrophilic substrate (4.5–5 nm), as estimated by SPR.[13]

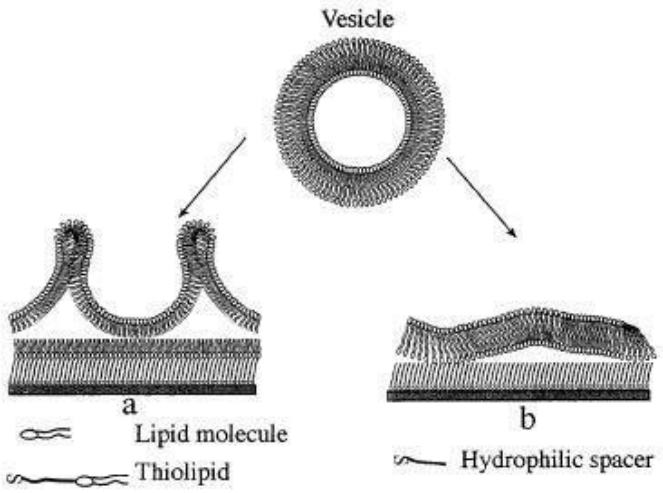

Figure 8. Schematic picture of: (a) splitting and spreading of a vesicle on a solid-supported thiolipid monolayer; (b) unrolling and spreading of a vesicle on a solid-supported hydrophilic spacer.

The kinetics of vesicle fusion, followed by monitoring the position of the minimum of the SPR reflectivity curves, depends on the composition and molecular shape of the vesicular lipids and on the nature of the substrate. As a rule, bilayer formation by vesicle unrolling onto a hydrophilic surface is faster than monolayer formation by vesicle fusion onto a hydrophobic surface. This is probably due to the fact that the processes involved in forming a planar bilayer starting from a vesicular bilayer are considerably less complex than those involved in forming a planar monolayer.[13,14]

The pathway of vesicle fusion on hydrophilic surfaces depends on several factors: the nature of the support (its surface charge, chemical composition and roughness), the nature of the lipid vesicles (their composition, charge, size and physical state), and the aqueous environment (its composition, pH and ionic strength). As a general trend, calcium ions are found to promote the adsorption and rupture of vesicles and lipid bilayer formation.[15] Effects are particularly strong on mica.[16] It has been suggested that the initial rapid stage of vesicle adsorption on hydrophilic surfaces

is controlled by vesicle adsorption at free sites of the surface, according to a Langmuirian type behavior. A second, lower stage is ascribed to vesicle unrolling and spreading processes. It has been proposed that the balance between the gain in adhesion energy (as given by the adhesion area) and the cost in the vesicle curvature energy (as given by the bilayer bending rigidity) is determinant for the adsorption, deformation and rupture of vesicles. Rupture occurs when strong adhesive forces cause the tension in the membrane of a partially fused vesicle to exceed the threshold for disruption of the membrane.[17]

Among hydrophilic substrates, those allowing the formation of lipid bilayers by vesicle fusion more easily are freshly oxidized surfaces of silica, glass, quartz and mica.[18] However, hydrophilicity is a necessary but not a sufficient condition to promote vesicle fusion. Surfaces of oxidized metals and metal oxides (e.g., TiO_2, Pt and Au) allow adsorption of intact vesicles but resist the formation of bilayers, presumably due to weak surface interactions.[19] Electrostatic, van der Waals, hydration and steric forces cause the noncovalently supported lipid bilayer to be separated from the solid surface by a nanometer layer of water.[20] This water layer prevents the support from interfering with the lipid bilayer structure, thus preserving its physical attributes, such as lateral mobility of the lipid molecules.

The quartz crystal microbalance with dissipation monitoring (QCM-D) has proved quite valuable to monitor the macroscopic features of vesicle deposition. A typical QCM sensor consists of a MHz piezoelectric quartz crystal sandwiched between two gold electrodes. The crystal can be brought to resonant oscillation by means of an a.c. current between the electrodes. Since the resonant frequency can be determined with very high precision (usually by less than 1 Hz), a mass adsorbed at the QCM surface can be detected down to a few ng cm^{-2}. At an ideal air/solid interface, there is a linear relationship between an increase in adsorbed rigid mass and a decrease in resonant frequency. The mass obtained from QCM-D measurements corresponds to the total mass coupled to the motion of the sensor crystal, including the mass of the adsorbed biomolecules and of the solvent bound or hydrodynamically coupled to the molecular film. This feature distinguishes mass measurements by QCM-D from those by SPR. In fact, the measured SPR signal originates from altered conditions for resonant

surface plasmon excitation due to changes in the interfacial refractive index. For a simple dielectric material there exists, as a first approximation, a nearly linear relationship between the change in refractive index caused by biomolecule adsorption and the number of biomolecules at the interface; on the other hand, SPR is practically insensitive to the presence of water molecules. Hence, the mass sensed by a QCM exceeds that estimated by SPR by the amount of water molecules bound or dynamically coupled to the adsorbed biomolecules. However, the dissipation monitoring of the QCM-D allows a distinction between lipid layers and loosely bound water molecules in adsorbed vesicles. In fact, under shear stress, lipid layers behave more elastically (or, differently stated, less viscously) than adsorbed vesicles, coupling strongly to the motion of the crystal surface. Conversely, adsorbed vesicles are substantially larger and less compact structures filled with water; moreover, water is also trapped between the vesicles and the surface. Consequently, vesicles are subject to larger deformations under shear stress. These viscoelastic features are invisible by simple resonance frequency determination. Viscoelasticity can, however, be visualized by measuring the energy loss, or dissipation (D) of the shear movement of the crystal in water. The dissipation D is measured by driving the crystal with a.c. current at the resonant frequency, followed by disconnection and analysis of the resulting damped sinusoidal oscillations. This dissipation parameter allows a distinction between intact, adsorbed vesicles (high dissipation) and lipid bilayer patches (low dissipation). Figure 9 shows the changes in resonance frequency (Δf) and in dissipation (ΔD) under different situations. If vesicles do not adsorb, no change in f or D takes place (Fig. 9A). If vesicles adsorb and remain intact, forming a supported vesicular layer, their high mass causes an appreciable frequency decrease, and also a high dissipation (Fig. 9B). If vesicles are initially adsorbed, but subsequently fuse forming a water-free lipid bilayer of lower mass, Δf shows a minimum before attaining a constant limiting value, while ΔD shows a maximum (Fig. 9C). Figure 9D exemplifies the case in which the vesicles adsorb and rupture instantaneously. Combined measurements by QCM-D and SPR have shown that isolated vesicles of egg-phosphatidylcholine (egg-PC) remain intact when bound to a silica support; a minimum critical vesicle coverage is required to initiate the conversion of surface-bound vesicles into

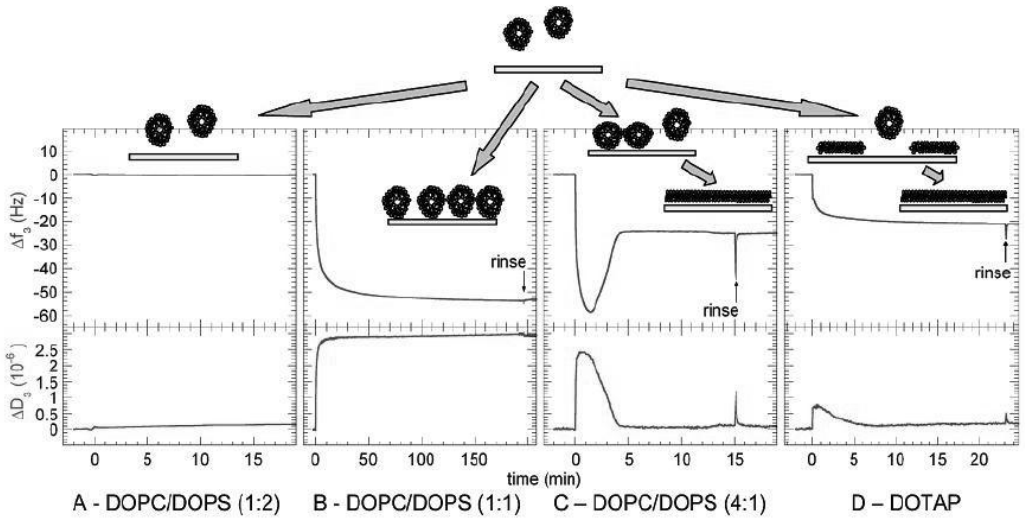

Figure 9. Lipid deposition pathways measured by QCM-D on silica. The legends indicate the lipids used: dioleoyltrimethylammonium-propane (DOTAP), dioleoylphosphatidylcholine (DOPC), and dioleoylphosphatidylserine (DOPS), with their molar mixing ratios. (Reprinted from Ref.[24] with kind permission from the American Chemical Society.)

lipid bilayer patches.[21] Use of the QCM-D permitted to confirm the formation of lipid bilayers on silica and of lipid monolayers on gold-supported alkanethiol monolayers by vesicle fusion, and the adsorption of intact vesicles on oxidized gold.[22]

Atomic force microscopy (AFM) has provided further direct evidence that silica can indeed be covered by isolated vesicles that remain stable for days.[23] Conversely, when adsorbing vesicles at low surface density on mica, they initially remain intact but rupture individually over a time interval ranging from minutes to hours.[16] The particularly smooth surface of mica imparts to vesicles and bilayer patches a certain lateral mobility, not to be confused with that of single lipid molecules. Thus, laterally mobile bilayer patches on mica tend to reshape into circular patches to minimize their line tension. Conversely, bilayer patches on silica frequently retain a strong irregular shape, providing evidence for lack of mobility. A satisfactory lateral mobility accelerates the formation of a complete lipid bilayer coating. In fact, the edges of lipid bilayer patches are thermodynamically unstable, and tend to interact with adjacent lipid material, e.g., by rupturing surface-bound vesicles or by coalescing with other bilayer patches.[24]

Initial adsorption of vesicles on hydrophobic surfaces is energetically disfavored, due to the presence of the hydrophilic polar heads on the outer surface of the vesicular membrane. Therefore, the vesicular membrane must split to allow its inner hydrophobic tails to get in contact with the hydrophobic surface. A possible pathway for vesicle fusion involves vesicle splitting, unrolling and spreading on the hydrophobic surface, as shown in Fig. 8a. The kinetics of vesicle fusion on the hydrophobic surface of gold-supported alkanethiol self-assembled monolayers was followed by SPR.[25] In the initial stage, the adsorbed layer thickness d increases linearly with the square root of time t, denoting control by vesicle diffusion to the surface according to Fick's first law. In a second stage, d increases roughly linearly with log t. Finally, the time dependence of d becomes typical of an adsorption process on an almost fully occupied surface. The curve of the surface coverage by vesicles against time was also monitored by SPR at different vesicle concentrations;[12] it was fitted to an equation practically identical with that derived for an electrode process controlled by diffusion and by a heterogeneous electron transfer step[26]. The resulting kinetic constant was ascribed to some surface reorganization of the

vesicles. The final increase in thickness following vesicle fusion amounts to 2.0–2.5 nm, as expected for a lipid monolayer, provided the vesicle concentration is not too high.[14]

When forming planar lipid monolayers and bilayers by vesicle fusion, the problem of vesicle mere adsorption or partial fusion on the substrate should be considered. When vesicles fuse spontaneously on a support, some of them may remain only partially fused, or even intact in the adsorbed state. When the surface density of vesicles is sufficiently high, their presence is revealed by an anomalously high thickness attained by the lipid film after vesicle fusion, as monitored by SPR. This phenomenon is particularly evident with supports consisting of mixtures, with comparable molar ratios, of two different molecules exposing to the bulk aqueous phase hydrophobic alkyl chains and hydrophilic functional groups, respectively.[6,27] With very high vesicle concentrations (5 mg/mL), monolayer thicknesses greater than 8 nm were reported on hydrophobic surfaces.[14] Thus, fusion of small unilamellar vesicles (SUVs) onto a binary mixture of hydrophobic cholesteryl-terminated molecules and hydrophilic 6-mercaptohexanol molecules yields AFM images showing heightened areas; their diameter being close to that of the SUVs denotes the presence of adsorbed vesicles.[4] The presence of a membrane protein, such as *cytochrome bo3*, in these vesicles increases the number density and the size of the heightened structures ascribable to adsorbed vesicles. Analogously, fusion of large unilamellar vesicles (LUVs) on a hydrophobic support exposing dipalmitoylphosphatidylethanolamine (DPPE) alkyl chains to the aqueous phase yields tapping-mode AFM (TM-AFM) images with a number of dome-shaped structures.[28] Some of these structures, whose diameter is close to that of the LUVs, tend to disappear after one hour, due to vesicle complete fusion. However, if the vesicles contain the membrane protein Na,K-ATPase, all the domelike structures are stable even after three hours. In general, adsorption of proteoliposomes (namely, vesicles incorporating membrane proteins) on hydrophobic surfaces prevents their complete spreading and fusion, due to the presence of protein molecules with extramembrane domains and to the hydrophilicity of the outer polar heads of the proteoliposomes.[15,29]

The presence of heightened areas in metal-supported lipid films formed by fusion of vesicles labeled with a fluorophore can

also be monitored by fluorescence microscopy. In fact, the energy of a photoexcited fluorophore is transferred nonradiatively to the metal support (quenching), if the fluorophore is at a distance from the metal surface shorter that a critical transfer distance (the Foerster radius). This critical distance amounts to about 20–30 nm for gold. Therefore, unquenched bright spots in the fluorescence microscopy images of gold-supported lipid films obtained by fusion of fluorophore-labeled vesicles mark the presence of heightened areas ascribable to adsorbed or hemifused vesicles.[30]

3. Langmuir-Blodgett and Langmuir Schaefer Transfer

Another procedure for forming a lipid monolayer on a hydrophobic substrate or a lipid bilayer on a hydrophilic substrate makes use of a Langmuir trough equipped with a movable barrier. By spreading a lipid dissolved in an organic solvent on the surface of the aqueous electrolyte contained in the trough and by allowing the solvent to evaporate, a lipid film is formed at the air/water interface. This film is compressed with the movable barrier until it is brought in proximity of the liquid crystalline state by adjusting the surface pressure. To form a lipid monolayer on a hydrophobic slab, this is immersed vertically through the lipid monolayer. This brings the hydrocarbon tails of the lipid monolayer, turned toward the air, in direct contact with the hydrophobic surface of the slab, which remains coated by a lipid monolayer (see Fig. 10A). This technique, called Langmuir-Blodgett (L-B) transfer, is also used to form a lipid bilayer on a hydrophilic slab.[31,32] In this case, the slab is initially immersed vertically through the lipid monolayer into the trough. No significant change in surface pressure is observed at this stage. The slab is then withdrawn at a speed slow enough to permit water to drain from the surface. During the withdrawal, the polar heads of the lipid monolayer are turned toward the surface of the hydrophilic slab, giving rise to noncovalent self-assembly (see Fig. 10B). The resulting decrease in the surface pressure of the lipid monolayer at the air/water interface is prevented by reducing its area with the moving barrier. A further lipid monolayer is then self-assembled on top of the first one by the so-called Langmuir-Schaefer (L-S) transfer. In practice, the lipid-coated slab is brought into horizontal contact with the lipid monolayer at the air/water interface, after compressing it at a preset surface pressure. Finally,

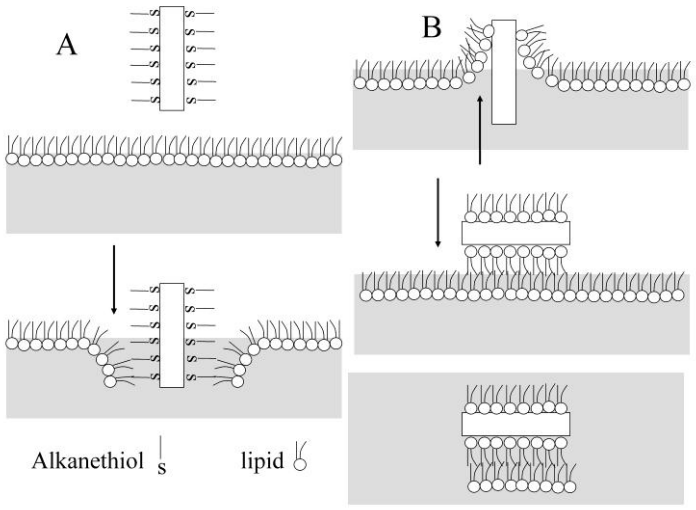

Figure 10. (A) Formation of a lipid monolayer on a hydrophobic alkanethiol-coated slab by Langmuir-Blodgett transfer; (B) Formation of a lipid bilayer on a hydrophilic slab by Langmuir-Blodgett transfer and subsequent Langmuir-Schaefer transfer.

the slab covered by the lipid bilayer is detached from the aqueous subphase. The combination of the L-B and L-S transfers is used principally for lipid bilayer deposition on hydrophilic surfaces of glass, mica, quartz, polymeric materials, graphite and, to a minor extent, on metals such as gold.[33]

An advantage of L-B and L-S transfers over vesicle fusion is that the strict composition of a mixed lipid monolayer on the trough surface is maintained after its transfer. Conversely, the composition of a mixed lipid layer on a substrate does not necessarily correspond to that of the vesicles used to form it, and varies strongly with the history of the sample preparation. On the other hand, an advantage of vesicle fusion over L-B and L-S transfers is that vesicles may easily incorporate membrane proteins, forming proteoliposomes. To this end, membrane proteins are usually stabilized in detergent micelles and then incorporated into the lipid vesicles upon removing the detergent molecules by dialysis. Fusion of proteoliposomes on a metal-supported thiolipid monolayer may

then cause the insertion of the membrane proteins in the resulting lipid bilayer.

4. Rapid Solvent Exchange

A further procedure for depositing a lipid monolayer is the *rapid solvent exchange*. This method is usually employed to self-assemble a lipid monolayer onto a hydrophobic surface exposing alkyl chains to the bulk aqueous phase. The method involves placing a small amount of lipid dissolved in a water miscible solvent, such as ethanol, onto the hydrophobic substrate and incubating it for a few minutes.[34,35] The ethanol solution is, then, vigorously displaced in a few seconds by a large excess of an aqueous buffer solution, taking care to avoid the formation of air bubbles at the surface. During the lipid addition and the subsequent rinsing with the aqueous solution, the lipid self-assembles to form a lipid monolayer and the lipid in excess is rinsed away.

5. Fluidity in Biomimetic Membranes

A fundamental property of biological membranes is the long-range lateral mobility of the lipid molecules. The fluidity of the plasma membrane, interposed between the cytosol and the extracellular space, should be preserved in supported biomimetic membranes. Free movement of lipid molecules enables the biomimetic membrane to react to the presence of proteins, charges and physical forces in a dynamic and responsive manner. A satisfactory fluidity allows biomimetic membranes to reorganize upon interaction with external perturbations, mimicking the functionality of living cell membranes. In particular, lateral mobility enables a biomimetic membrane to incorporate large membrane proteins from their detergent solutions by making space for them; it also determines the spontaneous separation of the components of a lipid mixture (demixing), giving rise to the formation of important lipid microdomains, called lipid rafts.

The fluidity and lateral mobility of biomimetic membranes can be characterized quantitatively by AFM[23] and fluorescence microscopy. Fluorescence recovery after photobleaching (FRAP) is one of the most popular ways of measuring molecular diffusion in membranes.[36] It relies on introducing a small amount of fluores-

cent probe molecules, usually covalently bound to lipids, into the membrane. A short burst of intense excitation light is projected onto the membrane, destroying the fluorescence of the fluorophore molecules in a well defined spot, a photochemical process called photobleaching. The gradual fluorescence recovery within the given spot is followed as a function of time, thus permitting an estimate of the lipid diffusion coefficient. In supported membranes, this coefficient typically ranges from 1 to 10 $\mu m^2\ s^{-1}$. When applied to lipid bilayers self-assembled on smooth supports such as silica, glass, quartz, mica or indium tin oxide (ITO), FRAP usually confirms a satisfactory lateral mobility of lipid molecules.[18,37] Conversely, biomimetic membranes consisting of a thiolipid monolayer tethered to a gold electrode, with a self-assembled lipid monolayer on top of it, does not exhibit lateral mobility. This is also true for the distal lipid monolayer noncovalently linked to the thiolipid monolayer, no matter if obtained by vesicle fusion or by Langmuir-Schaefer transfer.[6,30] A biomimetic membrane consisting of a hydrophilic spacer tethered to gold, with a lipid bilayer formed on top of it, was reported to exhibit fluorescence recovery after photobleaching, if the noncovalently bound lipid bilayer was formed by Langmuir-Blodgett and Langmuir-Scheafer transfers.[6] Fluorescence recovery in the gold-supported biomimetic membrane could only be observed for a short period of time, due to the gradual energy transfer from the fluorophore molecules to gold (quenching). No fluorescence recovery could be observed by forming the lipid bilayer on top of the hydrophilic spacer by vesicle fusion. Evidently, the unavoidable presence of adsorbed and hemifused vesicles prevents lateral mobility of the lipid molecules of the distal monolayer. The strict connection between the presence of adsorbed vesicles and the lack of lateral mobility allows conclusions on lateral mobility to be drawn by monitoring the presence of adsorbed vesicles by a QCM-D.

Electrostatic interactions between vesicles and support play an important role in vesicle fusion. Thus, variously charged gold-supported mixed monolayers of alkanethiols ω-functionalized with the neutral -OH group, the positive $-NH_3^+$ group or the negative $-COO^-$ group induce the fusion of oppositely charged vesicles, as monitored by FRAP.[38] Conversely, the fusion of vesicles made of neutral, zwitterionic lipids takes place only if the charge of the mixed functionalized alkanethiols exceeds a minimum value; this

is explained by electrostatic attraction between the charge of the mixed thiols and the oppositely charged end of the dipole of the zwitterionic lipid molecules.

As distinct from solid supports, such as gold or silver, mercury imparts lateral mobility to lipid monolayers directly self-assembled on its surface, thanks to its liquid nature. This is demonstrated by rapid spontaneous phase separation, with microdomain formation, in a lipid monolayer self-assembled on top of a DPTL thiolipid monolayer tethered to a mercury microelectrode.[39] The presence of microdomains was directly verified from the images of the distal lipid monolayer by using two-photon fluorescence lifetime imaging microscopy (2P-FLIM).

V. THE VARIOUS TYPES OF BIOMIMETIC MEMBRANES

In examining the various types of biomimetic membranes, we will first consider simple experimental models consisting of a single lipid monolayer, self-assembled either on mercury or on an alkanethiol monolayer tethered to a metal electrode. Subsequently, biomimetic membranes comprising a lipid bilayer will be examined, in the order of approximately increasing complexity.

1. Mercury Supported Lipid Monolayers

A simple and easily prepared biomembrane model obtained by noncovalent self-assembly consists of a phospholipid monolayer supported by a hanging mercury drop electrode. The use of a lipid-coated mercury electrode as a biomimetic membrane was introduced by Miller[40] and subsequently adopted in a modified version by Nelson.[41] The lipid coating is obtained by spreading a solution of the lipid in pentane on the surface of an aqueous electrolyte, allowing the pentane to evaporate and immersing a hanging mercury drop electrode in the electrolyte. This procedure gives rise to a lipid monolayer, with the hydrocarbon tails directed toward the hydrophobic mercury surface and the polar heads directed toward the solution. The defect-free support provided by liquid mercury to the lipid monolayer and the complete absence of pentane in the film impart high mechanical stability, resistance to electric fields

and reproducibility to the monolayer. This self-assembly procedure exploits the fact that mercury is the most hydrophobic metal. This by no means implies that mercury has no affinity for the oxygen of water; in fact, at the potential of zero charge, the water molecules adsorbed on bare mercury are slightly oriented with the oxygen turned toward mercury, although less than on all other metals.[42] However, as the adsorbing lipid molecules have to decide where to turn their hydrophilic polar head to attain a minimum in their adsorption free energy, they choose to turn it toward the aqueous phase, where the polar head can form hydrogen bonds with the adjacent water molecules.

Thanks to the liquid state of the mercury support, this simple biomembrane model is fluid and allows lateral mobility of the lipid molecules. However, it has no hydrophilic ionic reservoir on the metal side of the lipid film, and consists of a single lipid monolayer. Consequently, it is not suitable for the study of the function of integral proteins. It can be used to investigate the behavior of the polar heads of the lipid monolayer with varying pH, the behavior of small lipophilic biomolecules incorporated in the lipid film and that of peripheral redox proteins adsorbed on the film surface.

Over the potential region of minimum capacitance, which ranges from –0.15 to –0.75 V/SCE, the film is impermeable to inorganic metal ions, whereas it becomes permeable outside this region. The differential capacitance C of a lipid monolayer on mercury over this region is about 1.7–1.8 μF cm^{-2}, namely twice the value for a solvent-free black lipid membrane (BLM). At positive potentials the region of minimum capacitance is delimited by a capacitance increase that precedes mercury oxidation; at negative potentials it is delimited by two sharp peaks that lie at about –0.9 and –1.0 V/SCE (peaks 1 and 2 in Fig. 11) and by a third peak at about –1.35 V/SCE in the case of DOPC. Peaks 1 and 2 of DOPC are capacitive in nature and are due to field induced two-dimensional phase transitions. The third peak in Fig. 11 exhibits hysteresis in the reverse potential scan[41,43] and is due to partial desorption of the lipid. Complete desorption takes place at potentials negative enough to cause a merging of the curve of the differential capacitance C against the applied potential E recorded on lipid-coated mercury with that obtained on bare mercury, under otherwise identical conditions.

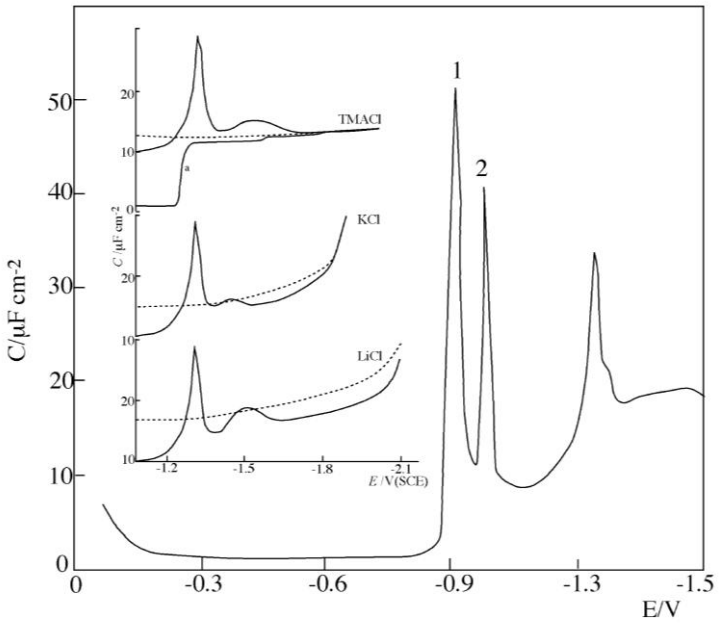

Figure 11. Curve of the differential capacitance *C* against potential *E vs.* SCE for DOPC-coated mercury in aqueous 0.1 M KCl. The inset shows *C* vs. *E* curves for bare (dashed line) and DOPC-coated (solid line) mercury in 0.1M solutions of tetramethylammonium (TMA) chloride, KCl and LiCl.[44]

At the far negative potentials at which lipid desorption is complete, the lipid molecules remain in close proximity of the mercury surface for hours in the form of positively charged micellar aggregates, and spread back readily on the electrode surface with a positive shift in potential.[44,45] This desorption/re-adsorption process was imaged by using epi-fluorescence microscopy and including a small amount of an amphiphilic fluorescent dye molecule in the lipid monolayer.[46] On a Hg electrode, as distinct from a Au electrode, fluorescence can be detected even if the fluorophore is at a small distance from the electrode. In fact, the fluorescence quenching efficiency, due to nonradiative energy transfer to the electrode, is by two to three orders of magnitude lower on Hg than on Au. Upon scanning the potential progressively in the negative

direction up to film desorption, the fluorescence intensity maintains a constant low level along the flat capacitance minimum; a large increase in fluorescence is observed at far negative potentials, indicating a separation of the lipid monolayer from the electrode surface. By scanning back the potential, the fluorescence decreases slowly down to the positive potential limit; however, neither the fluorescence nor the capacitance recovers the pristine value, denoting a defective reformed monolayer. In contrast to a similar system on gold[47], the fluorescent particles or aggregates on Hg are freely mobile, preventing an image analysis yielding their number density and size.

As a rule, incorporation of neutral hydrophobic organic compounds, such as polynuclear aromatic hydrocarbons,[48] polychlorinated biphenyls and phenothiazine,[49] into DOPC monolayers on Hg causes a negative shift and a depression of peaks 1 and 2; this is often accompanied by a slight decrease in the differential capacitance minimum. This effect becomes more pronounced with an increase in the aromaticity and hydrophobicity of the compound. Thus, while the effect of benzene and naphthalene is negligible, it becomes appreciable with hydrocarbons with three, four or five aromatic rings.[50] Hydrophobicity alone, as measured, say, by the octanol/water partition coefficient, is not sufficient to explain this effect; thus, undecane and dodecane have a high partition coefficient but no observable effect on lipid monolayers. The slight decrease in the flat capacitance minimum which is often observed with an increase in the bulk concentration of these compounds is probably to be ascribed to a thickening of the film following their incorporation in the lipid monolayer; this should more than compensate for the expected increase in capacitance stemming from the higher dielectric constant of aromatic compounds compared to that, $\cong 2$, of the lipid tails. The concomitant decrease in the height of the reorientation peaks 1 and 2 and their broadening is due to a decrease in the cooperativity of the reorientation of the lipid molecules, caused by the intercalation of the foreign molecules.

Phospholipid-coated mercury electrodes have been used to measure the intrinsic protonation constants of DOPC, dioleoylphosphatidylethanolamine (DOPE), dioleoylphosphatidylserine (DOPS)[51] and dioleoylphosphatidic acid (DOPA),[52] the surface dipole potential of DOPC, DOPS and DOPA,[53] as well as the change in the dipole potential of DOPS and DOPA with a change

in the charge density of the polar heads of these phospholipids[54] and upon adsorption of certain anti-tumor drugs.[55] These investigations were conducted by measuring the differential capacitance C and the charge density $\sigma_M$of lipid-coated mercury at a special homemade hanging mercury drop electrode.[56] In particular, σ_M was measured by contracting a lipid-coated mercury drop while keeping its neck in contact with the lipid reservoir spread at the water/argon interface, so as to allow a free exchange of lipid material between the lipid monolayer that coats the mercury drop and the lipid film spread on the aqueous solution.[57] This procedure ensures that the thickness and all other properties of the lipid monolayer remain unaltered during the contraction. The charge following the contraction divided by the decrease in drop area yields directly the charge density σ_M on the mercury surface. The experimental data were analyzed on the basis of a model of the membrane/solution interphase that accounts for the presence of charged ionizable groups either exposed to the aqueous phase or buried well inside the polar head region.[51] The behavior of DOPS was found to be particularly involved, with its phosphate group buried somewhere inside the polar head region, and the carboxyl and ammonium groups exposed to the aqueous phase. It was concluded that the overall charge density of a DOPS monolayer varies from slightly negative to slightly positive values as the bulk pH of the bathing solution is varied from 7 to 4.[54] Generalizing this model to account for the expansion of a lipid-coated Hg drop completely immersed in an aqueous solution and for the resulting tilt in the self-assembled phospholipid molecules, the dipole potentials of DOPS and DOPC monolayers were estimated at +140 – +150 mV, positive toward the interior of the film. The fact that these monolayers have very similar dipole potentials indicates that this dipole potential is not to be ascribed to the serine or choline group of their polar heads, but rather to a group common to these two lipids and buried deeper inside the polar head region. This can be reasonably identified with the glycerol backbone.

The effect of lipophilic ions on the capacitance minimum of lipid-coated mercury may be summarized as follows. If the compound is simply *adsorbed* on top of the lipid monolayer or intercalated between the polar heads, it does not affect the tail region, whose capacitance C_t is much less than that of the head region and close to that, C_m, of the whole lipid monolayer. In this case the

capacitance, C_c, of the film of the compound will be in series with C_m, causing a decrease in the overall capacitance $C \cong (C_m^{-1} + C_c^{-1})^{-1}$. In general, this decrease is low, because the polarizability of the compound (and, hence, its C_c value) is higher than that of the lipid tails. While remaining merely adsorbed in the polar head region, the compound may also determine a condensation and an increase in the alignment of the lipid monolayer, resulting in its thickening and in a decrease in capacitance. On the other hand, if the compound penetrates the hydrocarbon tail region, the fraction θ of the electrode surface covered by the compound will have a capacitance C_c higher than that, C_m, of the pure lipid domains. As a rough approximation and disregarding any edge effects at the boundary between the two different domains, the overall capacitance is given by $C = \theta C_c + (1 - \theta)C_m$ and is, therefore, higher than that of the pure lipid film. The cationic phenothiazine derivatives cause a moderate increase in the capacitance minimum.[49,58] The anionic diuretic furosemide causes an initial slight decrease in the capacitance minimum at low bulk concentrations[59] and then an increase at higher concentrations.[58,59] This may indicate that these anions start interacting with the polar heads at low concentrations, before penetrating the tail region at higher concentrations. All these ions depress and broaden peaks 1 and 2, just as neutral compounds. The cationic antibiotic polymyxin narrows the minimum capacitance region on the negative side and decreases the capacitance minimum by about 0.35 μF cm^{-2}.[60] This indicates that this peptide does not penetrate the hydrocarbon tail region.

Lipoproteins are molecular aggregates that transport water-insoluble lipids in the blood plasma: they contain a core of neutral lipids, coated with a monolayer of phospholipids in which special proteins (apolipoproteins) and cholesterol are embedded. The interaction of apolipoprotein A-I with DOPC-coated mercury proceeds in steps when increasing progressively its bulk concentration, $c_{A\text{-}I}$.[61] For $c_{A\text{-}I} \leq 4$ μg cm^{-3} the differential capacitance minimum C is not affected, but the concomitant decrease in the orientation peaks of DOPC points to an interaction of apoA-I with the polar heads of the lipid, possibly electrostatic, through its hydrophilic amino acids. With a further increase in $c_{A\text{-}I}$ the plot of C versus $c_{A\text{-}I}$ shows a first sigmoidal step, with a plateau at ~ 4 μF cm^{-2},

which is then followed by a further sigmoidal step, with a plateau at ~ 7.5 μF cm^{-2}. These C versus $c_{A\text{-}I}$ steps correspond to two consecutive penetration steps into the hydrocarbon tail region, probably associated with two different conformational changes of apoA-I. 10 mol % cholesterol in the DOPC monolayer suppresses the second penetration step, while 25 mol % suppresses both steps. This may be explained by the cholesterol molecules rigidifying the lipid monolayer, thereby preventing it from associating with some penetrating domains of apoA-I.

Small lipophilic ions such as tetraphenylphosphonium ($TPhP^+$) and tetraphenylborate ($TPhB^-$) prefer to be located in the polar head region ($x = \beta$) and in direct contact with the electrode surface ($x = 0$) rather than in the much less polarizable intermediate hydrocarbon tail region. We can therefore envisage two potential energy wells for these ions at $x = 0$ and $x = \beta$, with a potential energy barrier in between.[62] The charge involved in a potential step from a value negative (positive) enough for the anion (the cation) to be entirely located at $x = \beta$ to a value positive (negative) enough to induce a complete translocation of the ion to $x = 0$, once decreased by the charge involved in the same potential step in the absence of the incorporated ion, yields directly the opposite of the charge density of the ion in the lipid film. This procedure allowed the determination of the adsorption isotherms of the $TPhP^+$ and $TPhB^-$ ions in DOPC and DOPS monolayers.[62] In interpreting these isotherms, discreteness-of-charge effects were considered.

6-Ketocholestanol (KC), a steroid that differs from cholesterol mainly by the presence of a carbonyl group, was reported to form pores inside a mercury-supported DOPC monolayer by a mechanism of nucleation and growth similar to that of a number of channel-forming peptides.[63] The potential steps responsible for pore formation by KC molecules give rise to the potentiostatic charge vs. time curves shown in Fig. 12, whose sigmoidal shape reveals two consecutive two-dimensional phase transitions. The first phase transition is ascribed to an increase in the alignment of the KC dipoles along the direction of the interfacial electric field, with the oxygen of the carbonyl group more fully turned toward the aqueous solution. The increase in differential capacitance from 1.2 to 6.5 μF cm^{-2} observed over the potential range between the two phase transitions is ascribed to the first phase transition giving rise

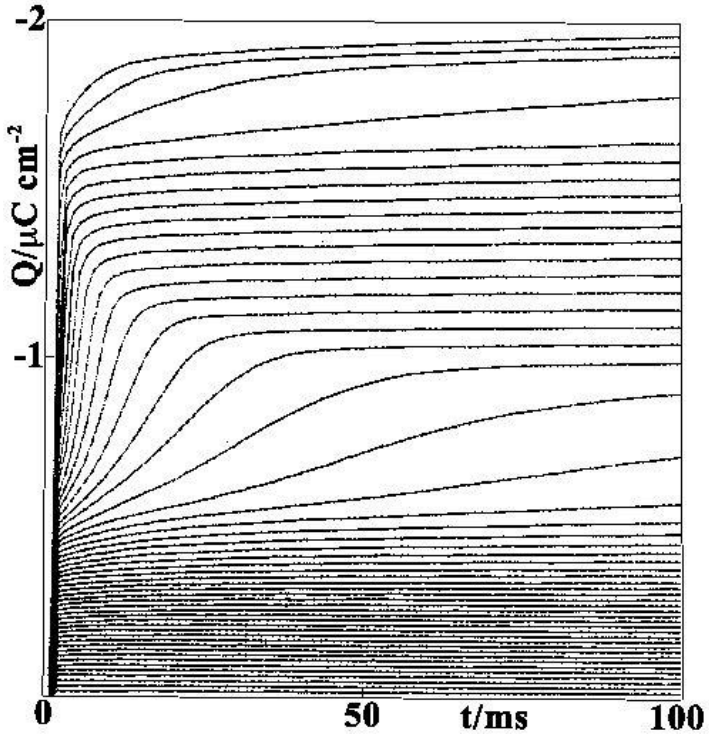

Figure 12. Charge vs. time curves following a series of potential steps from a fixed initial potential E_i= –0.250 V/SCE to final potentials E varying by –10 mV increments from –0.250 to –0.750 V on a mercury electrode coated with a lipid monolayer consisting of 67 mol% DOPC + 33 mol% 6-ketocholestanol and immersed in aqueous 0.1 M KCl.[63]

to bundles of KC molecules, with the oxygens turned toward the interior of the bundles. In these hydrophilic pores the inorganic ions can move back and forth following the a.c. signal, causing an increase in differential capacitance. The decrease in differential capacitance from 6.5 to 1.8 μF cm^{-2} after the second phase transition suggests that this transition involves the disruption of the pores and a return to a random distribution of DOPC and KC molecules within the mixed monolayer. The permeability of the lipid film to Tl^+ ions induced by the first phase transition, and its abrupt decrease induced by the second phase transition, support the formation and subsequent disruption of pores across the lipid monolayer.

Ubiquinone-10 (UQ) is an important, ubiquitous biomolecule that is present in many membranes and acts as a proton and electron carrier in the respiratory chain of the mitochondrial membrane. It consists of a quinone ring, which can be reduced to the corresponding quinol, and is provided with a long, rigid isoprenoid chain imparting a high affinity for lipids. The mechanism of its reduction inside a phospholipid monolayer supported by mercury was investigated by carrying out a series of consecutive potential steps from a fixed initial value E_i, where UQ is still electroinactive, to progressively more negative potentials, E_f, and by measuring the charge $Q(t,E_f)$ following each step, as a function of both time t and potential E_f.[64] The faradaic charge, $Q_f(t,E_f)$, was obtained by subtracting the capacitive charge measured in the absence of UQ from $Q(t,E_f)$. From the linear dependence of E_f upon log t, at constant $Q_f(t,E_f)$ and pH, and upon pH, at constant $Q_f(t,E_f)$ and t, it was concluded that UQ electroreduction to ubiquinol, UQH_2, takes place via a one-electron transfer in quasi equilibrium, followed by the rate-determining uptake of a proton; this rate determining step is followed by the rapid uptake of a further electron and a further proton, yielding UQH_2. The generic chronocoulometric procedure employed for UQ was also adopted to study the electrochemical behavior of dioactadecylviologen[65] and of vitamine K_1,[66] an essential constituent for blood coagulation, upon incorporating these molecules in a self-assembled DOPC monolayer supported by mercury.

Ion channels are responsible for the flow of hydrophilic ions across biomembranes along their electrochemical potential gradient, namely from the membrane side where the electrochemical

potential of the ion is higher to that where it is lower (passive transport). A widely investigated ion channel is gramicidin, a linear pentadecapeptide with helical structure that turns its hydrophobic groups toward the exterior of the helix and its hydrophilic carboxyl groups toward the interior. The length of a gramicidin channel is of 1.3 nm, about one half the thickness of a biomembrane. To span a biomembrane, two helical monomers of gramicidin form a helical dimer, with the N-terminuses of the dimer interacting in the center of the membrane. The resulting hydrophilic pore allows the transport of monovalent cations, such as alkali metal ions, across the membrane. The monomer of gramicidin incorporated in a mercury-supported phospholipid monolayer was reported by Nelson to act as an ion channel toward Tl^+ ion, thus allowing its penetration across the monolayer and its electroreduction to thallium amalgam.[67-71] From a cyclic voltammetric and a chronoamperometric investigation of Tl^+ ion electroreduction through the gramicidin channel, Nelson proposed a Chemical-Electrochemical (CE) mechanism, in which the rate-determining step is a preceding homogeneous chemical step associated with Tl^+ entry into the channel, prior to Tl^+ electroreduction.[69,70] This electrode process at a mercury-supported phospholipid monolayer incorporating gramicidin was employed by Nelson as a model system to probe the effect of lipid charge, solution composition and incorporation of biologically active compounds on ion channel transport. Thus, it was shown that a negatively charged DOPS monolayer increases the rate of Tl^+ transport with respect to a neutral DOPC monolayer, while polyvalent cations, such as Mg^{2+} and Dy^{3+}, have an opposite effect.[70] This is ascribed to the electrostatic interaction of this charge with Tl^+ ions in the immediate vicinity of the lipid film, with a resulting influence on their local concentration. The behavior of the same system by potential-step chronocoulometry was interpreted by Becucci et al.[72] on the basis of a mechanism that includes the diffusion of thallous ions toward the lipid film and a potential-independent heterogeneous step consisting of the dehydration of the ion and its binding to a site located at the mouth of the ion channel. The further step involving the surmounting of a potential energy barrier located somewhere in the middle of the channel is considered to be in quasi-equilibrium, and hence its potential dependence is of the Nernstian type. Rueda and coworkers[73], by investigating this system by EIS, postulated an additional

homogeneous chemical step mimicking the deactivation and release of a Tl^+-gramicidin intermediate from the electrode surface, in competition with the surmounting of the potential energy barrier located within the channel.

Two lipophilic neutral molecules are commonly incorporated into membranes with the aim of altering their dipole potential, namely phloretin, which creates a dipole potential negative toward the interior of the lipid film, and 6-ketocholestanol, which creates a dipole potential positive toward the interior, due to the presence of a carbonyl group.[74,75] As expected, incorporation of phloretin in the lipid monolayer containing gramicidin has no effect on the kinetics for thallous ion reduction.[72] In fact, the favorable dipole potential created by phloretin, negative toward the interior of the film, cannot accelerate the overcoming of the potential energy barrier more than predicted by a Nernstian-type behavior. Conversely, the unfavorable dipole potential, positive toward the interior of the film, created by incorporating 23 mol % 6-ketocholestanol in the DOPC monolayer, slows down this intermediate step by increasing the height of the potential energy barrier within the ion channel. This leads to a decrease in the rate constant for the surmounting of the barrier, which has the typical Butler-Volmer dependence upon the applied potential.[72]

2. Alkanethiol-Lipid Hybrid Bilayers

Great interest has been focused on self-assembled films that are attached to a solid support by formation of a covalent linkage between the self-assembled molecules and the solid support, yielding structures of long-term, mechanical stability. Monolayers of alkanethiols on gold are probably the most widely used and best characterized of all self-assembled films to date. Self-assembly involves the anchoring of the thiol to the gold surface through the sulfhydryl group, often accompanied by its deprotonation and electron transfer from the sulfur atom to the metal. The hydrocarbon chains are, therefore, directed toward the aqueous solution. The self-assembly is normally carried out by keeping the electrode immersed in an ethanol solution of the thiol from 12 to 24 hr for Au or Ag and from 5 to 20 min for Hg.

The deposition of a phospholipid monolayer on top of an alkanethiol monolayer tethered to gold can be accomplished by sev-

eral different preparation techniques, by exploiting the attractive hydrophobic interactions between the hydrocarbon tails of the alkanethiol and those of the phospholipid. The most common procedure for lipid deposition onto alkanethiol monolayers is vesicle fusion. The architecture of the mixed alkanethiol/lipid bilayer, in which the lipid forms a well-ordered, non-interdigitated monolayer on the alkanethiol, with its polar heads directed toward the aqueous solution, was confirmed by surface enhanced Raman spectroscopy (SERS), reflection absorption infrared spectroscopy (RAIRS), neutron reflectivity and EIS. A dipalmitoylphosphatidylcholine (DPPC) monolayer on top of a gold-supported alkanethiol monolayer in air was found by RAIRS to be highly ordered, with 95% of all-trans conformers.[76] SERS indicates that short chain alkanethiols, which are relatively disordered, are more affected by addition of a phospholipid monolayer than longer chain alkanethiols. Neutron reflectivity in D_2O of a DPPC/octadecanethiol bilayer on Au yields a scattering length density (SLD) profile that was fitted to a model of three layers: the sulfur layer, a hydrocarbon layer consisting of the alkyl chains of both the alkanethiol and DPPC, and the polar head region of DPPC.[77] At 60°C, where DPPC is in the liquid crystalline state, the thickness of the hydrocarbon layer region equals 3.3 nm, and that of the polar head region equals 1.0 nm. However, the flat minimum of the SLD profile, corresponding to a totally unhydrated region, is only about 2.2 nm wide, because the polar head region, which is estimated to contain 10 water molecules per DPPC molecule, is also significantly hydrated. AFM images of the gold-supported hybrid bilayer provide clear evidence that the phospholipid monolayer on top of the alkanethiol monolayer is substantially complete and homogeneous. Electrochemical impedance spectra of alkanethiol/phospholipid bilayers on gold have been analyzed with an equivalent circuit consisting of a capacitance C_{hb}, simulating the hybrid bilayer, with in series the resistance R_Ω of the aqueous solution.[25,78] By considering the capacitance C_t of the thiol monolayer in series with that, C_m, of the phospholipid monolayer, C_{hb} is given by $C_tC_m/(C_t + C_m)$. Upon measuring independently the differential capacitance C_t of the sole thiol monolayer on gold, the above equation allows an estimate of C_m. For a palmitoyloleoylphosphatidylcholine (POPC) monolayer on top of an octadecanethiol monolayer tethered to gold, C_m amounts to about

1.8 μF cm^{-2}, in good agreement with values obtained both at solvent-free black lipid membranes (BLM) and at an octadecanethiol/DOPC bilayer self-assembled on a hanging mercury drop electrode.[79] The latter hybrid bilayer is readily prepared by first immersing the mercury drop for one or two minutes in a thiol solution in ethanol; the phospholipid monolayer on top of the alkanethiol monolayer is then obtained by immersing the thiol-coated mercury drop into an aqueous solution on whose surface a phospholipid film has been previously spread.

Solid-supported alkanethiol/phospholipid bilayers are unsuitable for incorporation of channel-forming peptides and membrane proteins, because they do not fulfill the requirements listed in Section II. Thus, no hydrophilic layer is interposed between the hybrid bilayer and the electrode surface, thus excluding the space and water required for the proper folding of the extramembrane domains of integral proteins. Moreover, the flexibility and fluidity of the chemisorbed alkanethiol monolayer in direct contact with the electrode is much less than that of BLMs; this lack of flexibility and fluidity makes these mixed bilayers practically impermeable to lipophilic molecules of biological importance, such as ubiquinone-10 and vitamin K_1, and to lipophilic ions.[79] The kinetics of inorganic redox couples exhibiting a Nernstian behavior on bare gold is almost completely suppressed by hybrid alkanethiol/lipid bilayers for alkanethiol chains with more than eight carbon atoms, pointing to an assembly that provides a substantial barrier to electron transfer and to hydrophilic ions.[79,80] Electron tunneling across these films takes place only at very high overpotentials.

The polypeptide melittin is the major component of the venom of the honey bee. This peptide carries five positive charges. From its aqueous solutions, melittin binds spontaneously to biomembranes and BLMs. At low concentrations, it induces voltage-gated channels in BLMs, while at concentrations higher than 1.2 μg/mL it causes their disruption.[81-84] When bound to lipid bilayers, melittin adopts a highly α-helical conformation, with most hydrophobic residues on one side and most hydrophilic residues on the opposite side of the helix long axis. At zero transmembrane potential, these amphipathic helices accumulate on the surface of the membrane, parallel to the plane of the bilayer. As the transmembrane potential is made negative on the opposite side of the membrane with respect to melittin, the helices form membrane-spanning aggregates

that induce pore conductance. Addition of melittin to a gold-supported alkanethiol/phospholipid bilayer increases the faradaic current for ferricyanide electroreduction, rendering it practically identical with that observed across the sole alkanethiol monolayer;[78,84] this suggests that melittin may permeate the fluid lipid monolayer, but not the underlying alkanethiol monolayer.

The integral protein cytochrome *c* oxidase (COX) spans the inner mitochondrial membrane and is the terminal component of the respiratory electron-transport chain. It catalyzes the redox reaction between the small peripheral protein cytochrome *c* in its reduced form, i.e., ferro-cytochrome *c*, and oxygen, with formation of ferri-cytochrome *c* and water; it also pumps protons from the matrix to the intermembrane space, where it interacts with ferro-cytochrome *c*. COX was reported to retain its functional redox activity after incorporation in a gold-supported hybrid octadecanethiol/lipid bilayer from its detergent solution.[85] Thus, the cyclic voltammogram of COX in this hybrid bilayer yields an oxidation and a reduction peak whose peak potentials are practically equidistant from the known standard potential of the cytochrome a_3 redox site of this enzyme. However, this result was obtained by choosing thiol concentrations and experimental conditions allowing the formation of large uncovered areas of the gold electrode, where COX could partition into the hybrid bilayer during the dialysis procedure. This system was subsequently improved by monitoring the exact amount of octadecanethiol required for the formation of a thiol submonolayer, using a quartz crystal microbalance.[86] Moreover, gold was replaced by silver as the substrate. The Ag-S bond being stronger than the Au-S bond was considered to increase the stability of the membrane. In addition, the fact that the alkyl chains of the tethered thiol molecules are less tilted on silver than on gold was believed to favor a closer approach of the enzyme to the electrode surface. The cyclic voltammogram of COX incorporated in the silver-supported hybrid bilayer shows an oxidation peak much higher than the reduction one. This was ascribed to a nonfaradaic charge flowing during the positive voltage scan, as a consequence of a conformational transition allowing ion movement into and out of the hybrid bilayer.

Alkanethiol-coated electrodes may be usefully employed for adsorbing membrane fragments whose proteins retain their normal activity. Thus, erythrocyte ghosts, i.e., fragments of the plasma

membrane obtained by osmotic lysis of erythrocyte cells, are readily adsorbed on alkanethiol-coated gold.[87] The thickness of the adsorbed erythrocyte membrane, as measured by ellipsometry, SPR and AFM, ranges from 3 to 4 nm. This is not an unreasonable estimate for the thickness of a single leaflet of the erythrocyte membrane, in view of the presence of transmembrane proteins, which are expected to contribute to the total thickness of the layer. Acetylcholinesterase, an erytrocyte marker enzyme associated with the outer leaflet of erythrocyte cells, retains its activity on this alkanethiol/erythrocyte hybrid bilayer for at least eight days. The fact that the enzyme binds to the outer leaflet of the erythrocyte membrane supports the view that the ghost membrane splits and spreads onto the thiol SAM exposing the outer leaflet to the bulk solution, as depicted in Fig. 8a. Alkanethiol-coated gold was also used to adsorb antigens for screening antibody production.[88,89] Usually, epitopes, i.e., peptide sequences representing the major antigenic sites of the antigen, are adsorbed onto the alkanethiol monolayer by vesicle fusion or by Langmuir-Blodgett transfer, thus creating a structured antigen-bearing surface. Antibodies raised against the peptide sequence show notable preferential binding to the peptide-covered part of the surface. The resulting increase in the thickness of the gold-supported film is followed by SPR. This procedure can also be used for studying receptor-ligand binding events. Thus, for instance, the enzyme pyruvate carboxylase, which catalyzes the carboxylation of pyruvate, requires the coenzyme biotin for catalytic activity. Biotin is a small molecule covalently bound to a lysine residue at the active site of the enzyme. Avidin is a protein that can bind biotin very tightly, making it unavailable for its function as a coenzyme. Lipid vesicles containing a biotinylated phospholipid are fused onto alkanethiol-coated gold. Injection of neutravidin gives rise to specific biotin-neutravidin interactions. The resulting increase in film thickness is again followed by SPR.[89]

Annexin A1 is a protein that reversibly binds to cellular membranes in a Ca^{2+}-dependent manner. It was adsorbed on a POPC:(palmitoyloleoylphosphatidylserine = POPS) (4:1) lipid monolayer assembled by vesicle fusion on an octanethiol monolayer tethered to the gold surface of a QCM.[91] Adsorption of annexin A1 to this hybrid bilayer in the presence of Ca^{2+} ions was monitored by the decrease in resonance frequency. No adsorption

was observed in the absence of Ca^{2+} ions, nor even in their presence, if the POPC-POPS mixture was replaced by pure POPC. This indicates that annexin A1 requires the simultaneous presence of a negatively charged membrane and Ca^{2+} ions to interact with membranes. The adsorption isotherm of annexin A1 to POPC:POPS (4:1) was found to satisfy the Langmuir isotherm and its association constant was determined at different Ca^{2+} ion concentrations.

3. Bilayer Lipid Membranes (BLMs)

An important advance in biomembrane methodology was established when Mueller et al.[92] reported a method for forming planar bilayer lipid membranes separating two aqueous phases. According to this method, a lipid solution in a nonpolar solvent such as decane is spread beneath an aqueous phase across an aperture several millimeters in diameter drilled through a partition (septum) of some hydrophobic material such as Teflon. This procedure for forming the lipid bilayer is called the *painting method*. The spontaneous organization of the amphiphilic lipid molecules into a bilayer is driven by the strong self-association of water molecules, which inhibits the mixing of water and amphiphile. Strong lateral intermolecular forces between the long hydrocarbon tails of the lipid molecules also contribute to this self-assembly. The layer of the lipid solution in the nonpolar solvent becomes gradually thinner, with rainbow interference colors appearing on it, followed by black spots; finally, the whole layer becomes completely black. The blackening marks the transition of the lipid layer from a multimolecular to a bimolecular film, called bilayer (or black) lipid membrane (BLM), which is a non-reflecting optically black film. The resulting system consists of a lipid bilayer in quasi equilibrium with an annulus of lipid solution in the nonpolar solvent, called torus or Plateau-Gibbs border, which forms a transition zone between the bilayer and the septum. This system has been studied extensively as a model for the lipid bilayer of cell membranes. Nonetheless, its usefulness has been questioned, because the thin lipid film contains solvent molecules dispersed within the bilayer and in the form of microlenses floating in the bilayer.[93-97] To what extent the presence of the organic solvent limits the usefulness of

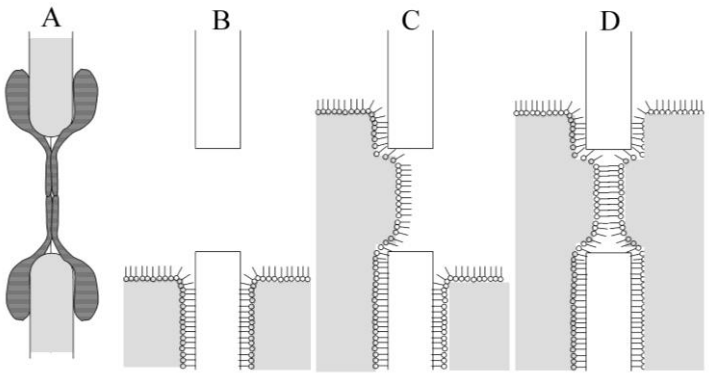

Figure 13. (A) Schematic picture of the cross-section of a black lipid membrane obtained by the painting method, with the Plateau-Gibbs border. (B-D) Preparation of the Montal-Mueller bilayer lipid membrane by raising the solution level on the left hand side of the aperture and, then, on its right hand side.

these BLMs has not been established, but it is clearly important to be able to form solvent-free planar bilayers.

A method for forming bilayers from lipid monolayers that eliminates solvent was developed by Montal and Mueller.[98]. Two polytetrafluoroethylene troughs containing an aqueous solution are separated by a thin (6.5–25 μm) septum through which a hole, 0.1–0.5 mm in diameter, is punched above the solution level. A lipid monolayer is spread from a pentane or hexane solution on each aqueous solution. After the solvent has evaporated, the water level is raised above the aperture first in one trough, and then in the other, bringing the alkyl chains of the monolayers into apposition (see Fig. 13). The Montal-Mueller technique is a particularly significant achievement because asymmetric bilayers can be formed[99] and proteins can be incorporated by first introducing them into the lipid monolayers.[100] The differential capacitance of this solvent-free BLM amounts to 0.8÷0.9 μF cm^{-2},[98] and it is higher than that, about 0.3÷0.4 μF cm^{-2}, of a BLM obtained by the painting method.[101] Evidently, the presence of organic solvent in the latter BLM decreases its differential capacitance.

BLMs have been extensively employed as matrixes for the incorporation of integral proteins, photoactive pigments and biomolecules involved in biophysical, biochemical and physiological studies. A major drawback of BLMs is their fragility, high sensitivity toward vibrations and mechanical shocks, and low resistance to electric fields; thus, they hardly last more than eight hours and collapse under potential differences (transmembrane potentials) greater than 100–150 mV between the solutions that bath the two sides of the BLM; moreover, they do not lend themselves to investigations with surface-sensitive techniques.

A simple procedure for forming BLMs was recently described by Poulos et al.[102] A squalene:decane (2:1) mixture containing 1% DPhyPC is added to a 1 M KCl aqueous solution in a small glass vial. Thanks to its immiscibility with water and its lower density, the organic solvent floats on the aqueous phase. In half an hour, a lipid monolayer is spontaneously formed at the organic/aqueous interface, with the polar heads turned toward the aqueous phase. A 1 μL droplet of an aqueous solution is then dropped into the organic phase, reaching by gravity the organic/aqueous interface without fusing with the aqueous phase. The lower, flattened portion of the droplet surface in contact with the lipid monolayer becomes rapidly coated by a lipid bilayer. Finally, an Ag/AgCl wire is immersed into the droplet, allowing the closure of the electric circuit via a further reference electrode immersed in the aqueous phase. This system allowed the recording of single channel currents of gramicidin, alamethicin and α-hemolysin.

Recently, attempts have been made to form more robust lipid bilayers (often referred to as *planar free-standing bilayers*) by spanning them over nanopores interposed between two aqueous and/or hydrogel phases. These free-standing bilayers have a fluidity probably comparable with that of biological membranes, thus imparting lateral mobility to lipid molecules and membrane proteins. The observed thirty times increase in stability by reducing the pore size by a factor of four demonstrates the benefit from using nanopores. Besides stabilizing lipid bilayers, small apertures increase the signal-to-noise ratio to an appreciable extent. Peptides and small channel-forming proteins insert spontaneously into these preformed bilayers. Bulky membrane proteins are incorporated either by fusion of proteoliposomes to preformed bilayers or by direct fusion of proteoliposomes to nanopores. Little is known

about the influence of nanopores on the fusion of proteoliposomes of similar size.

By comparing free-standing bilayers on Teflon chips with pore diameters ranging from 25 to 250 μm, the capacitance was found to be about equal to 0.6 μF cm^{-2}, a value typical of solvent-containing BLMs.[103] These bilayers were stable for many hours even at applied voltages up to 400 mV. The ion-channel activity of alamethicin and α-hemolysin could be recorded with a high signal-to-noise ratio, by using low-noise patch-clamp amplifier technology. Evans' group reported a device consisting of a 100 μm micromachined hole in a gold surface suspended over an aqueous reservoir. An octadecanethiol[104] or perfluorothiol monolayer[105] was tethered to the gold surface, to impart a hydrophobicity similar to that of the bilayer-forming solution to the hole rim. A lipid bilayer was then painted across the aperture with a plastic stick. Incorporation of the channel-forming peptides gramicidin and alamethicin allowed the recording of their single-channel activities.

Polycarbonate membranes commercially used for ultrafiltration are a porous material, with irregularly arranged pores of uniform size of about 1 μm. Favero et al.[106] covered one side of the membrane with a gold layer that was subsequently hydrophobized by tethering an alkanethiol monolayer on top of it. After gently dropping an egg-PC solution in *n*-hexane on the gold-coated side of the polycarbonate membrane, free-standing bilayers were spontaneously formed in the pores. By incorporating gramicidin D, the following order of increasing conductance, $NH_4^+ > K^+ >> Li^+$ was verified, in accordance with the known selectivity coefficients of this peptide. By setting up an apparatus allowing continuous conductance measurements under flowing conditions, the same authors[107] tested the functional activity of an ionotropic glutamate receptor incorporated in this microarray of BLMs. By injecting 0.1 μM glutamate in the flowing solution and by then removing it with pure buffer, a notable increase in conductance was recorded, followed by a return to the initial low value. Enhancement in conductance by injecting the coagonist glycine, and conductance suppression by injecting the antagonist Mg^{2+} ions, were verified. Although the feasibility of functional assays for membrane proteins was demonstrated, ultrafiltration membranes have a number of limitations. Thus, the stability of these membranes is about 10 h

with 25% cholesterol; the achieved sealing of about 10 MΩ cm^2 is too low for sensitive measurements;[108] the pore distribution is random, resulting in merged pores that may affect the bilayer stability; the membrane is about 10 nm thick, with a resulting high *aspect ratio* (i.e., pore size to membrane thickness); the stability of coated gold on polymer carbonate may be too low for continuous use.

Nanoporous alumina membranes with highly ordered pores of 60 and 280 nm in diameter have been frequently used by Steinem and coworkers to support free-standing lipid bilayers. In their earlier work, a differential capacitance of about 1 μF cm^{-2} was obtained for bilayers formed by fusing giant vesicles on nanopores of 30 and 50 nm diameter.[109] In a further development, the nanoporous alumina supports were coated with gold, and 1,2-dipalmitoyl-*sn*-glycero-3-phosphothioethanol was tethered to its surface via its thiol group.[110] The gold surface so hydrophobized favors the spanning of lipid bilayers across the nanopores of the alumina membrane, upon painting its gold-coated side with a DPhyPC solution in *n*-decane. The membrane was clamped between two Teflon half-cells. The formation of lipid bilayers in this *nano-bilayer lipid membrane* (nano-BLM) was followed by measuring the differential capacitance of the membrane by EIS up to the attainment of its maximum limiting value. The impedance spectra were fitted to an RC mesh, simulating the lipid bilayer, with the solution resistance R_Ω in series with it. Upon regarding the resistance of the thiol-coated gold much higher and its capacitance much lower than those of the pores, the resistance and capacitance of the whole membrane were referred exclusively to the active area of the pores, yielding a specific capacitance of 0.5–0.6 μF cm^{-2} and a specific resistance of up to 0.16 GΩ cm^2. As opposed to the membrane capacitance, the membrane resistance strongly depends on the quality of the preparation and the age of the nano-BLM. What is important for recording single channel currents by a low-noise patch-clamp amplifier is the resistance R_m of the whole nano-BLM, which must be higher than 1 GΩ to reduce the background electrical noise to the order of 1–2 pA. R_m decreases gradually in time, due to the progressive rupture of the individual lipid bilayers spanning the single pores. This gradual decrease in resistance causes a progressive increase in the current baseline, but the back-

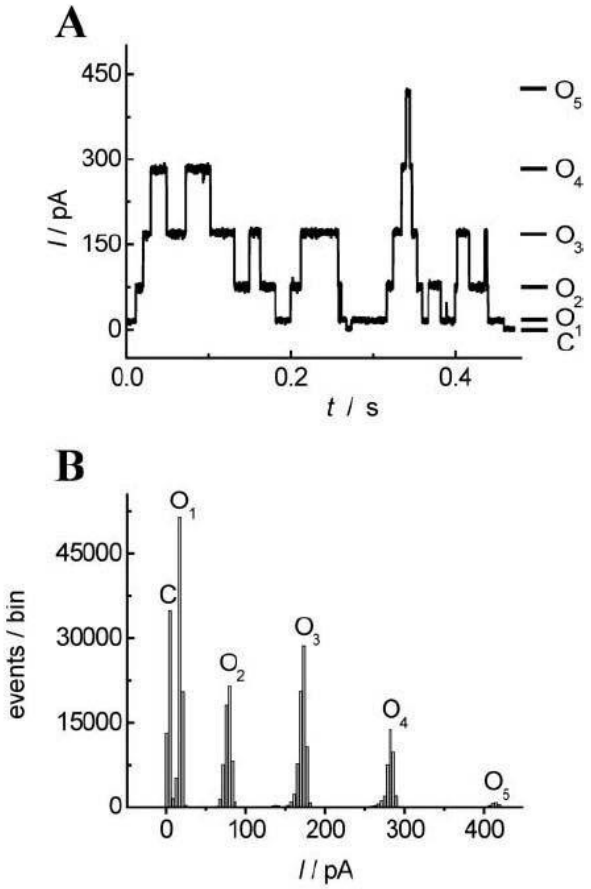

Figure 14. (A) Representative current trace showing single pore fluctuations induced by alamethicin. The nano-BLM was symmetrically bathed in 0.5 M KCl and a holding potential of 70 mV was applied. Data were filtered at 1 kHz. The whole burst of fluctuations is due to a single pore event, fluctuating between conductance levels O_1–O_5. O_1 = 16.4 pA; O_2 = 79.1 pA; O_3 = 171.7 pA; O_4 = 281.6 pA; O_5 = 415.2 pA. C = 3.0 pA reflects the current baseline with the channel closed. (B) Corresponding current amplitude histogram. (Reprinted from Ref. [110] with kind permission from Elsevier.)

ground noise remains low enough to allow the monitoring of single channel currents, provided R_m is maintained above 1 GΩ. From a statistical analysis, the lifetime of nano-BLMs with resistance higher than 1 GΩ was estimated at 1.5 days. Single channel currents of gramicidin, alamethicin[110] (see Fig. 14) and OmpF porin[111] were recorded, and the corresponding current amplitude histograms were reported.

OmpF porin is an integral membrane protein located in the outer membrane of *Escherichia coli.* It is a non-specific transport channel that allows the diffusion of small, polar molecules (600–700 Da in size) through the cell outer membrane, where it forms a trimer. The characteristic conductance states of the three OmpF monomers could be observed with the nano-BLM. Fast openings and closures of a single monomer, superimposed on the slow kinetics of the channel, was also recorded. Moreover, the blockade of the ion flow as a result of interaction of the antibiotic ampicillin with OmpF porin was verified. These experiments show that single channel currents of bulky proteins, such as OmpF porin, whose cross-sectional area amounts to about 80 nm^2, can be monitored using nano-BLMs with highly ordered pores of 60 nm in diameter. These nano-BLMs were also used to record the photocurrents generated by purple membrane fragments adsorbed on the lipid bilayers spanning the micropores.[112] Purple membranes from *Halobacterium salinarium* are very rich in the proton pump bacteriorhodopsin, which pumps protons from the cytoplasmic to the extracellular side of the bacterium membrane upon photoactivation by green light. The purple membrane fragments were added to the compartment exposing the gold-coated side of the alumina membrane. After their adsorption on the lipid bilayers spanning the nanopores and their illumination, the purple membrane fragments with the extracellular side facing the lipid bilayers cause protons to translocate through the proton pump. This movement generates a current transient that decays with a characteristic decay time; the current tends to a nonzero stationary value, revealing a small permeability of the nano-BLM to protons. Addition of the lipophilic proton ionophore CCCP increases the level of the stationary current by facilitating the diffusion of protons pumped by bacteriorhodopsin across the lipid bilayer.

Silicon nitride membranes with 800 nm pores arranged in regular arrays were hydrophobically functionalized, and bilayers were

then formed in the pores by the painting method.[113,114] The stability of these free-standing bilayers was found to depend on the nature of the lipid. Bilayers formed from the cylindrically shaped phosphatidylethanolamine exhibit a membrane resistance higher than 1 GΩ for more than one week, while those formed from DPhyPC remain above this threshold value for two days. Bilayers of the naturally occurring soy PC mixtures are stable for only about 2 h, but a reduction of the pore size from 800 to 200 nm increases their stability by a factor of 30. Membrane sheets with a well-defined orientation were transferred onto a regular array of holes, 50-600 nm in diameter, in a silicon nitride chip, 100–500 nm thick.[115] By pressing the chip against a supported layer of cultured cells and by then removing it, the cells rupture and membrane fragments remain attached to the chip, spanning the holes. The chip was integrated into a microfluidic chamber suitable for optical imaging.

Tien et al.[116] devised a biomimetic membrane formed at the end of a salt-bridge tubing. Briefly, a freshly cut salt-bridge tubing attached to the end of a Ag/AgCl(KCl) reference electrode is firstly dipped into an alkane solution of the lipid and then transferred into an aqueous solution, so as to form a lipid bilayer. In this case, the hydrophilic surface required for bilayer formation is provided by the freshly cut agar gel containing KCl. The resistance of these supported BLMs is usually irreproducible from one membrane to another. More recently, replacing water by a hydrogel as a hydrophilic medium has permitted to achieve a notable increase in stability of lipid bilayers in micropores. Thus, for instance, a lipid bilayer formed across a Teflon aperture was protected with a layer of photopolymerized poly(ethylene glycol) dimethacrylate, and proteins were incorporated by allowing them to diffuse slowly through the previously formed gel.[117] Covalent conjugation of the lipid bilayer to the encapsulating hydrogel was found to increase preservation of the lipid-containing solvent reservoir (the Plateau-Gibbs border) surrounding the membrane, thereby extending the membrane lifetime. To further reduce the flow of organic solvent away from the Plateau-Gibbs border, the Teflon septum was replaced by a glass cover slide where a 500 μm hole was drilled.[118] The hydrophilic glass surface was made hydrophobic by functionalizing it with 3−methacryloxypropyltrimethoxysilane, to provide cross-linkable vinyl groups on the glass surface. In this way, the hydrogel precursor could covalently bind to the vinyl groups of the

silane-coated glass substrate during the process of hydrogel polymerization, sealing the solvent annulus. This allowed the capacitance of the membrane to maintain its value of about 0.4 μF cm^{-2}, typical of a solvent-containing bilayer, for 12 days. In a different approach, a lipid bilayer was protected on both sides by precast gel slabs, and the electrical properties of nicotinic acetylcholine receptor[119] and of the peptides valinomycin and gramicidin[120] were examined, upon incorporating them in the bilayer. An appreciable decrease in the noise level was achieved by Kang et al.[121] by fabricating a chip in which a bilayer containing a single α-hemolysin channel was incapsulated by forming an agarose gel around it. A Teflon septum with a 100 μm diameter aperture was clamped between the cis and trans compartments of a chamber. A buffer solution in liquid agarose at 45°C was added to both compartments, maintaining the liquid level below the orifice of the septum. After spreading a DPhPC solution in pentane on the surface of the liquid agarose and allowing pentane to evaporate, the agarose level in the two compartments was raised by adding further warm agarose solution. By adopting this Montal and Mueller procedure (cf. Fig. 13), a lipid bilayer was obtained with a capacitance of 0.8-1 μF cm^2, typical of a solvent-free bilayer. The subsequent insertion of a preformed heptameric α-hemolysin channel into the lipid bilayer was monitored by an abrupt current jump. The chamber was then cooled to allow the agarose to form a gel, and the single nanopore chip was cut away from the chamber. The chip was stable and storable for at least three weeks at 4°C and endured mechanical disturbance.

With BLMs, the transmembrane potential can be readily adjusted and varied by applying a given potential difference across two identical reference electrodes (say, two Ag/AgCl electrodes) immersed in the bulk solutions bathing the two sides of the membrane. This procedure is not usually applicable to vesicles, due to their small size. However, a sophisticated and elegant electrophysiological technique, called *patch-clamping*, allows an ultramicropipette, whose tip has an inner diameter of a few micrometers, to penetrate both cells[122] and giant unilamellar vesicles (GUVs). The ultramicropipette contains an electrolyte solution with a reference Ag/AgCl electrode inside, while an identical reference electrode is immersed in the external solution. This allows the trans-

membrane potential to be measured and varied at will. Other widely employed biomembrane models are unilamellar lipid vesicles (also called liposomes). Due to their small size, they cannot be studied by electrochemical techniques. Rather, they can be investigated by spectroscopic techniques using fluorescent or spin labeled molecular probes. Electrical methods are used to apply square wave electric field pulses to cell suspensions, for the investigation of pore formation in biomembranes induced by electric fields (electroporation).[123]

In an effort to overcome the drawbacks of BLMs, more robust biomimetic membranes have been fabricated, by immobilizing lipid bilayers on solid surfaces. They are normally obtained by self-assembly, which can be driven exclusively by noncovalent, hydrophobic interactions or with the additional contribution of covalent linkages. In spite of notable improvements in this direction, some major problems of solid supported membranes arise when attempting to use them for analytical applications; the very small space between the bilayer and the support (from 2 to 10 nm) is rapidly saturated by the transported species. This makes quantitative dynamic measurements difficult.

4. Solid Supported Bilayer Lipid Membranes (sBLMs)

The term *solid supported bilayer lipid membrane* (sBLM) or, simply, *solid supported membrane*, is commonly used to denote a biomimetic membrane consisting of a lipid bilayer in direct contact with a solid support. These biomimatic membranes are typically formed on a hydrophilic solid support by immersing it in an aqueous dispersion of small unilamellar vesicles (SUVs), which slowly rupture and spread on the surface of the support. Alternatively, they can be formed by Langmuir-Blodgett and Langmuir-Schaefer transfers. When appropriately formed, these sBLMs are separated from the support surface through a hydration layer of water, estimated between 6 and 15 Å thick.[124,125] Several theoretical and experimental investigations of water near polar hydrophilic surfaces suggest that it is more ordered than bulk water, with higher viscosity and lower dielectric constant.[126,127] In accordance with these predictions, the characteristics of the lipid bilayer have been found to be structurally coupled with the support properties, such as its charge[128], wettability[129] and topography[130]. Frictional or electro-

static coupling between the support and at least the proximal leaflet of the lipid bilayer may induce undesirable asymmetries in compositional, structural, mechanical and dynamic properties of the lipid bilayer.[131] The lubrification effect of the water layer imparts a significant long-range lateral mobility to the lipid bilayer. However, significant frictional coupling between the bilayer and the underlying substrate slows down lateral diffusion, which may be accompanied by a breakdown of the two-dimensional fluid nature of the membrane.

The above biomembrane models are not suitable for studying the function of integral proteins. In fact, these proteins have hydrophilic domains protruding outside the lipid bilayer. To avoid their denaturation and to promote their function, the incorporation of integral proteins into biomembrane models must ensure that their protruding hydrophilic domains are accommodated in a hydrophilic medium on both sides of the lipid bilayer. Not surprisingly, embedded membrane-spanning proteins usually show no lateral diffusion, because of their interaction with the substrate[132], even though some of them maintain their function if their active site is far from the solid substrate.

The majority of sBLMs are formed on nonconducting supports such as silica, glass or mica.[18,32,37] Consequently, they are not amenable to electrochemical measurements. Thus, for instance, sBLMs on silica were recently formed from mixtures of native *Escherichia coli* bacterial inner membrane (IM) vesicles, which contain membrane proteins, diluted with egg-PC vesicles.[132] These sBLMs were investigated by QCM, AFM, attenuated total internal-reflection Fourier-transform infrared spectroscopy (ATR-FTIR) and FRAP. Samples with less than 40% IM were found to form sBLMs by vesicle fusion. They were fluid, as shown by FRAP, and those with 30% IM contained the protein, as confirmed by ATR-FTIR. Conversely, the samples with more than 40% IM were dominated by vesicle adsorption. By forming a sBLM on silica, side by side with an alkanethiol/lipid hybrid bilayer on gold, it was found by FRAP that the lipid molecules of the distal monolayer of the sBLM could move laterally, mixing freely with those of the hybrid bilayer.[133] Moreover, the distal and proximal monolayers of the sBLM on silica could also mix by flip-flop.

In what follows, a few examples of sBLMs investigated by electrochemical techniques will be examined. Phospholipid bi-

layers on Au(111) single crystal faces have been prepared by Lipkowski and coworkers either by vesicle fusion[134] or by Langmuir-Blodgett and Langmuir-Schaefer transfers.[33] The latter procedure yields bilayers with a higher packing density and with smaller tilt angles of the alkyl chains with respect to the surface normal. These bilayers have been characterized by charge density measurements, photon polarization modulation infrared reflection absorption spectroscopy (PM IRRAS)[134,33] and neutron reflectivity.[135] The minimum differential capacitance of these bilayers is about equal to 2 μF cm^{-2}, and is attained at charge densities σ_M on the metal higher than –8 μC cm^{-2}. The differential capacitance being greater than that of a solvent-free BLM denotes the presence of a number of defects, while neutron reflectivity reveals the presence of water molecules within the lipid bilayer. As σ_M becomes negative of –8 μC cm^{-2}, the lipid bilayer starts to detach from the electrode, but remains in close proximity to the electrode surface. In fact, neutron reflectivity indicates that the lipid bilayer is suspended on a thin cushion of the aqueous electrolyte, which screens the metal charge and contains a large fraction of the overall interfacial potential difference; consequently, the electric field across the lipid bilayer becomes weak. This suspended lipid bilayer is essentially defect-free and its structure resembles that of lipid bilayers supported by a quartz surface. The IR data demonstrate that the carbonyl and phosphate groups are more hydrated when the bilayer is adsorbed on the electrode surface at $\sigma_M > -8$ μC cm^{-2} than when it is detached from the electrode at more negative charge densities.[134] Neutron reflectivity shows that a significant amount of water enters the polar head region of the lipid bilayer when it is in contact with the metal surface. The detachment of the lipid bilayer from the electrode surface is accompanied by a decrease in the tilt angle of the alkyl chains with respect to the surface normal from about 55° to 35°, with a resulting increase in bilayer thickness. The PM IRRAS measurements indicate that, as long as the lipid bilayer remains attached to the metal surface, changes in the local electric field by several orders of magnitude have only a small effect on the orientation of the phospholipid molecules.[136] Electrochemical scanning tunneling microscopy (EC-STM) images of adsorption of dimyristoylphosphatidylcholine (DMPC) on Au(111) show that the lipid molecules are initially adsorbed flat, with the alkyl chains

oriented parallel to the surface;[137] the resulting ordered monolayer resembles that formed by alkanes. With time, the molecules reorient and the monolayer is transformed into a hemimicellar film. In the presence of a high vesicle concentration in solution, the hemimicellar state is transformed further into a bilayer.

A sBLM formed by fusing vesicles consisting of a mixture of 50 mol% cholesterol and 50 mol% dihexadecyl-dimethyl-ammonium bromide on boron doped (p-type) silicon covered with native oxide was investigated by EIS.[138] The positively charged lipid was chosen to favor vesicle spreading on the negatively charged Si/SiO_2 surface. The impedance spectrum was simulated by an equivalent circuit consisting of two RC meshes in series, with the resistance R_Ω of the aqueous solution in series with them. One RC mesh simulates the electrode, regarded as a combination of the Si space-charge region, the SiO_2 oxide and the thin water layer interposed between the semiconductor surface and the lipid bilayer; the other RC mesh simulates the lipid bilayer. The resistance and capacitance of the electrode amount to about 19 MΩ cm^2 and 2.2 μF cm^{-2}, respectively, those of the lipid bilayer to 0.98 MΩ cm^2 and 0.75 μF cm^{-2}. Values of the two capacitances are close, but the resistance of the electrode is much greater than that of the lipid bilayer, due to the 1.3–1.4 nm thick silicon oxide. The time constants of the two RC meshes are, therefore, appreciably different and the corresponding frequency ranges are sufficiently apart to allow an accurate estimate of the corresponding parameters. Incorporation of gramicidin from an aqueous solution decreases the resistance of the lipid bilayer by more than one order of magnitude in the presence of Na^+ ions, and even more in the presence of K^+ ions. This agrees with the cation selectivity scale of gramicidin. When the Si/SiO_2 substrate was coated with a lipid bilayer consisting of a mixture of 1,2-dioleoyl-3-trimethyl-ammonium propane (DOTAP) and DOPC, the resistance R_m of the bilayer was found to attain a maximum value for 10 mol% of the positively charged lipid.[8] Electrostatic forces are those of longest range between a lipid bilayer and a substrate, but other forces are also operative, such as attractive van der Waals forces and repulsive hydration and steric forces. In view of the major role played by electrostatic forces, the rapid decrease of R_m for DOTAP mole fractions greater than 10% can be tentatively explained by electrostatic repulsion between the partially formed SiO_2-supported lipid

bilayer and the fusing vesicles. The repulsion among the charged lipid molecules of the SiO_2-supported bilayer may also favor the entrapment of inorganic ions in the polar head region and their subsequent movement along small fluctuating membrane-spanning pores, with a resulting decrease in R_m.

A sBLM formed by fusing DMPC-cholesterol vesicles on the optically transparent semiconductor indium tin oxide (ITO) was investigated by EIS.[139] The vesicles also contained 10 mol% of a positively charged lipid to favor their interaction with the negatively charged ITO surface. The impedance spectrum was analyzed with the same equivalent circuit used for the Si/SiO_2 substrate. In this case, gramicidin was incorporated in the ITO-supported lipid bilayer by incubating it with gramicidin-containing vesicles. Upon incorporating gramicidin, the resistance R_m of the lipid bilayer was strongly reduced in the presence of a Na^+ salt with an organic anion not permeating membranes, whereas its capacitance did not change remarkably. Conversely, R_m was practically unaffected in the presence of a Cl^- salt with an organic cation not permeating membranes. This experiment confirms the functional activity and ion selectivity of gramicidin, which is known to be highly selective toward monovalent inorganic cations. The outer membrane proteins OmpF and OmpA from *Escherichia coli* were reconstituted in vesicles that were fused on ITO.[139] In an aqueous solution of NaCl, the resistance of the ITO-supported lipid bilayer was strongly reduced by incorporating OmpF, whereas it was only slightly decreased by incorporating OmpA. Such a behavior was explained by the fact that only OmpF is a pore-forming protein, whereas OmpF does not form pores. Note that the functional activity of OmpF was preserved because, on the cytosolic side of the bacterial membrane, it has no extramembrane domain that might be endangered by direct contact with the ITO surface.

Freshly formed surfaces of Pt, Au, Ag, Cu, Ni or stainless steel are hydrophilic. Self-assembly of a lipid bilayer on these surfaces is realized by cutting the end of a Teflon-coated hydrophilic metal wire while keeping it dipped in a decane or squalene solution of the lipid, and by then immersing the freshly cut metal surface in an aqueous solution for 5–10 min.[140] During this period, the lipid solution in excess creeps between the metal wire and its Teflon coating, leaving a self-assembled lipid bilayer on the metal surface. The differential capacitance of this film, 0.3–0.5 $\mu F\ cm^{-2}$,

is lower than that, about 0.8–0.9 μF cm^{-2}, of solvent-free BLMs, thus denoting the incorporation of alkane molecules, and its resistance (~0.5 MΩ cm^2) is also lower. The potential range covered by this solid-supported bilayer before its breakdown is appreciably wider than that at conventional BLMs, attaining values as high as 1.5 V. Since the metal surface can be rough after cutting, it can induce defects in the overlying lipid bilayer. These sBLMs, devised by Tien, were used by this author and coworkers[141] to carry out a feasibility study of an antigen-antibody reaction. The hepatitis B surface antigen was incorporated into the bilayer and was then allowed to interact with the corresponding monoclonal antibody in the bathing solution. The antigen-antibody interaction results in a notable linear decrease in the bilayer resistance with an increase in the antibody concentration, up to 50 ng mL^{-1}. These sBLMs were also used with the aim of realizing electrodes for biosensor applications.[141] In this connection, nonbiological liposoluble molecules such as ferrocene, tetracyanoquinodimethane (TCNQ) and tetrathiafulvalene (TFF) were incorporated in the bilayer and employed as electron carriers between the electrode and a hydrophilic redox couple present in the aqueous solution.[142] As an example, vinyl-ferrocene incorporated in a platinum-supported lipid bilayer acts as an electron carrier between the electrode and the peripheral, water-soluble protein ferri-cytochrome *c*.[143] The lipid bilayer provides a natural, biocompatible, surface for cytochrome *c* binding, with a resulting enhancement both in the equilibrium constant for cytocrome *c* adsorption on the bilayer and in the electron transfer rate between electrode and protein, with respect to a gold electrode in the presence of bipyridyl.[144] Fullerene C_{60} incorporated in a lipid bilayer supported by ITO was shown to facilitate electroreduction of ferricyanide ion and, upon illumination, to accelerate the photoinduced electron transfer from electron donors in solutions, (e.g., water, EDTA), to the electrode.[145]

In general, two possible mechanisms may be responsible for transmembrane electron transport between the electrode and a hydrophilic, lipid insoluble, redox couple present in the aqueous solution:

(1) a redox reaction at the bilayer/water boundary between the hydrophilic redox couple and a lipophilic redox couple pre-

sent in the bilayer, which shuttles electrons to or from the electrode surface;

(2) an electron tunneling across the bilayer, possibly assisted by some lipophilic molecule possessing conjugate π-bonds, and therefore capable of providing an electron-conductive pathway across the lipid bilayer.

The latter view, uphold by Tien and some other authors[146], is inspired by the existence in natural membranes of sites, small in extent, where electron transfer between hemes occurs as a result of the overlapping of the orbitals of neighboring molecules. However, the probability of electron tunneling through the entire thickness of a lipid bilayer, even in the presence of molecules with conjugated double bonds such as ferrocene, TCNQ or TFF[142], seems doubtful. In fact, it would require overpotentials higher than those observed experimentally.

A different procedure for the realization of a lipid bilayer noncovalently attached to a silver surface was adopted by Salamon, Tollin et al.[147] It consists of spreading a small amount of a solution of a lipid in a suitable solvent across a small orifice in a Teflon sheet sandwiched between a thin silver film, deposited on the external surface of a prism, and an aqueous solution. The hydrophilic surface of silver attracts the polar heads of the lipid molecules, thus forming a lipid monolayer with the hydrocarbon tails directed toward the bulk lipid phase. This phase becomes progressively thinner through the accumulation of the excess lipid and its solvent at the edge of the Teflon orifice, with formation of an annulus (the Plateau-Gibbs border), until the orifice is covered by a lipid bilayer enclosed between the silver surface and the aqueous solution. The authors claim that a water layer remains in contact with the silver electrode during this process, thus favoring the incorporation of integral proteins into the bilayer. The above sBLMs, noncovalently attached to the metal support, are reported to be stable for 25–35 h. However, the capacitance C of these bilayers, measured by EIS, is about one order of magnitude greater than that of a conventional BLM, denoting an appreciable amount of defects.[148] By a detailed analysis of the minimum, depth and half-width of the SPR reflectivity curves of these silver-supported lipid bilayers, Salamon and Tollin studied the structural changes following the incorporation of a number of integral proteins into the bilayer and the interaction of

these proteins with their associated water-soluble proteins (e.g., incorporation of rhodopsin and its interaction with the G-protein transducin[149], incorporation of cytochrome *c* oxidase and its interaction with cytochrome c.)[150] This allowed the authors to distinguish conditions under which nonspecific electrostatic interactions prevail over those characterized by the predominance of specific hydrophobic interactions. Salamon and Tollin have subsequently improved the technique by interposing a thin dielectric layer of SiO_2, acting as a waveguide, between the silver layer and the lipid bilayer, which was now self-assembled on the hydrophilic SiO_2 surface.[151] This system allows an estimate of the refractive index and the extinction coefficient of the composite film not only with *p*-polarized light (i.e., in the direction perpendicular to the bilayer plane), as in conventional SPR, but also with *s*-polarized light, i.e., in the direction parallel to the bilayer plane. These parameters measure the anisotropic character of the lipid membrane structure. This technique, called *coupled plasmon-waveguide resonance spectroscopy* (PWR), has provided useful pieces of information on the structural changes accompanying the incorporation in a lipid bilayer of the integral protein cytochrome b_6f and its interaction with the peripheral, water-soluble protein plastocyanin;[152] the structural changes involved in the incorporation of different receptors and in their ligand binding have also been investigated. The PWR spectroscopy has also been used to monitor the formation of microdomains in mixed sphingomyelin-DOPC mixtures (called lipid rafts) and the sorting of receptors into each microdomain.[153] The microdomain size evaluated from the lateral resolution of the PWR sensor is very high (100–300 μm). While providing useful structural information on (lipid bilayer) - (integral protein) - (peripheral protein) systems, this technique cannot provide direct evidence for the functional activity of these systems and a verification that the differential capacitance of the lipid film is that expected for a well-behaved lipid bilayer.

5. Tethered Bilayer Lipid Membranes (tBLMs)

As a rule, tethered bilayer lipid membranes refer to architectures in which the lipid bilayer is separated from the support through a monomolecular layer tethered to the support via a sulfhydryl or disulfide group (for gold, silver or mercury supports) or via a

silane group (for silica and glass supports). The monolayer interposed between the support surface and the lipid bilayer should have a well-defined composition and geometrical arrangement, as distinct from polymer-cushioned bilayer lipid membranes. TBLMs will be classified on the basis of the nature of the molecules composing the tethered monolayer, as follows:

(1) spacer-based tBLMs;
(2) thiolipid-based tBLMs;
(3) (thiolipid-spacer)-based tBLMs.

We will examine these three types separately.

(*i*) *Spacer-Based tBLMs*

The spacer may consist of an alkanethiol, functionalized with a hydrophilic group (e.g., a hydroxyl, carboxyl or amino group) at the apposite end of the alkyl chain with respect to the sulfhydryl group. More frequently, it consists of a thiolated or disulfidated hydrophilic chain. The spacer is tethered to a support via its sulfhydryl or disulfide group and a lipid bilayer is self-assembled on top of it, often by vesicle fusion. The interior of ω-functionalized alkanethiol monolayers is hydrophobic, as opposed to that of thiolated hydrophilic chains. However, even the latter spacers do not necessarily ensure a satisfactory hydration if they are too closed packed. In both cases, a thin water layer, about 1 nm thick, is normally interposed between the spacer monolayer and the lipid bilayer, as in the case of sBLMs; this provides a small ionic reservoir for channel-forming peptides incorporated in the lipid bilayer moiety. Since the lipid bilayer is not covalently linked to the support, it is expected to be sufficiently fluid to accommodate relatively bulky membrane proteins, unless they have large extramembrane domains on both the cytosolic and the extracellular side. The lateral mobility of lipid molecules on a hydrophilic spacer was verified by FRAP in about 10 min on very smooth gold surfaces[6], but a sufficient fluidity may probably be verified at longer times even on rougher surfaces. The capacitance of the lipid bilayer in these tBLMs is close to 1 $\mu F\ cm^{-2}$, but its resistance assumes relatively low values, of the order of 0.5 $M\Omega\ cm^2$.

A tBLM consisting of a 3-mercaptopropionic acid (MPA) tethered to gold, with a bilayer of the positively charged lipid dimethyldioctadecylammonium bromide (DODAB) on top, was used to incorporate gramicidin.[154] The lipid bilayer was stabilized by electrostatic interactions with the spacer. To this end, a pH of 8.6 was used to completely deprotonate the MPA monolayer, and the ionic strength of the solution was kept sufficiently low by using 1,1-valent electrolytes of concentration less than 50 mM. The ion-channel activity of gramicidin was verified by EIS upon simulating the lipid bilayer by a resistance and a Warburg impedance in series, and by a capacitance in parallel with the first two elements. The Warburg impedance was introduced to account for cation diffusion in the bulk aqueous phase. The same tBLM was used to incorporate the 25 kDa *Clavibacter* ion channel (CAC), which exhibits anion selectivity.[155] CAC incorporation decreases the resistance of the lipid bilayer from 3 to 5 times. The conductivity induced by CAC increases exponentially with potential, and linearly with chloride or with CAC concentration. Lipid bilayers formed on gold-supported alkanethiol monolayers ω-functionalized with an amino group were found to exhibit a film thickness more than twice that on alkanethiol monolayers ω-functionalized with a carboxyl group, by using SPR.[11] Combining surface plasmon fluorescence spectroscopy (SPFS) with SPR by fluorescently labeling the lipid films, the fluorescence intensity of the lipid bilayer on the $-NH_2$ surface was found to be almost three orders of magnitude higher than that on the –COOH surface. It was concluded that many adsorbed vesicles were present on the $-NH_2$ surface.

Another procedure for preparing spacer-bilayer assembies on electrodes consists of anchoring a polyethyleneoxy hydrophilic spacer to a hanging mercury drop electrode via a terminal sulfhydryl anchoring group by immersing the mercury drop in an ethanol solution of the spacer for about 20 min.[156] After extracting the spacer-coated mercury drop from the ethanol solution, it is slowly brought into contact with a lipid film previously spread on the surface of an aqueous electrolyte, by taking care to keep the drop neck in contact with the lipid reservoir. This disposition allows a free exchange of lipid material between the lipid reservoir on the surface of the aqueous electrolyte and the spacer-coated drop. This procedure gives rise to the formation of a lipid bilayer in contact

with the spacer-coated drop, by exploiting the spontaneous tendency of a lipid film to form a bilayer when interposed between two hydrophilic phases. The fluidity of the tBLM was tested by recording the cyclic voltammogram for the electroreduction of ubiquinone-10 incorporated in the lipid bilayer. The voltage-dependent ion channel activity of melittin incorporated in the tBLM was verified by EIS. A similar mercury-supported tBLM was fabricated by using a thiolated hexapeptide molecule with a high tendency to form a 3_{10}-helical structure as a spacer.[157] This thiopeptide had two triethylenoxy side chains to impart it a satisfactory hydrophilicity. The resulting tBLM was characterized by chronocoulometry and EIS and its suitability as a biomimetic membrane was tested by incorporating ubiquinone-10 and valinomycin.

(*ii*) *Thiolipid-based tBLMs*

A *thiolipid* molecule consists of a hydrophilic polyethyleneoxy or oligopeptide hydrophilic chain terminated at one end with a sulfhydryl or disulfide group for anchoring to the support and covalently linked at the other end to two alkyl chains simulating the hydrocarbon tails of a lipid (see Fig. 1A). A tethered thiolipid monolayer exposes a hydrophobic surface to the bulk aqueous phase and provides one half of the lipid bilayer. The other half is obtained by forming a lipid monolayer on top of the thiolipid monolayer, usually by vesicle fusion. Aqueous solutions of lipids, solubilized with a detergent in the form of micelles, have also been employed for this purpose, upon diluting the solution with an electrolyte below the critical micelle concentration of the detergent.[158]

(*a*) *Gold-supported thiolipid-based tBLMs*

Polyethyleneoxy-based thiolipid monolayers and (polyethyleneoxy-based thiolipid)/phospholipid bilayers tethered to gold have been characterized by SPR, EIS and cyclic voltammetry, and the synthesis of the thiolipids has been described.[158-160] The cross-sectional area of a hydrophilic polyethyleneoxy chain is smaller than that of the two alkyl chains, if it is in its fully extended conformation, but not if it is coiled. In the former case it is sufficiently hydrated to provide a satisfactory ionic reservoir; conversely, in the latter case it may accommodate only a limited amount of water

molecules. Whether the conformation is extended or coiled depends both on the interfacial electric field and on the nature of the metal support. TBLMs fabricated with polyethyleneoxy-base thiolipids exhibit capacitances in the range from 0.5 to 0.7 μF cm^{-2} and resistances in the range from 5 to 10 MΩ cm^2, which are comparable with the values found for conventional BLMs; however, somewhat higher capacitance values (1 μF cm^{-2}) have been reported for long spacers.[161] A particularly convenient tBLM of this type, called DPTL, was synthesized in the Max Planck Institute of Polymer Science in Mainz.[1] It consists of a hydrophilic tetraethyleneoxy chain covalently linked to a lipoic acid residue for anchoring to the metal at one end, and bound via ether linkages to two phytanyl chains at the other end (see Fig. 1A). Its cross-sectional area is of about 55 $Å^2$.

Thiolipopeptides consist of an oligopeptide chain terminated at one end with a sulfhydryl group and covalently linked at the other end to the polar head of a phospholipid. They are considered to assume a helical structure, rather than a β-sheet structure.[162] In this case, their cross-sectional area amounts to about 75 $Å^2$. They are usually obtained by tethering to a gold electrode a *thiopeptide* consisting of an oligopeptide chain terminated with a sulfhydryl group at one end and with a carboxyl group at the other end. This thiopeptide monolayer is then coupled *in situ* with dimyristoylphosphatidylethanolamine (DMPE).[163] TBLMs fabricated with thiolipopeptides have been employed for the incorporation of a number of integral proteins; they exhibit high capacitances (from 2 to 10 μF cm^{-2}) and low resistances, of the order of 10^4 Ω cm^2, which are more than three orders of magnitude lower than those of conventional BLMs.[164-166] The low resistance is ascribed to a not perfectly homogeneous coverage of the thiolipid monolayer by the distal lipid monolayer; this coverage is estimated at about 70% of full coverage and makes the tBLMs insufficiently insulating.[163] This is indicative of the presence of an appreciable number of pinholes and other defects in the bilayer, as well as of a certain disorder of the hydrocarbon chains. It was suggested that the thiolipopeptide monolayer actually consists of a mixture of the thiolipopeptide and of the corresponding uncoupled thiopeptide. This conclusion was based on the observation that gold-supported tBLMs formed from a presynthesized thiolipopeptide did not per-

mit the functional activity of incorporated proteins.[30] Such a functionality was recovered only by mixing the thiolipopeptide with a hydrophilic thiol, such as mercaptohexanol.

A structural and functional characterization of a DPTL monolayer tethered to gold was recently reported by Vockenroth et al.[167] using neutron reflectivity (NR) and EIS. The tetraethyleneoxy moiety was found to be only partly hydrated at the more positive potentials. However, at –0.600 V vs. Ag/AgCl(0.1 M KCl) a pronounced increase in the neutron scattering length density of the spacer was observed, denoting an increased amount of water transferred into this region. Leitch et al.[168] drew similar conclusions using polarization modulation infrared reflection absorption spectroscopy (PM-IRRAS). Thus, the fraction of nonhydrated C=O of the lipoic acid ester group was found to be about 50% at the more positive potentials and to attain a value of about 30% at –0.600 V, which denotes an increasing hydration of the spacer at these negative potentials. Analogous conclusions were also drawn by McGillivray et al.[35] by using NR, EIS and Fourier-transform IRRAS (FT-IRRAS) to investigate a gold-supported thiolipid monolayer similar to DPTL, with a hydrophilic spacer moiety consisting of a hexaethyleneoxy chain directly bound to a sulfhydryl group. FT-IRRAS revealed a significant disorder in the spacer region and a substantial order in the hydrocarbon tail region. Moreover, NR showed that the spacer region had a thickness smaller than its fully extended length and only 5 vol% exchangeable water, despite its significant disorder. Since the incorporation of proteins with extramembrane domains requires a significant hydration of the spacer, the thiolipid monolayer was then diluted with short β-mercaptoethanol (βME) molecules. This permitted water molecules to be accommodated in the more spacious thiolipid-βME mixture. By self-assembling a lipid monolayer on top of this mixed monolayer, McGillivray et al.[35] obtained a tBLM with a differential capacitance comparable with that of conventional BLMs. Moreover, NR data revealed the presence of an appreciable amount of exchangeable water in the spacer moiety of this tBLM.

Thiolipid-based tBLMs, when anchored to solid supports such as gold or silver, do not meet the requirement of fluidity and lateral mobility. The thiolipid molecules are rigidly bound to the metal surface atoms. In principle, the lipid molecules on top of the thiolipid monolayer may be free to move laterally. In practice, howev-

er, their lateral mobility is hindered by the presence of adsorbed or hemifused vesicles and by the roughness of the metal support (see Section IV.5). Moreover, the hydration of the polyethyleneoxy moiety of thiolipids anchored to gold is low, while the incorporation of proteins with extramembrane domains requires a significant hydration of the spacer. Only small peptides and ionophores can be accommodated in the lipid bilayer moiety of polyethyleneoxy-based tBLMs, via incorporation from their aqueous solutions.

A typical example is the depsipeptide valinomicin, an ion carrier that complexes a potassium ion with its carbonyl groups. Valinomycin cages potassium ions and shuttles them across the bilayer from the aqueous solution to the hydrophilic polyethylenoxy chain, moving back and forth. Upon incorporating valinomycin in the tBLM, the impedance spectrum was fitted to an equivalent circuit consisting of three circuit elements in series: a capacitance C_s simulating the spacer, a R_mC_m mesh simulating the lipid bilayer, and a resistance R_Ω, simulating the aqueous solution.[161,169] In a KCl solution, the conductance, $1/R_m$, of the lipid bilayer moiety was found to increase proportionally to the bulk valinomycin concentration, c_v. The lipid bilayer capacitance, C_m, remained practically constant with varying c_v using the DPTL thiolipid[169], but increased linearly with c_v using a different thiolipid.[161] The high selectivity of valinomycin toward potassium ion with respect to sodium ion was verified. The impedance spectra of a gold-supported DPTL/DPhyPC tBLM incorporating valinomycin were also interpreted with a SPICE computer program designed to simulate processes across membranes with an electrical network;[169] this amounts to solving the Nernst-Planck equation for field-assisted diffusion of permeating ions across a membrane with the appropriate boundary conditions. However, in doing so, the potential difference across the tBLM, measured with respect to an Ag/AgCl(sat. NaCl) reference electrode, was identified with its extrathermodynamic absolute potential difference (see also Ref. 170). A gold-supported DPTL/DPhyPC tBLM was also used to incorporate the M2 peptide, which forms a straight α-helix spanning lipid bilayers.[171] Bundles of M2 α-helixes form a hydrophilic pore in the membrane, by turning their polar residues toward the interior of the pore and their nonpolar residues toward its exterior. M2 is one of the four membrane-spanning segments composing each of the five subunits that constitute the nicotinic acetylcholine

receptor. As distinct from valinomycin and gramicidin, the M2 peptide does not insert spontaneously into a lipid bilayer from the bulk solution. Therefore, its incorporation was achieved by preloading the vesicles used for the formation of the distal leaflet of the tBLM with it. The M2 pore allows the passage of small monovalent cations such as Na^+ and K^+, but not larger cations such as tetramethylammonium (TMA). Upon incorporating M2, the resistance of the lipid bilayer is reduced to one fifth of its value in KCl solution, but increases again by exchanging the KCl solution with a TMACl solution.

In spite of the lack of lateral mobility and low hydration of these tBLMs, attempts have been made to incorporate the exotoxin α-hemolysin from *Staphylococcus aureus*, a water soluble, monomeric, 293-residue polypeptide that forms heptameric pores in lipid bilayers. Three different polyethyleneoxy-based tBLMs have been employed: $HS(CH_2CH_2O)_6(CH_2)_{17}CH_3$ (THEO-C_{18}),[172] DPTL and DPHDL,[173] which differs from DPTL by the presence of six ethyleneoxy units, instead of four, and of two lipoic acid residues, instead of one. With all thiolipids, incorporation of α-hemolysin causes a decrease in resistance and an increase in capacitance of the tBLM. The effect of α-hemolysin on the tBLM obtained by self-assembling an egg-PC monolayer on the THEO-C_{18} thiolipid is bimodal and poorly reproducible. In some experiments, the fitting of two RC meshes in series to the impedance spectra indicates that the parameters ascribed to the hexaethyleneoxy moiety are practically unaffected. This suggests that the protein penetrates only the distal monolayer of the tBLM. In a second group of experiments, the resistance ascribed to the hexaethyleneoxy moiety decreases by two orders of magnitude. As a whole, the changes in the hexaethyleneoxy and hydrocarbon moieties induced by α-hemolysin suggest that this toxin penetrates the tBLM partially or totally. The resistance of the DPHDL monolayer was very low (0.33 kΩ cm^2) when compared with that, 9.9 MΩ cm^2, of the DPTL monolayer. This denotes a loosely packed DPHDL monolayer. However, the formation of a DPhyPC monolayer on top of it by vesicle fusion seems to heal some of its defects. Upon incorporating α-hemolysin, the resistance of the lipid bilayer moiety of the DPHDL/DPhyPC tBLM decreases by three orders of magnitude, and that of the DPTL/DPhyPC tBLM by one order of magnitude.

In view of the well-known lysing effect of α-hemolysin on biomembranes, we cannot exclude a similar effect on these tBLMs, with membrane breakdown.

By replacing the lipoic acid residue of DPTL with a trichloropropyl-silane group, a supramolecule (DPTTC) was obtained, which was self-assembled on a SiO_2 surface via the trichlorosilane tether.[174] The SiO_2 layer was very thin (about 0.2 nm), being the native oxide layer of a highly p-doped silicon wafer. Consequently, a tBLM obtained by forming a lipid monolayer on top of the DPTTC monolayer tethered to the silicon wafer could be investigated by EIS. The impedance spectrum of the resulting tBLM was simulated by two RC meshes in series, with the omnipresent solution resistance R_Ω in series with them. The two RC meshes simulated the oxide layer and the lipid bilayer tethered to it, respectively. The functionality of this tBLM was tested by verifying the ion-channel activity and ion selectivity of valinomycin and gramicidin. Valinomycin decreases the resistance of the lipid bilayer in the presence of KCl by three orders of magnitude, while the corresponding capacitance remains practically unaltered. The highly insulating properties of this tBLM have potential for biosensing applications on semiconductor chips. A tBLM was also formed on aluminum oxide (AlO_x) sputtered on template-stripped gold.[175] An *anchor-lipid* was immobilized on the AlO_x film, about 2.7 nm thick, via Langmuir-Blodgett transfer. The anchor-lipid differs from DPTL by the replacement of the lipoic acid residue with a $-P{=}O(OEt)_2$ group for anchoring to the AlO_x surface. A DPhyPC monolayer was deposited on top of the anchor-lipid monolayer by vesicle fusion. The natural porosity of the AlO_x film, not visible at AFM, was intended to enlarge the ionic reservoir beneath this tBLM. The thin AlO_x film on gold allowed an EIS and SPR characterization of the system. The impedance spectrum of the tBLM was fitted by a parallel combination of a resistance and a constant phase element (instead of a capacitance), in series with the electrolyte resistance, R_Ω. The lipid bilayer had a resistance of about 17 $M\Omega\ cm^2$ and a capacitance of 10 $\mu F\ cm^{-2}$. The resistance is similar to that of gold-supported tBLMs, but the capacitance is one order of magnitude higher. This suggests that the tBLM adheres to some extent to the pores of the AlO_x layer. Incorporation of valinomycin in the lipid bilayer decreases its resistance by more than one order

of magnitude in the presence of K^+ ions, but not in that of Na^+ ions, confirming the ion selectivity of this ionophore.

Au-supported thiolipopeptide-based tBLMs have been reported to incorporate a few bulky proton pumps. Thus, Naumann et al. incorporated the proton pump ATPase CF_0F_1 from chloroplasts and that, ATPase EF_0F_1, from *Escherichia coli*, in a tBLM fabricated with a hydrophilic oligopeptide spacer.[164,165] SPR yields a thickness of about 5 nm for the lipid bilayer in the absence of the proton pump and of 7 to 9 nm in its presence.[163] The square-wave voltammogram of the lipid film incorporating the ATPase, as recorded at pH 7.4 in the absence of the activating compound ATP, shows a small reduction peak at -0.7 V vs. Ag/AgCl(sat. KCl), due to hydrogen evolution. Progressive additions of ATP to the aqueous solution bathing the biomimetic membrane cause a gradual increase in the reduction peak; this was ascribed to an increase in the proton concentration within the hydrophilic oligopeptide spacer adjacent to the electrode surface, due to proton pumping from the aqueous solution by the activated ATPase. A confirmation comes from the suppression of the reduction peak by tentoxin, an extremely specific inhibitor of the ATPase from chloroplasts. In a subsequent work, Naumann et al.[30] verified by FRAP that the distal lipid leaflet, obtained by fusion of egg-PC liposomes mixed with a fluorescence labeled lipid, did not show lateral mobility. They also confirmed the functional activity of the H-ATPase by monitoring by EIS a decrease in the membrane resistance upon addition of ATP. This decrease was observed at potentials much more positive than those at which hydrogen ion electroreduction on gold takes place. Since a decrease in resistance monitored by EIS involves a back-and-forth movement of protons across the membrane and the H-ATPase is not an ion channel, we may hypothesize that the protons, after being translocated by the proton pump toward the electrode, move rapidly backward by nonspecific diffusion across a leaky membrane.

Cytochrome *c* oxidase (COX) was incorporated in an analogous Au-supported, thiolipopeptide-based tBLM.[166] The integral protein COX is the terminal component of the respiratory electron-transport chain and spans the inner mitochondrial membrane. It catalyzes the redox reaction between the small peripheral protein cytochrome *c* in its reduced form, i.e., ferro-cytochrome *c*, and oxygen, with formation of ferri-cytochrome *c* and water; it also

pumps protons from the matrix to the intermembrane space, where it interacts with ferro-cytochrome *c*. In the absence of ferro-cytochrome *c*, the square-wave voltammogram of the tBLM incorporating COX shows a reduction peak due to the electroreduction of protons on the gold surface at –0.70 V, as usual; increasing additions of ferro-cytochrome *c* cause a progressive decrease of this peak; this decrease was ascribed to a decrease in the proton concentration within the thiopeptide spacer, due to proton pumping from the spacer to the aqueous solution. This direction of the proton flux was explained by the fact that ferro-cytocrome *c* can only interact with the COX protein molecules that turn their intermembrane-space side toward the aqueous phase, which is also the direction of COX proton pumping in biomembranes. The addition of cyanide, which is known to inhibit proton transport by binding to the binuclear center of COX, eliminates the effect of ferro-cytochrome *c*. As already stated, thiolipopeptide-based tBLMs have a differential capacitance much higher and a resistance much lower than those of conventional BLMs, thus denoting poor electrical properties and an appreciable field-assisted permeability to protons. The lipid monolayer on top of the thiolipopeptide monolayer shows no detectable mobility. This was demonstrated by fusing lipid vesicles labeled with a fluorescent probe, photobleaching a spot of the resulting tBLM with a laser beam and monitoring any fluorescence recovery after photobleaching (FRAP) in this spot; no recovery was observed after ten minutes.

The above conclusions as to proton pump incorporation in thiolipopeptide-based tBLMs should be examined in light of the observation that vesicles have a low propensity to fuse on the hydrophobic surface exposed to the aqueous solution by a thiolipid monolayer, especially if they incorporate an integral protein; rather, they are adsorbed or partially fused (cf. Section IV.2). Incorporation of the above proton pumps from their solutions in detergent may easily take place in the membrane of adsorbed or partially fused vesicles, since the vesicular membrane is clearly interposed between two aqueous phases. An analogous situation may be envisaged with proteoliposomes that are adsorbed or partially fused on the thiolipid monolayer from their suspending solution. In this respect, the functional activity of the above proton pumps might well be successfully verified even with vesicles or proteoliposomes adsorbed and/or partially fused on a thiolipid mono-

layer, without the need for a spacious ionic reservoir beneath a well-behaved lipid bilayer. In fact, their activation would cause an increase in the proton concentration on top of the thiolipid monolayer (in the case of F_0F_1 ATPase activated by ATP) or its decrease (in the case of COX activated by ferrocytocrome *c*). In view of the relative permeability of the leaky thiolipopeptide monolayers to protons, this would determine an increase or a decrease in the proton electroreduction current on gold, as actually observed.

A tBLM consisting of a gold-supported thiolipopeptide, with a soybean-PC monolayer on top, was used to incorporate the odorant receptor OR5 from *Rattus norvegicus* during its *in vitro* synthesis.[176] The vectorial insertion of the protein into the tBLM in a functional and oriented form was verified. The incorporation and orientation of the protein were shown by immunolabeling in combination with surface plasmon enhanced fluorescence spectroscopy (SPFS). Reversible ligand binding was demonstrated by surface-enhanced infrared reflection absorption spectroscopy (SEIRAS). Total internal fluorescence (TIRF) imaging, confocal fluorescence correlation spectroscopy (FCS) and FRAP allowed the incorporation density and the translational mobility of OR5 to be quantified.[177]

A gold-supported thiolipopeptide-based tBLM was also employed to incorporate the acetylcholine receptor (AChR), a ligand-gated channel protein present in the postsynaptic membrane of the muscle cell. The binding of acetylcholine to the receptor protein causes a conformational change in the protein that allows the influx of Na^+ ions into the muscle cell. The venoms of certain snakes contain peptide neurotoxins (e.g., α-bungarotoxin) that are competitive inhibitors of the AChR. The thickness of the lipid bilayer of the tBLM, as estimated by SPR, increases from about 4.5 to about 6.5 nm upon AchR incorporation.[178] This suggests a relatively high packing density of the AchR molecules arranged perpendicular to the bilayer. Addition of α-bungarotoxin causes a slow but appreciable increase in thickness, thus denoting the binding of this toxin to the binding sites of AChR, possibly accompanied by major conformational changes. This test confirms that at least a portion of the AchR protein is oriented with the extracellular domain pointing outside of the lipid bilayer, since α-bungarotoxin binds to this domain. The inhibitory effect of α–bungarotoxin on the ion-channel activity of AchR was not verified.

Gold-supported DPTL/DPhyPC tBLMs on microchips have recently been employed to measure single channel currents of peptides and proteins. To this end, a microelectrode array device consisting of many (100×100 μm^2) *sensor* pads was employed (see Fig. 15).[179-181] A DPTL monolayer was tethered to the gold-coated sensor pads from a DPTL solution in ethanol; then, a lipid monolayer was formed on top of it by vesicle fusion. In view of the very small surface area of the pad, the resistance of the resulting tBLM ranged from 1.5 to 17 GΩ. This resistance was high enough to reduce the background electrical noise to the low level required for the use of the patch-clamp technique. A droplet of a buffered aqueous solution was applied to a given tBLM-coated gold pad. Then, a conventional patch pipette containing an Ag/AgCl electrode and filled with the same buffer solution was inserted into the droplet. The electrical circuit of the patch-clamp amplifier was closed with a tungsten-tipped electrode that was positioned onto a gold-coated *probe* pad electrically wired to the given sensor pad.

This devise has allowed the recording of single channel currents of gramicidin A,[189] the high-conducting Ca^{2+}-activated K^+ (BK or Maxi-K) channel, the synthetic M2δ ion channel[180] and the mechanosensitive channel of large conductance (MscL) from *Escherichia coli*.[191] All these peptides and proteins were incorporated into lipid vesicles, before fusing them onto the DPTL-coated sensor pad. With the exclusion of the gramicidin channel, the unitary conductance of the remaining ion channels was found to be from one third to one tenth lower than that obtained with conventional BLMs. In this connection, one cannot exclude the possibility that, even in this case, the channels responsible for single channel currents are located in the membrane of adsorbed or partially fused vesicles. In fact, if this is the case, then the capacitive coupling between the vesicular membrane and the tBLM is expected to decrease the unitary conductance of the channels. The channel lifetimes for both open and closed states were normally found in good agreement with those obtained under similar conditions in conventional patch-clamp experiments. Plots of the current against the applied voltage are roughly linear and pass through the origin of the coordinate system, with the only exception of gramicidin. However, it is not clear whether the voltage is referred to the Ag/AgCl reference electrode or whether the curves were forced to pass through the origin.

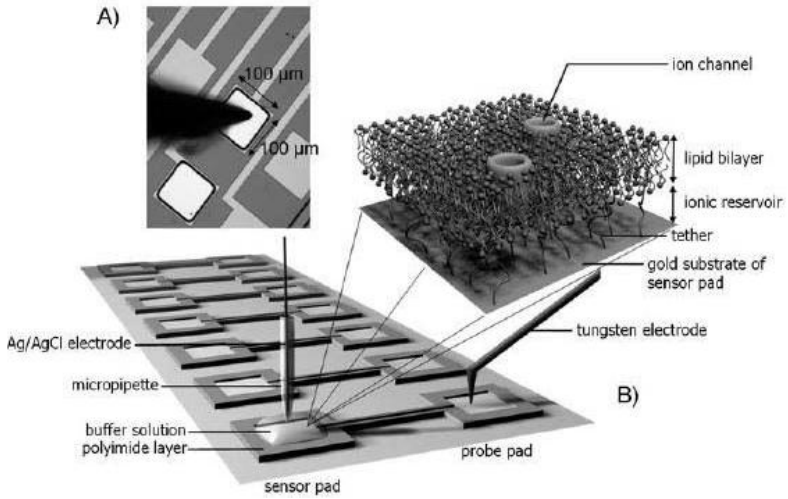

Figure 15. The tethered bilayer membrane array. A) An optical microscope image of the probe pad and the tungsten electrode tip. B) Graphical representation of the tethered bilayer membrane array. The lower left corner shows the gold sensor pad covered with a tBLMs that incorporates ion channels. An Ag/AgCl electrode situated in a patch micropipette was used as an electrode and was inserted into the buffer drop. The gold substrate of the sensor pad was connected by a thin gold line to the probe pad onto which a tungsten tip was lowered as a counter electrode. The inset shows the tBLM formed at the gold surface of the sensor pad. (Reprinted from Ref. [181] with kind permission from Elsevier.)

The capacitance and resistance of DPTL/DPhyPC tBLMs on gold microelectrodes of circular shape, with diameters ranging from 4000 to 8 μm, was examined as a function of the electrode size.[182] For the larger electrodes, the capacitance is directly proportional to the electrode area, while the resistance is inversely proportional to it. For the smaller electrodes, the capacitance decreases linearly and the resistance increases linearly with a decrease in the electrode diameter. This indicates that the capacitance and resistance of the larger electrodes are dominated by the electrode area, while the circumference seems to have the dominant role at smaller electrodes. Consequently, for small electrode sizes, a slight disorder of the bilayer structure at the edge of the electrode has a major influence on the electrical properties of the membrane. This conclusion is supported by the consideration that the micro-tBLMs used for the recording of single channel currents have resistances ranging from 1.5 to 15 GΩ. These resistances are high enough to reduce the level of the background noise down to the range of a few pA. However, the corresponding specific resistances are much less than those attained with identical tBLMs anchored to macroscopic gold electrodes of areas of the order of 1×10^{-2} cm^2. In fact, the specific resistance of the latter tBLMs amounts to about 15 MΩ cm^2. If a 100×100 μm^2 micro-tBLM had such a specific resistance, it should have a resistance of 150 GΩ. The loose packing of micro-tBLMs may explain why they may incorporate relatively bulky proteins much more easily than macro-tBLMs, without having to dilute the thiolipid with a short spacer.

(*b*) *Mercury-supported thiolipid-based tBLMs*

As distinct from Au-supported thiolipid-based tBLMs, Hg-supported thiolipid-based tBLMs do not require the use of thiolipid-spacer mixtures to incorporate channel-forming proteins. Thanks to the fluidity imparted to the thiolipid monolayer by the liquid mercury surface, these tBLMs may incorporate bulky proteins, such as OmpF porin from *Escherichia coli*[183] and the HERG potassium channel,[184] in a functionally active state. Upon incorporating gramicidin[2] or valinomicin,[3] the tetraethyleneoxy (TEO) moiety of DPTL in aqueous KCl solution undergoes a conformational change ascribable to its elongation, as the applied potential

is stepped from a fixed initial value of –0.200 V/SCE to a final value of –0.500 V/SCE.[3] As the final value of this potential step becomes progressively more negative, the charge of K^+ ions accommodated in the TEO spacer increases rapidly, attaining a maximum limiting value of about 45 μC cm^{-2} at –0.8 V/SCE.[185] This corresponds to three potassium ions per DPTL molecule, denoting an appreciable hydration of the spacer. Moreover, EIS measurements of the surface dipole potential of the TEO spacer tethered to mercury yield values that compare favorably with the dipole moment of TEO molecules measured in organic solvents;[186] this suggests a substantial order of the TEO chains in Hg-supported tBLMs. Incidentally, tBLMs supported by Au[165] or Ag[187] do not allow ionic charge measurements carried out by stepping the applied potential to final values negative of ~ –0.650 V. In fact, the resulting charge vs. time curves show a linear section with a relatively high and constant slope that is maintained for an indefinitely long time.[165,197] The constant current responsible for this linear increase in charge is ascribed to a slight water electroreduction with hydrogen formation. The high hydrogen overpotential of mercury avoids this inconvenience. When comparing interfacial phenomena on different metals, rational potentials should be used, namely potentials referred to the potential of zero charge (pzc) of the given metal in contact with a nonspecifically adsorbed 1,1-valent electrolyte. The pzc equals –0.435 V/SCE for Hg[188] and –0.040 V/SCE for polycrystalline Au.[189] Therefore, an appreciable hydration of the TEO moiety, possibly accompanied by its elongation[3], takes place in the proximity of a rational potential of about zero on Hg, but at a much more negative rational potential of about –0.600 V on Au,[167,168] close to the DPTL desorption from this metal. A drawback in the use of mercury-supported tBLMs is represented by the notable difficulty in using surface sensitive techniques for their structural characterization.

With respect to solid metal supports, mercury has the advantage of providing a defect free, fluid and readily renewable surface to the self-assembling thiolipid/lipid bilayer. Moreover, it imparts lateral mobility to the whole mixed bilayer. In addition, the self-assembly of a lipid monolayer on top of a thiolipid monolayer is readily carried out by simply immersing a thiolipid-coated mercury drop in an aqueous electrolyte on whose surface a lipid film has been previously spread.[3] Thanks to the hydrophobic inter-

actions between the alkyl chains of the thiolipid and those of the lipid, this simple procedure gives rise to a lipid bilayer anchored to the mercury surface via the hydrophilic spacer moiety of the thiolipid. By avoiding the use of vesicles, this procedure excludes any artifacts due to partially fused vesicles. These advantageous features make the incorporation of membrane proteins in mercury-supported thiolipid-based tBLMs easier and safer than in solid-supported tBLMs.

A tBLM obtained by self-assembling a DPhyPC monolayer on top of a DPTL-coated mercury electrode was investigated by impedance spectroscopy over a frequency range from 1×10^{-2} to 1×10^{5} Hz and over a potential range of 0.8 V, both in the absence and in the presence of the ion carrier valinomycin.[3] The impedance spectra obtained upon incorporating valinomycin in this tBLM from aqueous 0.1 M KCl are particularly rich of characteristic features, especially when reported in a $\omega Z'$ versus $\omega Z''$ plot (the M plot; cf. Section III). This plot shows four partially fused semicircles (see Fig. 5), which can be straightforwardly fitted by an equivalent circuit consisting of a series of four RC meshes. Each semicircle corresponds to a RC mesh; the diameter of the semicircle measures the reciprocal, $1/C$, of the capacitance of the RC mesh, while the angular frequency ω at the maximum of the semicircle measures the reciprocal of its time constant, $\tau = RC$. The angular frequency increases in the direction of increasing $\omega Z''$. The R and C values relative to the four RC meshes vary appreciably with the applied potential. To this end, a generic approximate approach was developed, which applies the concepts of impedance spectroscopy to a model of the electrified interface and to the kinetics of potassium ion transport assisted by valinomycin across the tBLM.[3] This permits the four RC meshes to be ascribed to four different slabs composing the tBLM. Proceeding in the positive direction of the abscissas, the first semicircle has the highest resistance and was ascribed to the lipoic acid residue, in direct contact with the electrode surface. The second semicircle has a capacitance of about 7 $\mu F\ cm^{-2}$, close to that of a monolayer of tetraethyleneoxythiol self-assembled on mercury, and was ascribed to the TEO moiety. The third semicircle in the absence of valinomycin has a capacitance close to 1 $\mu F\ cm^{-2}$, a value typical of a conventional solvent-free BLM, and was reasonably ascribed to the lipid bilayer moiety.

Finally, the last semicircle has the same resistance as the electrolyte solution and a very low capacitance, of the order of 1 nF cm^{-2}, and was ascribed to the electrolyte solution adjacent to the tBLM.

The same tBLM was used to incorporate the peptide melittin, whose α-helical monomers aggregate in the lipid bilayer to form an ion channel.[190] The impedance spectrum was again fitted to an equivalent circuit consisting of four RC meshes, and the capacitance C_m and resistance R_m of the mesh ascribed to the lipid bilayer moiety were examined as a function of the applied potential and of the lipid composition of the bilayer. The bilayer conductance, $1/C_m$, was found to increase abruptly above the background level at a sufficiently negative applied potential, attaining a maximum value, in agreement with the voltage-gated nature of the melittin channel. In fact, it is known that the melittin molecules lie flat on the surface of biomembranes and penetrate them only when the transmembrane potential on the opposite side of the biomembrane becomes sufficiently negative. The conductance increases with the composition of the distal monolayer of the tBLM in the order DOPC:cholesterol (60:40) < DOPC < DOPC:sphingomyelin:cholesterol (59:15:26) < DOPS. When using the ternary mixture, which may form lipid rafts, a fifth RC mesh of high capacitance and low resistance is clearly visible in the M plot; it disappears at the same applied potential at which the conductance increases abruptly. This behavior was tentatively ascribed to the formation of a melittin layer on top of the lipid rafts of the distal mixed lipid monolayer: at the applied potential at which the melittin molecules penetrate the lipid bilayer, this melittin layer is disrupted. The sigmoidal charge vs. time curves following a potential step from a value at which melittin channels are not formed to one at which they are formed was interpreted on the basis of a generic kinetic model.[191] This model accounts for the potential-independent disruption of melittin clusters adsorbed flat on the lipid bilayer, induced by the potential-dependent penetration of the resulting monomers into the lipid bilayer; the potential-independent aggregation of the monomers inside the bilayer with channel formation is then treated on the basis of a mechanism of nucleation and growth. This explains the initial induction period responsible for the sigmoidal shape of charge vs. time curves.

The channel-forming protein OmpF porin from *Escherichia coli* was incorporated in a mercury-supported DPTL/DPhyPC bi-

layer, and the resulting impedance spectrum in aqueous KCl was fitted by an equivalent circuit consisting of four RC meshes.[183] The dependence of the resulting circuit elements upon the applied potential was interpreted on the basis of an approximate approach based on a model of the electrified interface and on the kinetics of the translocation of potassium and chloride ions across the lipid bilayer. Incorporation of OmpF porin increased the conductivity of the lipid bilayer moiety of the tBLM over a narrow potential range straddling the zero value of the potential difference across the lipid bilayer moiety.

Gramicidin is a peculiar channel-forming peptide whose helical structure differs from the α-helix of common peptides and membrane proteins by the fact that it has a lumen large enough to allow the passage of simple desolvated monovalent cations. Since its length is about one half that of a biomembrane, it spans the membrane by forming a dimeric channel. The C-terminuses of the two gramicidin monomers composing a dimer contain three tryptophan residues that form hydrogen bonds with the polar heads of the lipid bilayer. Consequently, the corresponding N-terminuses are directed toward each other, in the middle of the lipid bilayer, just as the dipole moments of the two monomeric units. A transmembrane potential different from zero is, therefore, expected to favor electrostatically one monomeric orientation at the expense of the other, thus destabilizing the dimer. Nonetheless, the stationary current due to the flow of potassium ions along gramicidin channels incorporated in a conventional BLM increases with an increase in the transmembrane potential, exhibiting an almost quadratic dependence.[192] This behavior was confirmed by incorporating gramicidin in a mercury-supported DPTL/DPhyPC bilayer and by carrying out a series of potential steps from a potential positive enough to repel potassium ions from the TEO spacer to progressively more negative potentials and by recording the resulting charge vs. potential curves.[2] The slope of the initial portion of these curves measures the stationary current due to the ionic flux. Plotting this current against the transmembrane potential yields a curve in good agreement with that obtained with conventional BLMs. To explain this behavior, it was assumed that the rate constant for dimer formation increases in parallel with an increase in the ionic flux. In fact, when the time elapsed between the passage of two consecutive cations through the junction between the two

monomers forming the conducting dimer starts to become comparable with, and ultimately shorter than, the time required for the dissociation of the two monomers, such a dissociation becomes increasingly less probable. The curve calculated on the basis of this assumption was in good agreement with experiment.

The HERG K^+ channel is present in the plasma membrane and consists of four identical subunits, each spanning the membrane with six α-helixes. It may exist in one of three conformations: a closed (C), an open (O) and an inactive (I) conformation.[193] At the rest potential, the transmembrane potential (measured with respect to the potential on the extracellular side of the plasma membrane, taken conventionally equal to zero) is negative, and the HERG channel is in the C conformation. If we carry out a positive potential step that annihilates the transmembrane potential (a process called depolarization) the channel passes slowly from the C to the O conformation, but very rapidly from the O to the I conformation; consequently, the resulting outward flux of potassium ions is small and lasts for about one millisecond. If we then carry out a subsequent potential step to a value more negative than the rest potential (a process called hyperpolarization), the channel passes rapidly from the I to the O conformation and slowly from the O to the C conformation. Consequently, the inward flux of potassium ions is much higher than the outward flux, and lasts for more that 100 ms. The HERG K^+ channel was incorporated in a mercury-supported DPTL/DPhyPC bilayer from its aqueous solution in the detergent Triton X-100.[184] At a potential of –300 mV/SCE, corresponding to a transmembrane potential of +150 mV, the channel is in the I conformation. By stepping the applied potential to –720 mV/SCE, corresponding to a transmembane potential of about –270 mV, the HERG channel passes rapidly from the I to the O conformation, and then slowly to the C conformation. Figure 16 shows the charge vs. time curve following this potential step. The charge first increases rapidly due to the charging of the double layer, and then more slowly, due both to the flux of potassium ions induced by the opening of the HERG channel and to the nonspecific ionic flux across the membrane. To extract the charge ascribed exclusively to the opening of the HERG channel, the same potential step was repeated after adding WEY, a specific inhibitor of the HERG channel. By subtracting the charge transient in the presence of WAY from that in its absence, the

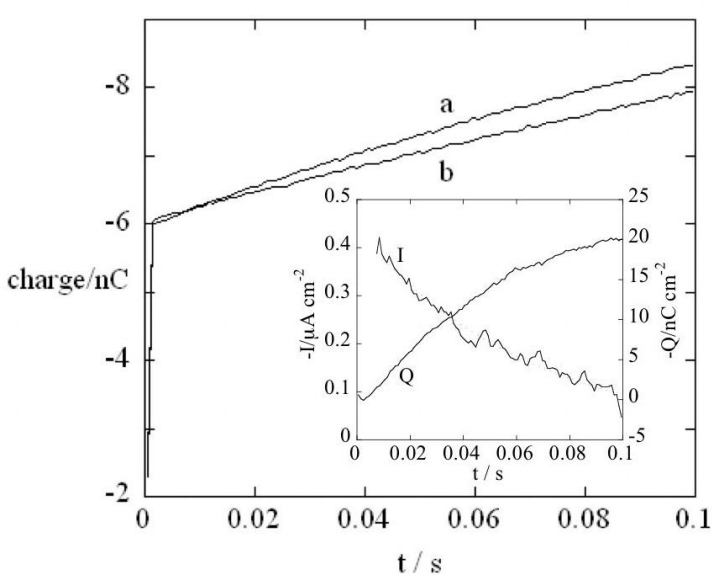

Figure 16. Charge vs. time *t* curves following a potential step from –0.300 to –0.720 V/SCE at a tBLM incorporating the HERG channel in 0.1 M KCl, both before (*a*) and after addition (*b*) of 5 μM WAY. The inset shows the curve of the charge *Q* against time t, obtained by subtracting curve (*b*) from curve (a), and the corresponding curve of the current *I* against *t*; both *Q* and *I* are ascribable to the HERG channel activation.[184]

charge vs. time curve due exclusively to the opening of the HERG channel was obtained, as shown by the inset of Fig. 16. The same procedure was followed to obtain the corresponding current versus time curve; this curve shows a monoexponential decay with time, with a time constant in good agreement with that obtained by the patch-clamp technique with conventional BLMs.

Sarcolipin (SLN) and phospholamban (PLN) are two small membrane proteins that modulate the function of Ca-ATPase of the sarcoplasmic reticulum. They were incorporated in a mercury-supported DPTL/DPhyPC bilayer to verify whether these two proteins may form ion-selective pores in biomembranes.[194-196] SLN inhibits the Ca-ATPase activity at low Ca^{2+} concentrations. However, it is also reported to increase the level of Ca^{2+} accumulation

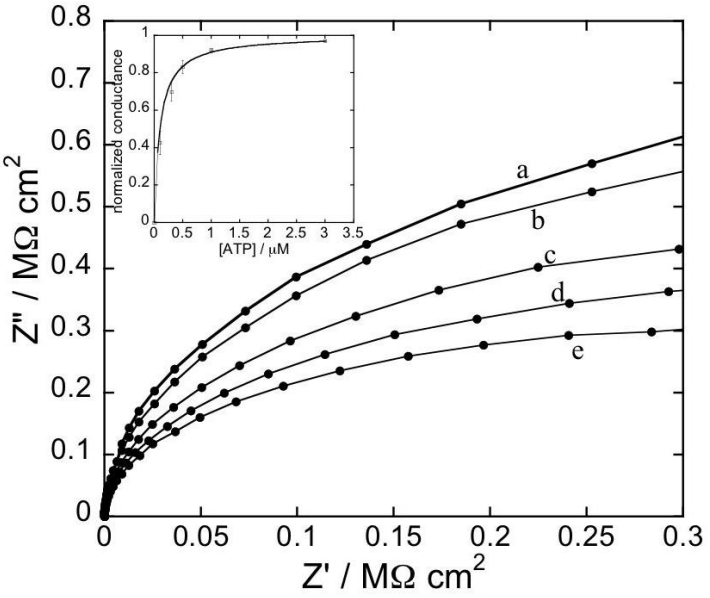

Figure 17. The solid circles are experimental points on a Z′′ vs. Z′ plot for a tBLM in a pH 5.3 aqueous solution of 0.05 M NaH_2PO_4 at -0.500 V vs. Ag/AgCl(0.1M KCl) in the absence of SLN (*a*), after incorporation of SLN from its 0.7 μM solution (*b*), and after subsequent additions of 0.1 (*c*), 0.3 (*d*) and 3 μM ATP (*e*). The solid curves are fits of a series of four RC meshes to the solid circles. The values of the resistance, R_m, of the lipid bilayer moiety resulting from the fits are: 0.90 (*a*), 0.70 (*b*), 0.53 (*c*), 0.42 (*d*) and 0.35 (*e*) MΩ cm^2. The corresponding C_m values are all close to 1 μF cm^{-2}. Inset: Conductance, $1/R_m$, normalized to its maximum value equated to unity, as a function of the ATP concentration. The error bars denote standard deviations. The solid curve is a fit of the Michaelis-Menten equation to the experimental points.[195]

in the lumen of the SR at high calcium ion concentrations. It consists of a single α-helix that spans the whole membrane. It was shown that SLN forms channels highly selective toward small inorganic anions, such as chloride ion.[194] The resistance of the tBLM immersed in a 0.05 M aqueous solution of the sodium salt of the tetravalent anion adenosyntriphosphate (ATP), which does not permeate biomembranes, does not change upon incorporating SLN. This indicates that SLN does not allow the translocation of

simple monovalent cations such as sodium ion. On the other hand, if the sodium salt of ATP is diluted with an equal volume of a NaCl solution containing the same concentration of Na^+ ions, the resistance decreases by about one order of magnitude, indicating that SLN allows the translocation of the small chloride anion across the lipid bilayer. Incorporation of SLN in a tBLM immersed in a pH 5.3 aqueous solution of 0.05 M NaH_2PO_4 causes only a slight decrease in the resistance of the lipid bilayer, as measured by the diameter of a *Z*" vs. *Z*' plot (Nyquist plot; cf. Section III); however, submicromolar additions of ATP decrease the resistance of the tBLM to an appreciable extent, as shown in Fig. 17.[195] Plotting the conductance against the ATP concentration yields a curve that tends asymptotically to a limiting value and can be satisfactorily fitted by the Michaelis-Menten equation, with an association constant for the SLN-ATP complex of about 0.1 μM (see the inset of Fig. 17).

This behavior was explained by regarding a SLN channel as consisting of a bundle of four or five SLN α-helixes that turn their hydrophilic side, containing two hydrophilic threonine residues, toward the interior of the bundle; this provides a hydrophilic pathway for small desolvated inorganic anions, such as chloride ion. Phosphate ion is somewhat bulkier than chloride ion. However, SLN contains a positively charged arginine residue (Arg6) just outside the lipid bilayer, on its cytoplasmic side. ATP was assumed to bind electrostatically to this arginine residue. The repulsion among the highly negatively charged ATP molecules bound to Arg6 should widen the lumen of the SLN channel, thus allowing the passage of phosphate ions. On the basis of this and other features of SLN, it was proposed that SLN is just the *P_i transporter* described by Lee and coworkers[197] on 1991 and whose nature was not known up to now. The role of SLN is that of translocating phosphate ions from the cytoplasm to the lumen of the sarcoplasmic reticulum, thus causing the precipitation of calcium phosphate and increasing the level of Ca^{2+} accumulation in the lumen.

Phospholamban (PLN) exists in equilibrium between the pentameric and monomeric forms. The pentamer releases to Ca-APTase a monomer, which forms a 1:1 complex inhibiting the affinity of Ca-ATPase for Ca^{2+}.[198] Phosphorylation of the monomer by ATP removes the inhibition. Both SLN and the PLN monomer have a single α-helix that spans the membrane. As distinct

from SLN, PLN has a large cytoplasmic domain. The two α-helixes are quite similar, having several identical residues. The main difference between the SLN and the PLN helix is represented by the presence of two hydrophilic threonines in the SLN helix, which occupy positions analogous to those of two hydrophobic cysteines, C41 and C46, in the PLN helix; the two cysteines play a fundamental role in the stabilization of the PLN pentamer, by forming hydrogen bonds. Incorporation of PLN in a mercury-supported DPTL/DPhyPC bilayer does not affect its resistance over the physiological range of transmembrane potentials.[196] It was concluded that the absence of the two threonine residues prevents the PLN pentamer from forming a hydrophilic pore. An analogous lack of ion channel activity was exhibited by the T18A mutant of SLN, where the Thr18 hydrophilic residue is replaced by a hydrophobic alanine residue.[195] This confirms the role played by the threonine residues in the ion channel activity of SLN.

A mercury-supported tBLM was formed at the tip of a microelectrode for measuring single-channel activity.[199] To this end, use was made of a platinum wire embedded in a thin glass capillary and terminated with a platinum microdisk, about 20 μm in diameter. Mercury was electrodeposited on this microdisk from a pH 1 mercurous nitrate aqueous solution, giving rise to a mercury spherical cap that was coated with a DPTL/DPhyPC bilayer. The resistance of this *tethered bilayer lipid micromembrane* ranged from 5 to 30 GΩ and was, therefore, high enough to decrease the electrical noise to the very low level required for the recording of single-channel currents by the patch-clamp technique. Its differential capacitance amounted to 1.0 μF cm^{-2}, denoting the formation of a well-behaved solvent-free lipid bilayer. The channel protein OmpF porin from the outer membrane of *Escherichia coli* was incorporated in this micromembrane from its aqueous solution in the detergent Triton X-100. Figure 18 shows the single channel currents due to the opening of the OmpF porin channel as a function of time at different applied potentials. A burst of single channel currents is observed at –400 mV/SCE, and to a minor extent at –500 mV, which corresponds to a zero transmembrane potential. This behavior is consistent with the well known property of OmpF porin, according to which this channel protein undergoes inactivation on both sides of the zero transmembrane potential.

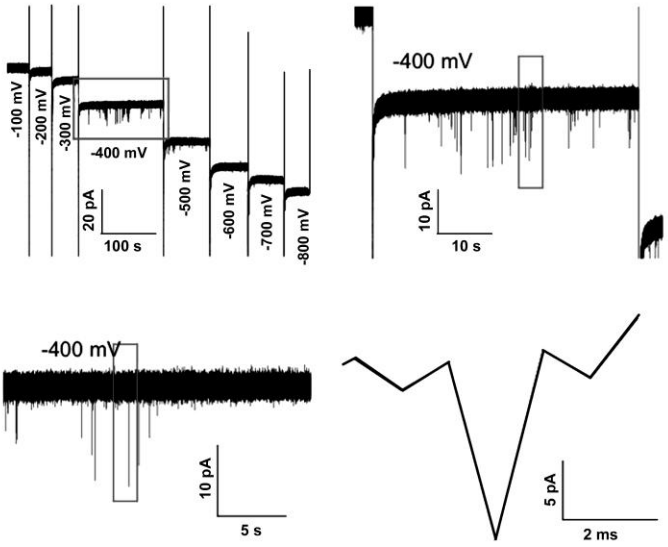

Figure 18. Single-channel traces of OmpF porin from *Escherichia coli* incorporated in a mercury-supported tethered bilayer lipid micromembrane immersed in aqueous 0.1 M KCl, at different applied potentials measured vs. a Ag/AgCl(3M KCl) reference electrode. Potentials must be decreased by 50 mV to refer them to the SCE.[199]

This micromembrane was also used to investigate the spontaneous formation of microdomains, when the distal monolayer is made up of a lipid mixture. Microdomains are in the gel state when they consist primarily of a lipid with a transition temperature from the gel to the liquid crystalline state (also called melting temperature, T_m) higher than room temperature, such as sphingomyelin. When these microdomains also contain cholesterol to an appreciable extent, they become fluid, albeit more ordered and tightly packed than the surrounding lipid matrix, consisting primarily of lipids with T_m lower than room temperature, such as DOPC. The latter microdomains, called *lipid rafts*, are qualified as *liquid-ordered*, to distinguish them from the *liquid-disordere* lipid matrix. Lipid rafts are microdomains, composed of glycolipids, sphingolipids and cholesterol, which are present in the outer leaflet

of plasma membranes. Rafts are receiving increasing attention since they are considered to regulate the membrane function in eukaryotic cells. The presence of microdomains was directly visualized from the image of the distal lipid monolayer, by using two-photon fluorescence lifetime imaging microscopy (2P-FLIM).[39] The distal monolayer consisted of a sphingomyelin:DOPC:cholesterol (47:47:6) mixture, with the addition of 1 mol% laurdan. Laurdan is a fluorophore that is known to distribute uniformly in coexisting gel, liquid-ordered and liquid-disordered phases. It emits in the blue region of the optical spectrum and has a longer lifetime in the gel phase, while it emits in the green region and has a shorter lifetime in the liquid-disordered phase. The fluorescence lifetime image of the distal lipid mixture shows a high degree of heterogeneity and is characterized by the coexistence of gel, liquid-ordered and liquid-disordered phases. Microdomains with an irregular percolative-like shape and lifetimes of 3450±50 ps are ascribed to the gel phase. Small roundish microdomains immersed in the surrounding matrix have lifetimes of 2830±50 ps and are attributed to the liquid-ordered phase. Finally, the matrix, with intermediate fluorescence lifetimes, is ascribed to the coexistence of the liquid–disordered phase and of liquid-ordered microdomains of size below the resolution of the microscope (about 0.4 μm radial).

(*iii*) (*Thiolipid-spacer*)-*Based tBLMs*

A mixture of a short hydrophilic spacer anchored to gold via a sulfhydryl or disulfide group (e.g., mercaptoethanol or dithiodiglycolic acid) and of a thiolipid with its terminal hydrophobic group (e.g., a cholesteryl[13,14] or a phytanyl group[34]) capable of pinning a lipid bilayer gives rise to a practically aqueous region sandwiched between the short spacer and the lipid bilayer (see Fig. 19); this may favor the accommodation of the extramembrane domains of relatively bulky membrane proteins. Deposition of a lipid bilayer onto such a mixture of a short spacer and of a thiolipid is usually carried out by vesicle fusion or by rapid solution exchange. The resulting lipid bilayer has a capacitance of about 0.5–0.6 μF cm^{-2} and a resistance higher than 5 MΩ cm^2. These values com-

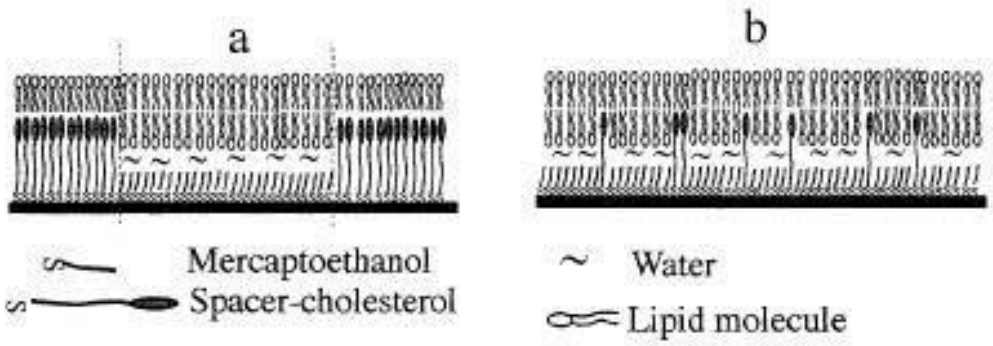

Figure 19. (a) Schematic picture of a micropatterned film consisting of distinct areas covered by a mercaptoethanol monolayer with a lipid bilayer on top, and by a monolayer of a hydrophilic spacer covalently bound to a cholesteryl group with a lipid monolayer on top. (b) Schematic picture of a mixed monolayer of mercaptoethanol and spacer-cholesterol molecules with a lipid bilayer on top.

pare favorably with those of conventional BLMs. Ion-channel activity of gramicidin and melittin incorporated in such a tBLM and ion-selectivity of gramicidin were verified by EIS.[34] However, here too, the lateral mobility of the lipid bilayer is hindered by the hydrophobic group of the thiolipid molecules, which provides a fraction of the proximal leaflet of the lipid bilayer.

The ability of the volume enclosed between the gold electrode and the lipid bilayer moiety of (thiolipid-spacer)-based tBLMs to accommodate water molecules and inorganic ions was estimated from the level of conductance induced by the incorporation of a given amount of the ionophore valinomycin. This ionic reservoir was simulated by a capacitance C_s and the lipid bilayer by an R_mC_m mesh. By using a number of thiolipids and spacers of variable length, Cornell and coworkers[34] found that the conductance, $1/R_m$, of the lipid bilayer increases with an increase in the length of the thiolipid and with a decrease in that of the spacer. In a subsequent paper, the same authors used a long thiolipid terminated with a benzyl disulfide anchor in order to increase the separation among the thiolipid molecules, and mixed it with different proportions of the short mercaptoacetic acid disulfide. The capacitance, C_s, of the ionic reservoir of the resulting tBLMs was regarded as consisting of the capacitance, C_H, of tightly bound inorganic ions in series with the capacitance, C_d, of diffuse layer ions, in analogy with the Helmholtz layer and diffuse layer capacitances at a bare gold electrode.[200] The separation between the C_H and C_d capacitances was estimated from the dependence of the overall capacitance C_s of the ionic reservoir on the bulk ionic concentration and on the applied potential. As a matter of fact, the situation within the ionic reservoir is somewhat different from that at a bare electrode because the inorganic ions are prevented from coming in direct contact with the electrode surface, due to the presence of the short spacer and of the benzyl ring.

Relatively bulky membrane proteins with extramembrane domains can be accommodated in the bilayer if the areas covered by the short thiolated spacer are sufficiently large. Differences in chain length[201] and chemistry[202] between thiolipids and spacers may hopefully favor the formation of phase-demixed domains on the nanoscale, facilitating protein incorporation. This seems to be the case with mixed monolayers of cholesteryl-based thiolipids and short thioalcohol spacers on gold.[203] Reductive desorption

peaks of these mixtures yield well-formed single peaks at mole fractions close to 100% of any of the two pure components, whereas two partially overlapping peaks are observed at intermediate mole fractions. This indicates that phase separation takes place over an intermediate mole fraction range. No tBLMs were observed by EIS when trying to fuse vesicles on tethered mixed monolayers with thiolipid mole fractions below this intermediate mole fraction range. These results were confirmed by friction AFM images in air, recorded with a hydrophilic cantilever tip. Hydrophobic heightened domains due to repulsion between the tip and the hydrophobic thiolipid were observed at intermediate mole fractions.

A relatively high resistance of 0.1 MΩ cm^2 was attained by fabricating a micropatterned monolayer of a thiolated triethyleneoxy chain covalently bound to a cholesteryl group, whose hydrophobic surface was covered by a lipid monolayer formed by vesicle splitting and spreading;[5] this micropatterned film had 15 μm × 15 μm square holes filled with a mercaptoethanol monolayer, whose hydrophilic surface was covered by a lipid bilayer formed by vesicle unrolling and spreading. The square holes filled with the short mercaptoethanol molecules and the lipid bilayer on top are believed to be preferential sites for the incorporation of integral proteins. In fact, the rigidity of the cholesteryl groups and their anchorage to the electrode via the thiolated triethyleneoxy chain make the mixed cholesteryl/lipid bilayer less suitable for protein incorporation than the liquid-crystalline lipid bilayer on top of the mercaptoethanol monolayer. Biofunctionality of this tBLM was confirmed by incorporation of the ionophore valinomycin and the channel-forming peptide gramicidin, which exhibited the expected ion selectivity. Instead of using a microcontact printing on gold, an alternative approach consisted in transferring a mixture of a thiolipid and of palmitic acid to a gold substrate by the Langmuir-Blodgett technique. The regularly distributed domains of palmitic acid on gold were then washed away in a suitable solvent, while the covalently bound thiolipid was not removed; the resulting domains of bare gold were then filled with a mercaptoethanol monolayer.[89] Besides microcontact printing and Langmuir-Blodgett transfer of phase-separated thiolipid monolayers, deep-UV photolithography was employed for patterning thiol layers on gold surfaces.[204]

Vesicle unrolling was facilitated by using a gold-supported monolayer consisting of a mixture of short-chain polyethyleneoxythiol hydrophilic spacers and of thiolipid molecules consisting of the same spacer covalently bound to a cholesteryl group.[13] These cholesterol derivatives serve as *anchoring units* that penetrate into the outer monolayer of unilamellar vesicles and increase both the fluidity of gel-phase bilayers and the rigidity of liquid-crystalline-phase bilayers. Vesicle fusion on monolayers of mixtures of these colesteryl-based thiolipids and spacers takes place only for fractional surface coverages of the thiolipid exceeding a minimum value. *In situ* investigation of these tBLMs by ATR-FTIR spectroscopy indicates that the distal leaflet of these tBLMs is comprised of pure lipid and the proximal one is comprised of a mixture of cholesteryl and lipid.[205] A particular tBLM was fabricated by anchoring to a smooth template-stripped gold surface a mixture of DPTL and of a spacer (TEGL) in which the two phytanyl chains of the DPTL molecules were replaced by a terminal hydroxyl group (see Fig. 1);[27] a lipid bilayer was then formed on top of this mixture by vesicle fusion. Contact mode and friction mode AFM images of the mixed DPTL-TEGL monolayer seem to exclude phase segregation. Ion-channel activity of gramicidin and melittin incorporated in this tBLM and ion selectivity of gramicidin were verified by EIS.

A gold-supported mixture of a triethyleneoxythiol covalently linked to a cholesteryl group, with a lipid monolayer on top, and of 6-mercaptohexanol, with a lipid bilayer on top, was used to incorporate cytochrome *bo3* (*cbo3*).[4] This is the primary membrane-bound terminal oxidase of *Escherichia coli*, which catalyzes the oxidation of ubiquinol-8 and the reduction of oxygen to water in a process coupled to proton translocation across the cell membrane. Upon incorporating *bo3* and ubiquinone-8 into this tBLM in the presence of oxygen, a reduction cyclic voltammogram was recorded at potentials negative enough to cause ubiquinone-8 electroreduction to ubiquinol-8 on gold. In this way, ubiquinol-8 transfers electrons continuously from the gold electrode to *cbo3*, where it is reoxidized by oxygen to ubiquinone-8, which moves back to the electrode surface. The height of the sigmoidal-shaped catalytic cyclic voltammograms increased with an increase in oxygen concentration, whereas it was completely suppressed upon addition of 1 mM cyanide ion.

A micropatterned layer, consisting of regions of thiolipid molecules with a lipid monolayer on top alternated with regions of mercaptoundecanoic acid with a lipid bilayer on top, was used to incorporate rhodopsin.[204,206] This integral protein contributes to the closing of the Na^+ channels of the plasma membrane of the outer segment of the vertebrate rod cell. When rhodopsin is photoactivated, it starts an enzyme cascade that amplifies the absorption of light by a factor of one million. The first step of this cascade is the interaction of the photoactivated rhodopsin with transducin, a peripheral protein that binds to guanosine-5'-diphosphate (GDP) in its inactive state, and to guanosine-5'-triphosphate (GTP) in its active state, as schematically depicted in Fig. 20. Transducin is

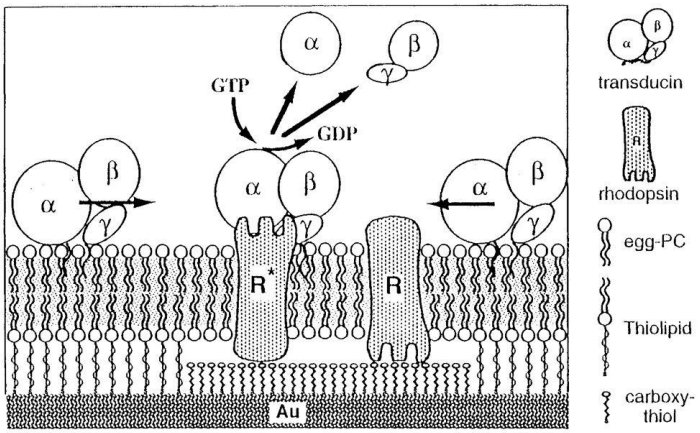

Figure 20. Schematic picture of rhodopsin–transducin coupling on patterned gold-supported bilayers, as described in the text. Rhodopsin is preferentially incorporated in the freely suspended bilayer domains, while transducin is adsorbed indifferently on anchored and freely suspended bilayer regions of the tBLM. When rhodopsin is photoactivated, transducin is depleted only in the freely suspended bilayer regions, and therefore diffuses from anchored to freely suspended bilayer domains. This lateral displacement of transducin and its release from defined domains are observed by one-dimensional imaging SPR. (Reprinted from Ref. [204] with kind permission from the American Chemical Society.)

composed of three subunits, designated α, β and γ. The GDP/GTP binding site is associated with the α subunit. Photoactivated rhodopsin (R*) interacts with the α subunit of transducin by catalyzing the replacement of bound GDP with GTP, which results in the dissociation of the α subunit from the β and γ subunits. Scanning the micropatterned film by SPR shows that rhodopsin is preferentially incorporated into the lipid bilayer on top of the mercaptoundecanoic acid, which is more fluid and has a more water-rich reservoir than the lipid bilayer consisting of the anchored thiolipid with a lipid monolayer on top. On the other hand, the peripheral protein transducin cannot distinguish between the two different lipid-coated regions and is equally adsorbed on both. The progressive increase in film thickness due to transducin binding to the micropatterned film is monitored by SPR, just as the rapid decrease in film thickness due to transducin desorption following rhodopsin photoactivation in the presence of GTP. After interrupting illumination, a slow increase in film thickness is observed, due to transducin rebinding.

The OmpF porin, a pore forming protein present in the outer membrane of *Escherichia coli*, was incorporated in a tBLM consisting of a mixture of a diethyleneoxy-based thiolipid and of a sulphanylpropionic acid spacer.[206,207] This ligand-gated channel acts as a receptor for the antibacterial toxin colicin N, which blocks the channel by binding to its mouth. The conductance of the lipid bilayer incorporating OmpF porin, as measured by EIS, amounts to 1.54 mS cm^{-2}. Progressive additions of colicin N cause a gradual decrease in conductance up to a minimum limiting value of 1.35 mS cm^{-2}. Setting the conductance value in the absence of colicin equal to unity and its limiting value in the presence of colicin equal to zero, the sigmoidal plot of the resulting *normalized* conductance against the logarithm of colicin concentration is practically identical to that obtained at a conventional BLM. However, the limiting value of the conductance at a conventional BLM is more than three orders of magnitude less than the initial value, while at the gold-supported tBLM it is only 15% less. This is due to the poor electrical properties of the lipid bilayer, which allows an appreciable nonspecific ionic flux.

6. Polymer-Cushioned Bilayer Lipid Membranes (pBLMs)

The spaciousness of the ionic reservoir of tBLMs may not be sufficient to accommodate bulky extramembrane domains of membrane proteins. The problem is particularly serious with cell-adhesion receptors, whose functional extracellular domains can extend to several tens of nanometers. Thus, the spreading of proteoliposomes doped with human platelet integrin $\alpha_{IIb}\beta_3$ and ATP synthase on quartz or glass substrates results in inhomogeneous patches of pinned proteins.[208,209] This problem can be circumvented by separating the lipid bilayer from the solid substrate using soft polymeric materials of typically less than 100 nm thickness, which rest on the substrate and support the bilayer. These stratified films are often referred to as polymer-cushioned or polymer-supported bilayer lipid membranes (for a review, see Ref. 210). This approach reduces the non-specific binding of proteins to the solid support and the frictional coupling between proteins and the support, preventing the risk of protein denaturation due to direct contact between protein subunits and the bare support surface. In some cases, the cushion may assist self-healing of local defects in lipid bilayers deposited on macroscopically large supports.

To form a thermodynamically stable polymer-lipid composite film on a solid support in aqueous solution and to avoid the formation of polymer blisters, several requirements should be fulfilled. Specifically, the spreading pressures should be positive for the lipid bilayer on the polymer and for the polymer on the solid support.[211] From a thermodynamic viewpoint, a stratified structure is only stable if each additional layer results in a gain in the total surface free energy. Moreover, the interaction between the lipid bilayer and the substrate surface must be repulsive. In fact, if the net force acting per unit area (disjoining pressure) is negative, continuous thinning of the interlayer results in the film collapse, i.e., dewetting, giving rise to regions of tight local contact between the lipid bilayer and the substrate surface (the so-called pinning centers). Polymer-cushioned membranes are fairly unstable if the attractive interfacial forces between the polymer and the lipid bilayer are relatively weak. In this case, the bilayer can easily detach from the polymer cushion. On the other hand, too strong attractive forces may decrease the lateral mobility of the bilayer. A compromise should, therefore, be found between a sufficient stability of the

polymer/lipid interface and lateral mobility. A possible strategy consists of enhancing the stability of polymer-cushioned membranes via attractive electrostatic interactions.[212] A different approach to stabilization of polymer-cushioned membranes was adopted by Naumann et al. [213] by tethering the polymer both to the substrate and to the membrane. To this end, a benzophenone silane photocoupling agent was tethered to a glass surface via the silane group. A lipopolymer-phospholipid mixture preorganized at the air/water interface was transferred to the benzophenone silane funtionalized glass surface by the Langmuir-Blodgett technique. The benzophenone moiety was then covalently linked to the C-H groups of the polymer chains by UV irradiation. Finally, a DMPC monolayer was transferred by the Langmuir-Schaefer technique from the air/water interface to the cushion, thus adding the distal leaflet of the bilayer to the polymer-cushioned membrane. Long-range lateral mobility within the bilayer was verified by FRAP at 40°C, when DMPC is in the liquid-crystalline state. However, a notable decrease in the lateral mobility of the distal lipid monolayer was observed by increasing the lipopolymer tethering density beyond a certain limit. A similar approach was used by Wagner and Tamm[225], who prepared lipid bilayers supported by a linear polyethyleneoxy chain derivatized at one end with a triethoxysilane group, for anchoring to a quartz support, and at the other end with DMPE for anchoring to the lipid bilayer. By reconstituting annexin V and cytochrome b_5 in the lipid bilayer, the lateral diffusion of these proteins was measured.

The advantage of using polymer supports can be appreciated when studying biological functions of incorporated cell receptors. Membranes supported by 5-nm thick cellulose films have been used to incorporate cell receptors of the integrin family. When probing the interaction between these pBLMs and giant vesicles exposing integrin-specific ligands, the adhesion free energy for the interaction was comparable with the value inferred from the integrin-ligand dissociation constant.[208] This strongly suggests that integrins fully retain their mobility and native functionality when incorporated in these pBLMs.

Polymer cushions have also been conveniently employed as supports of cellular membranes. Human erythrocyte *ghosts* (i.e., red blood cells after removal of their cytoplasm) were adsorbed over cellulose cushions.[215,216] After incubation of the ghosts for 60

min, the orientation of the erythrocyte membrane was identified with two immune-fluorescence labels. This labeling proved that polymer-supported human erythrocyte membranes are almost free from local defects and expose the cytoplasmic domain to the bulk aqueous phase. The success of this deposition suggests that cellulose cushions fulfill the conditions of complete wetting of cellular membranes and finely tune the cell-surface interactions. However, FRAP experiments showed no sign of lateral diffusion, probably due to the presence of spectrine cytoskeletons.

Usually, polymer cushions are anchored to supports such as glass, silica and mica, by using polymers derivatized with alkyl silanes[20] or triethoxysilane for covalent linkage to silanols at the surface of the silicate substrates.[225] More rarely, they are anchored to gold or to semiconductors such as GaAs via thiolated polymers. Covalent coupling of polymers to silane or thiol anchors can be achieved through epoxy groups, photoactive groups and so-called active esters.[217] A variety of polymeric materials have been employed. These include polyacrylamide,[218] polyethyleneimine, dextran,[219] trimethylsilylcellulose,[220] chitosan[221] and hyaluronic acid[222].

Wong et al.[223,224] characterized lipid bilayers supported by a polyethyleneimine cushion on a quartz substrate by neutron reflectometry and found that thickness, surface roughness and coverage of the polymer depend strongly on the method of preparation. Kühner et al.[218] prepared 30–40 μm thick polyacrylamide gels on glass and coated them with monolayers and bilayers, using Langmuir-Blodgett techniques. When examined by epifluorescence microscopy, these bilayers exhibited residual domain structure. Lateral mobility of a lipid-linked 20-residue peptide antigen was verified in these bilayers. In an extension of this work, the electrophoretic mobility of charged lipids was determined in monolayers that were supported by agarose gels;[225] bilayers did not form on these substrates. In another study, bilayers were formed on a polyvinyl substrate that had functionalized diethylene amino groups for reaction with lipid head groups.[226] Although homogeneous bilayers with high lateral mobility were obtained under some conditions, the hydrophilic linkers were too short to accommodate membrane proteins in this system. Elender et al.[219] were able to form uniformly fluorescent bilayers of DMPC and 20 mol% cholesterol on 600-800 nm cushions of dextran supported by Si/SiO_2 and glass. The

lateral diffusion coefficient and mobile fraction of the lipids were high in this system, which, however, was very unstable in the absence of cholesterol. All above polymer-supported lipid bilayers were deposited on non-conducting supports and, consequently, they are not amenable to electrochemical measurements. These bilayers were often patchy and with several defects.

Polymer-cushioned lipid bilayers on conducting supports have been investigated only rarely. Spinke et al.[227,228] described a polymer-supported lipid bilayer anchored to gold. These authors used a methacrylic terpolymer consisting of a hydrophilic main chain that acts as a spacer, a disulfide unit that anchors the polymer to the gold surface, and a hydrophobic lipid-like part that forms a first lipid monolayer upon self-assembly. A second lipid monolayer was formed on top of the first by fusion with DMPC vesicles. The fusion was followed by SPR, which revealed a maximum increase in film thickness by about 2 nm after 4 h.

Polymer-cushioned lipid bilayers have frequently been investigated on the indium-tin-oxide (ITO) semiconductor. In case of a lipid bilayer deposited on a regenerated (and thus hydrophilic) cellulose cushion, the swollen polymer film behaves like an aqueous electrolyte. Selective ion transport via ion channels and carrier proteins incorporated in the membrane was, therefore, quantitatively evaluated by determining the electric resistance of the membrane.[229] On ITO electrodes, the presence of polymer cushions significantly reduces local defect densities and results in an electric resistance from 5 to 50 times higher than that of a lipid bilayer directly deposited on ITO. [8,138,139]

A hydrophobic cellulose derivative provides not only an environment to a lipid monolayer, but also acts as an electric insulator with an electric resistance as high as 20 MΩ cm^2. When a lipid monolayer is deposited on a semiconductor surface pre-coated with such a polymer insulator, the whole system consists of a conductor-insulator-semiconductor set-up. As the film thickness can be controlled with nm accuracy, the potential drop across the polymer insulator can be controlled precisely. The system can be tuned so as to detect the charging and discharging of the polar heads of the lipid monolayer by monitoring changes in the semiconductor space charge capacitance. When optimized, this simple device should reach a sensitivity of about 1 e/30 nm^2.[230]

7. S-Layer Stabilized Bilayer Lipid Membranes (ssBLMs)

Monomolecular crystalline arrays of protein subunits, called S-layers, are common surface structures of archea and bacteria.[233-237] They constitute the outermost component of the cell envelope of these procaryotic organisms. S-layer subunits can be aligned in lattices with oblique, square or hexagonal symmetry. Since S-layers are monomolecular assemblies of identical protein subunits, they exhibit pores of identical size and morphology. Most S-layers have a rather smooth outer surface and a more corrugated inner surface. In gram-negative archea, S-layers are the only component external to the cytoplasmic membrane; pillar-like extensions of the subunits of the S-layers may even penetrate into the polar head region of the membrane. Conversely, in gram-positive bacteria, the rigid wall component in direct contact with the cytoplasmic membrane is primarily composed of peptidoglycan, a polymer consisting of sugars and amino acids that forms a mesh-like layer. A group of non classical cell wall polymers, called *secondary cell wall polymers* (SCWPs), are covalently bound to muramic acid residues of peptidoglycan and attached non-covalently, presumably by a lectin-type interaction, to the S-layer proteins. SCWPs are composed of disaccharide repeating units and contain pyruvate ketals that provide a negative charge. In gram-negative bacteria, a thin peptidoglycan layer is interposed between an inner membrane and an outer membrane, with an S-layer non-covalently bound to the latter.

Since S-layer subunits of most bacteria interact with each other through non-covalent forces, they can be set free with high concentrations of agents that break hydrogen bonds, such as guanidine hydrochloride or urea. Once the S-layer lattice of a bacterial cell is completely disintegrated and the disintegrating agent is removed by dialysis, the S-layer subunits have the unique capability to reassemble spontaneously in suspension, at the liquid/air interface, on solid surfaces, on spread lipid monolayers and on liposomes. Recrystallization starts at several distant nucleation points on the surface and proceeds until neighboring crystalline areas meet. It this way, a closed mosaic of differently oriented monocrystalline domains is formed. Recrystallization of isolated S-layer proteins on differently charged solid supports reveals an electroneutral outer and a net negative or net positive inner S-layer surface.

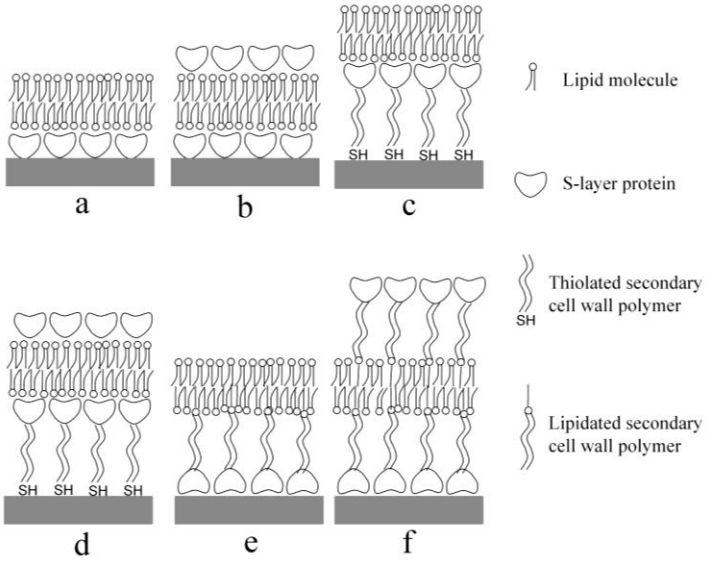

Figure 21. Schematic picture of S-layer stabilized solid supported lipid membranes. (a) S-layer directly recrystallized on gold, with a lipid bilayer on top. (b) Same as (a), with an additional S-layer recrystallized on top of the lipid bilayer. (c) Thiolated secondary cell wall polymers (SCWPs) directly bound to gold and interacting with a S-layer, with a lipid bilayer on top. (d) Same as (c), with an additional S-layer recrystallized on top of the lipid bilayer. (e) S-layer directly recrystallized on gold and interacting with lipidated SCWPs, which anchor a lipid bilayer. (f) Same as (e), with lipidated SCWPs inserted into the distal lipid monolayer and interacting with an additional S-layer.

The natural tendency of S-layers to interact with membranes has been exploited to insert them as an intermediate layer between a lipid bilayer and a substrate, giving rise to the so-called *S-layer stabilized bilayer lipid membranes* (ssBLMs). Thus, in the case of bacterial S-layer proteins, it has been demonstrated that protein domains or functional groups of the S-layer lattice interact via electrostatic forces with some head groups of lipid molecules. In addition, the affinity of S-layer proteins for the corresponding SCWPs, which are recognized as specific binding sites, can be used to fabricate complex architectures (see Fig. 21). Thus, a mon-

olayer of SCWPs, suitably thiolated at one end, can be anchored to a gold support, and a S-layer can be spontaneously recrystallized on top of it; finally, a lipid bilayer can be self-assembled on top of the S-layer. Optionally, the lipid bilayer so formed can be further stabilized by recrystallizing an additional S-layer on top of it. Alternatively, a loose monolayer of lipidated SCWP molecules can be bound to a S-layer previously recrystallized on a substrate; a lipid bilayer self-assembled on top of the SCWP monolayer is then firmly anchored by the lipid moieties of the SCWPs, which penetrate the proximal lipid leaflet. Optionally, the lipidated SCWP molecules present on the outer lipid leaflet can be bound to a further S-layer. All these architectures have a stabilizing effect on the associated lipid bilayer, leading to an improvement in its lifetime and robustness. The assembly of S-layer structures from solution to a solid substrate, such as an Au-coated glass slide, can be followed by SPR or by a QCM-D.[233] The self-assembling process is completed after approximately 45 min. The mass increase followed by QCM-D corresponds to a thickness of about 8-9 nm, in agreement with the value estimated by SPR.

A well-characterized S-layer protein, SbqA from *Bacillus sphaericus* CCM 2177, was used as an ultrathin crystalline, water containing hydrophilic layer between a gold electrode and a lipid bilayer.[234] The SbqA protein recrystallizes in monomolecular square lattices with the neutral outer surface exposed to the aqueous phase and the negatively charged inner surface attached to the gold electrode. A morphological unit, about 170 nm in diameter, consists of four protein monomers. The pores are of identical size and morphology, with a diameter of about 3.5 nm. A SqbA-coated gold substrate was pressed against a polyethylene plastic sheet attached vertically to the open side of a chamber, as shown in Fig. 22a. An orifice, about 1×10^{-3} cm^2 in area, was made through the plastic sheet by punching it with a perforating tool. Alternatively, a piece of SUM was interposed between the gold surface and the plastic sheet (Fig. 22b). SUM (S-layer ultrafiltration membrane) is an isoporous structure with very sharp molecular exclusion limits, manufactured by depositing under pressure up to three stacked S-layer-carrying cell wall fragments on a commercial polyamide microfiltration membrane (MFMs), with an average pore size of approximately 0.4 μm. The 1–4 μm sized S-layer fragments are deposited on the microfiltration membrane as shingles on a roof.

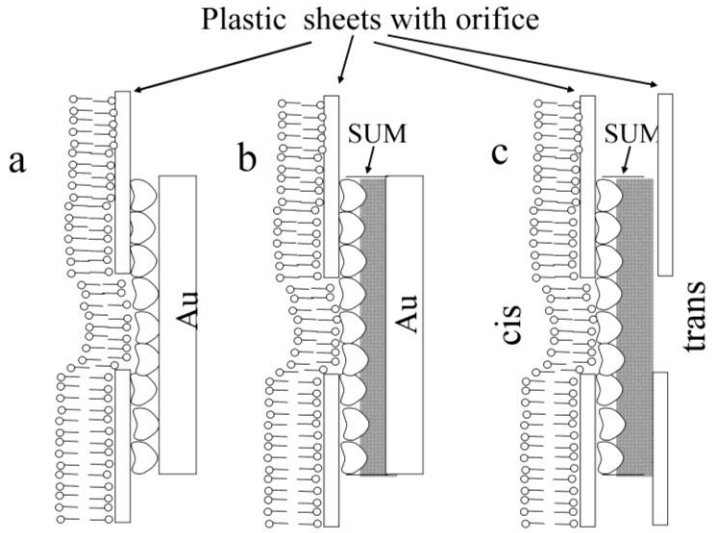

Figure 22. (a) Gold-supported SbpA layer pressed against a perforated plastic sheet, with a lipid bilayer transferred onto the SbpA layer by the Langmuir-Blodgett technique. (b) Same as (a), apart from the replacement of the SbpA layer by SUM. (c) Lipid bilayer supported by SUM and interposed between two bulk aqueous phases.

The side of the SUM with attached the S-layer lattices was turned toward the chamber. A DPhyPC lipid bilayer on top of the SqbA- or SUM-coated gold was formed by a modified Langmir-Blodgett technique. To this end, the chamber was filled with an aqueous electrolyte above the orifice level, a DPhyPC solution is *n*-hexane was spread on the electrolyte surface and the organic solvent was allowed to evaporate. By lowering the electrolyte level below the orifice, a first lipid monolayer was deposited on the coated gold, and a second monolayer was deposited by raising again the electrolyte level.

A tetraetherlipid (TEL) was also used in place of DPhyPC. This is a bipolar, membrane-spanning phospholipid consisting of a 72 member microcycle formed by two glycerol units that are bridged by two biphytanoyl chains. While in phospholipids the alkyl chains are connected to the glycerol moieties by ester bonds, in tetraetherlipids they are connected by four ether bonds, provid-

ing an enhanced robustness under acidic conditions and at high temperatures (up to 100°C). To self-assemble a TEL monolayer (which corresponds to a phospholipid bilayer) on the surface of the coated gold, it is just sufficient to raise the level of the electrolyte, on whose surface a TEL has been previously spread, above the orifice level. The electrochemical properties and the stabilities of the DPhyPC bilayers and of the TEL monolayers were verified by EIS, upon fitting the data by a simple RC mesh. In fact, for practical purposes, the resistance R_Ω of the electrolyte could be neglected. The specific capacitances were 0.53 and 0.69 μF cm^{-2} for DPhyPC bilayers and 0.75 and 0.77 μF cm^{-2} for TEL monolayers resting on SbpA and SUM, respectively. Membrane resistances of up to 80 MΩ cm^2 were observed for DPhyPC bilayers on SbpA. In addition, lipid bilayers supported by SbpA exhibited a long-term robustness of up to two days. Upon incorporating the voltage-gated ion channel alamethicin at open circuit, the membrane resistance dropped from about 80 MΩ cm^2 to about 950 Ω cm^2, whereas the capacitance did not change. Subsequent addition of the inhibitor amiloride caused a modest increase in resistance. The ion-channel activity of the ion carrier valinomycin and its selectivity toward K^+ ions with respect to Na^+ ions were also verified.

In a different approach, the gold support was replaced by an aqueous electrolyte.[235] In this case, the polyethylene plastic sheet was folded in half and interposed between two compartments. An orifice was punched in the two adjacent plastic sheets and a piece of SUM was placed over the aperture, between the two sheets, with the S-layer covered side turned toward the cis compartment (Fig. 22c). Both compartments were filled to just above the aperture with an aqueous electrolyte; a DPhyPC-(dipalmitoylphosphatidic acid) lipid bilayer was then formed on the cis side of the SUM by the same modified Langmuir-Blodgett procedure previously described. For comparison, an unsupported, conventional BLM was also formed across the aperture using the same lipid mixture and the same Langmuir-Blodgett technique. Conventional BLMs and SUM-supported lipid bilayers showed a specific capacitance of 0.6–0.7 μF cm^{-2}. The S-layer produced a stabilizing effect on the lipid bilayer. Thus, the dielectric breakdown voltage of the conventional BLM was 220 mV, whereas the SUM-supported lipid bilayer did not rupture upon application of three

voltage ramps of up to 500 mV, and had lifetimes of up to 8 h. In such a comparison, the potential difference across the SUM was regarded as negligible in view of its very low resistance of about 5 mΩ. Incorporation of α-hemolysin in the SUM-supported lipid bilayer allowed the recording of single channel currents, which were of comparable height with those on conventional BLMs. TEL monolayers were also deposited by the modified Langmuir-Blodgett technique on a SUM interposed between two aqueous phases, in place of phospholipid bilayers.[236] Recrystallization of a S-layer on top of SUM-supported TEL monolayers increased the lifetime of the membrane from about 7 to about 21 h, while leaving the specific conductance unaltered. Gramicidin was incorporated in SUM-supported membranes composed of DPhyPC, TEL and mixtures of DPhyPC and TEL, and single-channel currents were recorded. The selectivity toward K^+ ions was found to be higher than that toward Na^+ ions, in accordance with the behavior at conventional BLMs. However, the conductivity at SUM-supported membranes was significantly lower than that at conventional BLMs. Attempts to span a pure TEL monolayer across the aperture in a plastic sheet without a SUM support by the modified Langmuir-Blodgett technique were unsuccessful.

8. Protein-Tethered Bilayer Lipid Membranes (ptBLMs)

In all the biomimetic membranes previously described and allowing the incorporation of proteins, the protein orientation in the membrane is purely casual. At most, if one of the two extramembrane domains of the protein is much bulkier than the other, incorporation in a tBLM occurs preferentially with the bulkier domain turned toward the aqueous phase, in view of the limited spaciousness of the hydrophilic moiety of the tBLM. Moreover, the packing density of the reconstituted proteins in the lipid bilayer is not well controlled. The need for a well-defined protein orientation with respect to the electrode surface is particularly felt with redox membrane proteins, in which the electrons involved in a chain of redox centers are conveyed across the membrane in a well-defined direction.

To overcome this problem, Knoll, Naumann and coworkers have developed a novel methodology based on tethering proteins, rather than lipids, to the electrode surface; the lipids are then al-

lowed to self-assemble around the tethered proteins.[237] To this end, a recombinant membrane protein is engineered to bear a stretch of six consecutive histidine residues. A gold surface is then functionalized by attaching a molecule terminated with a nitrilotriacetic (NTA) moiety at one end and with a sulfhydryl group for anchoring to gold at the other end. Complexation of Ni^{2+} ions to both the NTA functionality and the histidines of the stretch causes the protein to be anchored to the gold surface from its solution in detergent, as shown in Fig. 23. To retain full functional integrity, the membrane protein is incorporated into a lipid bilayer. For this purpose, the protein layer tethered to gold is mixed with detergent-destabilized lipid vesicles of DMPC. By removing the detergent

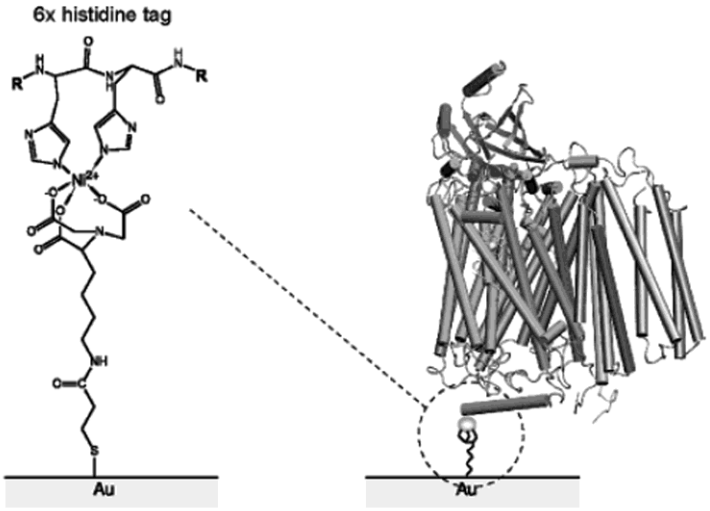

Figure 23. Adsorption of cytochrome *c* oxidase on the Ni-NTA modified Au surface via the His-tag at the C-terminus of subunit I. Two nitrogen atoms of the imidazole rings from two of the histidines of the His stretch coordinate the Ni^{2+} ion. The coordinating histidines residues are not necessarily adjacent in the primary sequence, as drawn in the figure. (Reprinted from Ref. [237] with kind permission from the American Chemical Society.)

with microporous biobeads, the tethered proteins are surrounded by lipid molecules that form a lipid bilayer around them, as verified by SPR and EIS; a water layer remains interposed between the lipid bilayer and the NTA moiety, acting as an ionic reservoir.

This approach has been adopted to investigate the function of cytochrome *c* oxidase (COX) from the proteobacterium *Rhodobacter sphaeroides*.[237] COX is the last enzyme in the respiratory electron transport chain of bacteria, located in the bacterial inner membrane. It receives one electron from each of four ferrocytochrome *c* molecules, located on the periplasmic side of the membrane, and transfers them to one oxygen molecule, converting it into two water molecules. In the process, it binds four protons from the cytoplasm to make water, and in addition translocates four protons from the cytoplasm to the periplasm, to establish a proton electrochemical potential difference across the membrane.

In this protein-tethered bilayer lipid membrane (ptBLM), the orientation of the protein with respect to the membrane normal depends on the location of the histidine stretch (his tag) within the protein. Two opposite orientations of the protein were investigated, either with the cytochrome *c* binding side pointing away from the electrode surface or directed toward the electrode, simply by engineering the his tag on the C terminus of subunit SU I or SU II, respectively. The individual steps of functionalization of the gold support, adsorption of the engineered protein and its reconstitution in the lipid bilayer were followed in situ by means of surface-enhanced infrared absorption spectroscopy (SEIRAS).[237] The functional activity of COX was verified by cyclic voltammetry with both protein orientations. In this connection, it should be noted that electron transfer in COX occurs sequentially through the four redox centers Cu_A, heme a, heme a_3 and Cu_B, in the direction from the binding site of cytochrome *c*, located on the outer side of the bacterial membrane, to its inner side. With the cytochrome *c* binding side pointing away from the electrode surface, the primary electron acceptor, Cu_A, is far from the electrode surface. Hence, in the absence of cytochrome *c*, the cyclic voltammogarm exhibits only a capacitive current. This indicates that COX is not electrically coupled to the electrode, and direct electron transfer does not take place. Under these conditions, the electrochemical impedance spectra were fitted to an equivalent circuit consisting of a capacitance C_s, with in series an R_mC_m mesh and the solution resistance

R_Ω; the capacitance C_s simulates the ionic reservoir and the R_mC_m mesh simulates the lipid bilayer.[238] The capacitance C_m and resistance R_m of the bilayer amount to about 6 μF cm^{-2} and 800 kΩ cm^2. This high capacitance and low resistance denote a loosely packed lipid bilayer, partly ascribable to the presence of a high protein content. As ferri-cytochrome *c* is added in the presence of oxygen, at potentials negative of 270 mV/NHE it starts to be electroreduced to ferro-cytochrome *c*. This triggers an electrocatalytic process whereby, in the enzymatic cavity of COX, ferro-cytochrome *c* is oxidized by oxygen to ferri-cytochrome *c*, which can be continuously electroreduced to ferro-cytochrome *c*. This gives rise to a reduction current in the negative potential region.

When the COX is oriented with the cytochrome *c* binding side pointing toward the electrode surface, the primary electron acceptor, Cu_A, is also oriented toward the electrode. In this case, the cyclic voltammogram in the absence of oxygen shows a single reduction peak at about –274 mV/NHE, due to the electroreduction of the enzyme, and a corresponding oxidation peak at about –209 mV/NHE.[239,240] The peak currents increase linearly with the scan rate, denoting a surface confined process. Moreover, scan rates < 1 V s^{-1} leave the peak potentials unaltered, indicating that the electron transfer is reversible (i.e., in quasi-equilibrium) at these scan rates. The fact that the reduction and oxidation peak potentials do not coincide was ascribed to some purely chemical protonation step within the protein. The midpoint potential is shifted by about -450 mV with respect to the standard potential of +230 mV/NHE, determined for the Cu_A redox center in isolated COX. This was explained by assuming that the first transient electron acceptor in the reduction process is not the Cu_A center, but rather the Ni(II) ion of the Ni(II)/Ni(I) redox couple of the Ni-NTA complex. At scan rates < 1 V s^{-1}, oxidation and reduction peaks are slightly asymmetric. A further increase in scan rate enhances this asymmetry, leading to the appearance of a second peak at scan rates > 20 V s^{-1}, as shown in Fig. 24. The resulting complex voltammogram of the four-redox-site COX protein was deconvoluted into four Gaussian components. Kinetic parameters of the four one-electron transfer steps, one for each redox center, were extracted from the plots of the four deconvoluted peak potentials against the logarithm of the scan rate (the so-called *trumpet* plot).

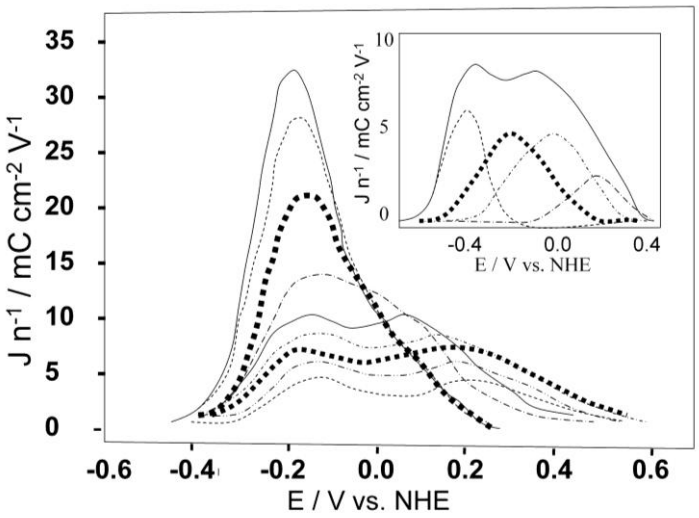

Figure 24. Oxidative branches (baseline-corrected) of the cyclic voltammograms of COX with the his tag attached to subunit II in the absence of oxygen, at scan rates between 1 and 600 V s^{-1} (current densities normalized by the scan rate, ≅ 1 V s^{-1}). Proceeding downwards, the scan rate increases in the order: 1, 3, 7.5, 20, 40, 300, 400, 500, and 600 V s^{-1}. Inset: Example of a deconvolution into four Gaussian components. (Reprinted from Ref. [239] with kind permission from Elsevier.)

Strong evidence that the electron transfer observed by cyclic voltammetry takes place directly within the enzyme was derived from Soret band excited surface-enhanced resonance Raman spectroscopy (SERRS) taken as a function of potential.[240,241] The cyclic voltammogram of COX oriented with the cytochrome *c* binding side directed toward the electrode was used to determine the functional activity of the enzyme as a function of its surface density.[242] This density was varied by diluting the thiol functionalized with the chelator nitrilotriacetic (NTA) moiety with a non-functionalized thiol that did not bind to the enzyme. At low COX surface densities, the bilayer does not effectively form, and protein aggregates are observed; on the other hand, at very high surface densities, very little lipid is able to intrude between the closely packed protein molecules. In both cases, redox activity is low. Redox activity is preserved in the biomimetic membrane only at

moderate surface coverages, in which a continuous lipid bilayer is present and the protein molecules are not forced to aggregate.

In the presence of oxygen, electrons transferred from the electrode to the redox centers of COX are irreversibly transferred to oxygen, leading to a notable increase of the reduction peak, which now lies at –202 mV/NHE, and to a continuous electron transfer. The cyclic voltammogram also shows a further reduction peak at –422 mV/NHE. This is due to the catalytic turnover of COX, which reduces oxygen to water and pumps protons into the interstitial space between the electrode and the lipid bilayer. Proton electroreduction at the electrode surface determines the second reduction peak. The absence of direct electron transfer and of proton electroreduction when COX is oriented with the cytochrome *c* binding site turned toward the solution confirms the orientation dependence both of direct electron transfer and of transmembrane proton transport.

VI. CONCLUSIONS

The use of electrochemical techniques such as cyclic voltammetry, EIS and charge transient recordings for the investigation of biological systems is becoming increasingly popular, just as the application of the concepts of electrochemical kinetics and of the structure of electrified interfaces to the interpretation of the electrochemical response.

Several efforts are presently made to realize biomembrane models consisting of a lipid bilayer anchored to a solid electrode through a hydrophilic spacer and satisfying those requirements of ruggedness, fluidity and high electrical resistance that are necessary for the incorporation of integral proteins in a functionally active state. A unique feature of these biomembrane models is the achievement of the maximum possible vicinity of a functionally active integral protein to an electrode surface (the electrical transducer). The capacitive currents resulting from the activation of ion pumps, transporters, channel proteins and channel-forming peptides incorporated in these biomembrane models can be analyzed over a broad potential range by electrochemical techniques, which are by far less expensive than other techniques presently adopted.

The realization of these biomembrane models allows fundamental studies of the function of integral proteins. Biomimetic membranes are ideally suited to elucidate many problems in molecular membrane biology, by permitting a reliable and rapid functional screening of a large number of mutant receptor proteins. This will open the way to the elucidation of structure-function relationships in ligand-receptor and protein-protein interactions. Moreover, the development of biomimetic systems that incorporate therapeutically or diagnostically important natural proteins will open the door to the realization of sensors targeting biological analytes. Making biomembrane models sufficiently insulating and free from pinholes and other defects that might provide preferential pathways for electron and ionic transfer across the lipid bilayer is a particularly challenging goal in the characterization of ion channel activity. It can be tackled by making the solid support as smooth as possible, by using micropatterned solid-supported lipid bilayers formed via microcontact printing on gold, or by synthesizing hydrophilic and amphiphilic spacers with an architecture that may favor highly compact monolayers.

Many practical applications are foreseen for these sensors, such as the detection of drug candidates modulating the function of ion channels and pumps or targeting membrane receptors. In this respect, there is strong need to develop novel, rapid and highly sensitive methods for drug screening, capable of selecting and analyzing a huge number of compounds. At present, screening of pharmacologically active compounds follows traditional procedures that apply time-consuming ligand-binding studies and receptor-function tests separately. Thus, for instance, the function of ion channels and transporters is traditionally characterized in detail by patch clamp studies, which investigate the proteins in their natural environment, the cellular membrane. These assays are tedious to perform and difficult to automate at high throughput, making the investigation of many samples difficult. The lack of knowledge about the different functions of these channels is due to a lack of specific inhibitors, which are unavailable due to the lack of efficient measuring systems. Present ligand-binding experiments identify only ligands to already known binding sites on the protein(s) of interest and neglect other potentially more interesting sites. Moreover, they cannot easily differentiate between agonists and antagonists. Thus, the direct, predominantly electrochemical de-

termination of the function of ion channels and pumps in biomembrane models reconstituted from purified components addresses a strongly felt need for the development of new drug candidates or diagnostic test systems.

ACKNOWLEDGMENTS

Thanks are due to Ente Cassa di Risparmio di Firenze for financial support to the authors' research on metal-supported biomimetic membranes. The technical support by Dr. Giovanni Aloisi in the preparation of the manuscript is gratefully acknowledged.

ACRONYMS

AFM	Atomic force microscopy
ATR-FTIR	Attenuated total internal-reflection Fourier-transform infrared spectroscopy
BLM	Bilayer lipid membrane
COX	Cytochrome *c* oxidase
DMPC	Dimyristoylphosphatidylcholine
DMPE	Dimyristoylphosphatidylethanolamine
DOPA	Dioleoylphosphatidic acid
DOPC	Dioleoylphosphatidylcholine
DOPE	Dioleoylphosphatidylethanolamine
DOPS	Dioleoylphosphatidylserine
DPhyPC	Diphytanoylphosphatidylcholine
DPPC	Dipalmitoylphosphatidylcholine
DPPE	Dipalmitoylphosphatidylethanolamine
DPTL	2,3-Di-*O*-phytanyl-sn-glycerol-1-tetraoxyethylene glycol-D,L-α-lipoic ester
Egg-PC	Egg-phosphatidylcholine
EIS	Electrochemical impedance spectroscopy
FRAP	Fluorescence recovery after photobleaching
GUV	Giant unilamellar vesicle
ITO	Indium tin oxide
NR	Neutron reflectivity
PBLM	Polymer-cushioned bilayer lipid membrane

POPC	Palmitoyloleoylphosphatidylcholine
PtBLM	Protein-tethered bilayer lipid membrane
QCM	Quartz crystal microbalance
QCM-D	Quartz crystal microbalance with dissipation monitoring
SBLM	Solid-supported bilayer lipid membrane
SEIRAS	Surface-enhanced infrared absorption spectroscopy
SERRS	Surface-enhanced resonance Raman spectroscopy
SPR	Surface plasmon resonance
SsBLM	S-layer stabilized bilayer lipid membrane
SUV	Small unilamellar vesicle
TBLM	Tethered bilayer lipid membrane
TEGL	Tetraoxyethylene glycol-D,L-α-lipoic acid ester
TEO	Tetraethyleneoxy

REFERENCES

[1]S. M. Schiller, R. Naumann, K. Lovejoy, H. Kunz, and W. Knoll, *Angew. Chem. Int. Ed. Engl.* **42** (2003) 208.

[2]L. Becucci, A. Santucci, and R. Guidelli *J. Phys. Chem. B* **111** (2007) 9814.

[3]L. Becucci, M. R. Moncelli, R. Naumann, and R. Guidelli, *J. Am. Chem. Soc*. **127** (2005) 13316.

[4]L. J. C. Jeuken, S. D. Connell, P. J. F. Henderson, R. B. Gennis, S. D. Evans, and R. J. Bushby, *J. Am. Chem. Soc.* **128** (2006) 1711.

[5]A. Toby, A. Jenkins, R. J. Bushby, N. Boden, S. D. Evans, P. F. Knowles, Q. Liu, R. E. Miles, and S. D. Ogier, *Langmuir* **14** (1998) 4675.

[6]M. Baumgart, M. Kreiter, H. Lauer, R. Naumann, G. Jung, A. Jonczyk, A. Offenhäusser, and W. Knoll, *J. Colloid Interf. Sci.* **258** (2003) 298.

[7]J. R. Macdonald and W. B. Johnson in *Impedance Spectroscopy. Emphasizing solid materials and systems*, Ed. by J. R. Macdonald, J. Wiley & Sons, New York, 1987, p.1.

[8]G. Wiegand, N. Arribas-Layton, H. Hillebrandt, E. Sackmann, and P. Wagner, *J. Phys. Chem. B* **106** (2002) 4245.

[9] (a) W. Knoll, *Annu. Rev. Phys. Chem.* **49** (1998) 569; (b) W. Knoll, I. Köper, R. Naumann, and E.-K. Sinner, *Electrochim. Acta* **53** (2008) 6680.

[10]B. Wiltschi, W. Knoll, and E.-K. Sinner, *Methods* **39** (2006) 134.

[11]K. Tawa, and K. Morigaki, *Biophys J*. **89** (2005) 2750.

[12]A. L. Plant, *Langmuir* **15** (1999) 5128.

[13]L. M. Williams, S. D. Evans, T. M. Flynn, A. Marsh, P. F. Knowles, R. J. Bushby, and N. Boden, *Langmuir* **13** (1997) 751.

[14]L. M. Williams, S. D. Evans, T. M. Flynn, A. Marsh, P. F. Knowles, R. J. Bushby, and N. Boden, *Supramol. Sci.* **4** (1997) 513.

[15]G. Puu and I. Gustafson, *Biochim. Biophys. Acta* **1327** (1997) 149.

[16]R. P. Richter and A. Brisson, *Biophys. J.* **88** (2005) 3422.

[17]R. Lipowsky and U. Seifert, *Mol. Crystals* **202** (1991) 17.
[18]E. Kalb, S. Frey, and L. K. Tamm, *Biochim. Biophys. Acta* **1103** (1992) 307.
[19]E. Reimhult, F. Hook, and B. Kasemo, *Langmuir* **19** (2003) 1681.
[20]E. Sackmann, *Science* **271** (1996) 43.
[21]C. A. Keller, K. Glasmästar, V. P. Zhdanov, and B. Kasemo, *Phys. Rev. Lett*. **84** (2000) 5443.
[22]C. A. Keller and B. Kasemo, *Biophys. J.* **75** (1998) 1397.
[23]R. P. Richter A. Mukhopadhyay, and A. Brisson, *Biophys. J.* **85** (2003) 3035.
[24]R. P. Richter, R. Bérat, and A. R. Brisson, *Langmuir* **22** (2006) 3497.
[25]S. Lingler, I. Rubinstein, W. Knoll, and A. Offenhäusser, *Langmuir* **13** (1997) 7085.
[26]P. Delahay and J. E. Strassner, *J. Am. Chem. Soc.* **73** (1951) 5219.
[27]L. He, J. W. F. Robertson, J. Li, I. Kärcher, S. M. Schiller, W. Knoll, and R. Naumann, *Langmuir* **21** (2005) 11666.
[28]A. Zebrowska and P. Krysinski, *Langmuir* **20** (2004) 11127.
[29] J. Jass, T. Tjärnhage, and G. Puu, *Biophys. J.* **79** (2000) 3153.
[30]R. Naumann, T. Baumgart, R. Gräber, A. Jonczyk, A. Offenhäusser, and W. Knoll, *Biosens. Bioelectr.* **17** (2002) 25.
[31]L. K. Tamm and H. M. McConnell, *Biophys. J.* **47** (1985) 105.
[32]H. M. McConnell, T. H. Watts, R.M. Weis, and A. A. Brian, *Biochim. Biophys. Acta* **864** (1986) 95.
[33]I. Zawisza, X. Bin, and J. Lipkowski, *Langmuir* **23** (2007) 5180.
[34]B. Raguse, V. Braach-Maksvytis, B. A. Cornell, L. G. King, P. D. J. Osman, R. J. Pace, and L. Wieczorek, *Langmuir* **14** (1998) 648.
[35]D. J. McGillivray, G. Valincius, D. J. Vanderah, W. Febo-Ayala, J. T. Woodward, F. Heinrich, J. J. Kasianowicz, and M. Lösche, *Biointerphases* **2** (2007) 21.
[36]D. Axelrod, D. E. Koppel, J. Schlessinger, E. Elson, and W.W. Webb, *Biophys. J.* **16** (1976) 1055.
[37]A. N. Parikh, *Biointerphases* **3** (2008) FA22.
[38]T. W. Cha, A. Guo, and X.-Y. Zhu, *Biophys. J.* **90** (2006) 1270.
[39]L. Becucci, S. Martinuzzi, E. Monetti, R. Mercatelli, F. Quercioli, S. Battistel, and R. Guidelli, *Soft Matter*, accepted.
[40]I. R. Miller, in *Topics in Bioelectrochemistry and Bioenergetics*, Ed. By G. Milazzo, Wiley, Chichester, 1981, p. 194.
[41]A. Nelson and A. Benton, *J. Electroanal. Chem.* **202** (1986) 253.
[42]S. Trasatti, in *Modern Aspects of Electrochemistry*, Ed. by B. E. Conway and J.O'M. Bockris, Vol. 13, Plenum, New York, 1979, p. 81.
43, A. Nelson and N. Auffret, *J. Electroanal. Chem.* **248** (1988) 167.
[44]F. Tadini Buoninsegni, L. Becucci, M. R. Moncelli, and R. Guidelli, *J. Electroanal. Chem.* **500** (2001) 395.
[45]D. Bizzotto and A. Nelson, *Langmuir* **14** (1998) 6269.
[46]D. Bizzotto, Y. Yang, J. L. Shepherd, R. Stoodley, J. Agak, V. Stauffer, M. Lathuillière, A. S. Akhtar, and E. Chung, *J. Electroanal. Chem*. **574** (2004) 167.
[47] J. Shepherd, Y. Yang, and D. Bizzotto, *J. Electroanal. Chem*. **524-525** (2002) 54.
[48]A. Nelson, *Anal. Chim. Acta* **194** (1987) 139.
[49]A. Nelson, N. Auffret, and J. Borlakoglu, *Biochim. Biophys. Acta* **1021** (1990) 205.
[50]A. Nelson, N. Auffret, and J. Readman, *Anal. Chim. Acta* **207** (1988) 47.
[51]M. R. Moncelli, L. Becucci, and R. Guidelli, *Biophys. J.* **66** (1994) 1969.
[52]M. R. Moncelli and L. Becucci, *J. Electroanal. Chem.* **385** (1995) 183.

[53]L. Becucci, M. R. Moncelli, R. Herrero, and R. Guidelli, *Langmuir* **16** (2000) 7694.
[54]M. R. Moncelli, L. Becucci, F. Tadini Buoninsegni, and R. Guidelli, *Biophys. J.* **74** (1998) 2388.
[55]R. Herrero, M. R. Moncelli, R. Guidelli, M. Carla', A. Arcangeli, and M. Olivotto, *Biochim. Biophys. Acta* **1466** (2000) 278.
[56]M. R. Moncelli and L. Becucci, *J. Electroanal. Chem.* **433** (1997) 91.
[57]L. Becucci, M. R. Moncelli, and R. Guidelli, *J. Electroanal. Chem.* **413** (1996) 187.
[58]M. R. Moncelli and L. Becucci, *Bioelectrochem. Bioenerg.* **39** (1996) 227.
[59]I. R. Miller, *J. Membrane Biol.* **101** (1988) 113.
[60]I. R. Miller, D. Bach, and M. Teuber, *J. Membrane Biol*. **39** (1978) 49.
[61]M-F. Lecompte, A.-C. Bras, N. Dousset, I. Portas, R. Salvayre, and M. Ayrault-Jarrier, *Biochemistry* **37** (1998) 16165.
[62]M. R. Moncelli, R. Herrero, L. Becucci, and R. Guidelli, *J. Phys. Chem.* **99** (1995) 9940.
[63]L. Becucci, M. R. Moncelli, and R. Guidelli, *J. Am. Chem. Soc*. **125** (2003) 3785.
[64]M. R. Moncelli, L. Becucci, A. Nelson, and R. Guidelli, Biophys. J. **70** (1996) 2716.
[65]R. Herrero, M. R. Moncelli, L. Becucci, and R. Guidelli, *J. Phys. Chem. B* **101** (1997) 2815.
[66]R. Herrero, F.Tadini Buoninsegni, L. Becucci, and M.R. Moncelli, *J. Electroanal. Chem.* **445** (1998) 71.
[67]A. Nelson, *J. Electroanal. Chem.* **303** (1991) 221.
[68]A. Nelson, *J. Chem. Soc. Faraday Trans.* **89** (1993) 2799.
[69]A. Nelson, *Langmuir* **12** (1996) 2058.
[70]A. Nelson, *Langmuir* **13** (1997) 5644 .
[71]M. Rueda, I. Navarro, G. Ramirez, F. Prieto, C. Prado, and A. Nelson, *Langmuir* **15** (1999) 3672.
[72]L. Becucci, M. R. Moncelli, and R. Guidelli, *Biophys. J*. **82** (2002) 852.
[73]F. Prieto, I. Navarro, and M. Rueda, *J. Electroanal. Chem.* **550-551** (2003) 253.
[74]J. C. Franklin and D. S. Cafiso, *Biophys. J.* **65** (1993) 289.
[75]E. Gross, R. S. Bedlack, Jr., and L. M. Loew, *Biophys. J.* **67** (1994) 208.
[76]C. W. Meuse, G. Niaura, M. L. Lewis, and A. L. Plant, *Langmuir* **14** (1998) 1604.
[77]C. W. Meuse, S. Krueger, C. F. Majkrzak, J. A. Dura, J. Fu, J. T. Connor, and A. L. Plant, *Biophys. J.* **74** (1998) 1388.
[78]A. L. Plant, *Langmuir* **9** (1993) 2764.
[79]F. Tadini Buoninsegni, R. Herrero, and M. R. Moncelli, *J. Electroanal. Chem*. **452** (1998) 33.
[80]A. L. Plant, M. Gueguetchkeri, and W. Yap, *Biophys. J.* **67** (1994) 1126.
[81]M. Pawlak, S. Stankowski, and G. Schwarz, *Biochim. Biophys. Acta*. **1062** (1991) 94.
[82]M. T. Tosteson, D. C. Tosteson, *Biophys. J*. **36** (1981) 109.
[83]C. Kempf, R. D. Klausner, J. N. Weinstein, J. Van Renswoude, M. Pincus, and R. Blumenthal, *J. Biol. Chem*. **257** (1982) 2469.
[84]W. Hanke, C. Metfessel, H.-U. Wilmsen, E. Katz, J. Jung, and G. Boheim, *Biochim. Biophys. Acta* **727** (1983) 108.
[85]J. K. Cullison, F. M. Hawkridge, N. Nakashima, and S. Yoshikawa, *Langmuir* **10** (1994) 877.
[86]J. D. Burgess, M. C. Rhoten, and F. M. Hawkridge, *Langmuir* **14** (1998) 2467.

[87]N. M. Rao. A. L. Plant, V. Silin, S. Wight, and S. W. Hui, *Biophys. J.* **73** (1997) 3066.
[88]M. Boncheva, C. Duschl, W. Beck, G. Jung, and H. Vogel, *Langmuir* **12** (1996) 5636.
[89]B. Duschl, M. Liley, G. Corradin, and H. Vogel, *Biophys. J.* **67** (1994) 1229.
[90]A. L. Plant, M. Brigham-Burke, E. C. Petrella, and D. J. O'Shannessy, *Anal. Biochem.* **226** (1995) 342.
[91]K. Kastl, M. Ross, V. Gerke, and C. Steinem, *Biochemistry* **41** (2002) 10087.
[92]P. Mueller, D. O. Rudin, H. T. Tien, and W. C. Wescott, *Circulation* **26** (1962) 1167.
[93]F. A. Henn and T. E. Thompson, *J. Mol. Biol.* **31** (1968) 227.
[94]D. M. Andrews and D. A. Haydon, *J. Mol. Biol.* **32** (1968) 149.
[95]R. E. Pagano, J. M. Ruysschaert, and I. R. Miller, *J. Membr. Biol.* **10** (1972) 11.
[96]S. H. White and T. E. Thompson, *Biochim. Biophys. Acta* **323** (1973) 7.
[97]S. H. White, D. C. Petersen, S. Simon, and M. Yafuso, *Biophys. J.* **16** (1976) 481.
[98]M. Montal and P. Mueller, *Proc. Natl. Acad. Sci. U.S.A.* **69** (1972) 3561.
[99]M. Montal, *Biochim. Biophys. Acta* **298** (1973) 750.
[100]M. Montal and J. I. Korenbrot, *Nature (Lond.)* **246** (1973) 219.
[101]K. Janko and R. Benz, *Biochim. Biophys. Acta* **470** (1977) 8.
[102]J. L. Poulos, T.-J. Jeon, R. Damoiseaux, E. J. Gillespie, K. A. Bradley, and J. J. Schmidt, *Biosens. Bioelectron.* **24** (2009) 1806.
[103]M. C. Peterman, J. M. Ziebarth, O. Braha, H. Bayley, H. A. Fishman, and D. M. Bloom, *Biomed. Devices* **4** (2002) 231.
[104]S. D. Ogier, R. J. Bushby, Y. Cheng, S. D. Evans, S. W. Evans, A. T. A. Jenkins, P. F. Knowles, and R. E. Miles, *Langmuir* **16** (2000) 5696.
[105]Y. Cheng, R. J. Bushby, S. D. Evans, P. F. Knowles, R. E. Miles, and S. D. Ogier, *Langmuir* **17** (2001) 1240.
[106]G. Favero, A. D'Annibale, L. Campanella, R. Santucci, and T. Ferri, *Anal. Chim. Acta* **460** (2002) 23.
[107]G. Favero, L. Campanella, S. Cavallo, A. D'Annibale, M. Perella, E. Mattei, and T. Ferri, *J. Am. Chem. Soc.* **127** (2005) 8103.
[108]A. Janshoff and C. Steinem, *Anal. Bioanal. Chem.* **385** (2006) 433.
[109]J. Drexler and C. Steinem, *J. Phys. Chem. B* **107** (2003) 11245.
[110]W. Römer and C. Steinem, *Biophys. J.* **86** (2004) 955.
[111]E. K. Schmitt, M. Vrouenraets, and C. Steinem, *Biophys. J.* **91** (2006) 2163.
[112]C. Horn and C. Steinem, *Biophys. J.* **89 (**2005) 1046.
[113]X. Han, A. Studer, H. Sehr, I. Geissbühler, M. Di Berardino, F. K. Winkler, and L. Tiefenauer, *Adv. Mater*. **19** (2007) 4466.
[114] L. X. Tiefenauer and A. Studer, *Biointerphases* **3** (2008) FA74.
[115]C. Danelon, J.-B. Perez, C. Santschi. J. Brugger, and H. Vogel, *Langmuir* **22** (2006) 22.
[116]X. Lu, A. Leitmannova Ottova, and H. T. Tien, *Bioelectrochem. Bioenerg.* **39** (1996) 285.
[117]T. J. Jeon, N. Malmstadt, and J. J. Schmidt, *J. Am. Chem, Soc.* **128** (2006) 42.
[118]T.-J. Jeon, N. Malmstadt, J. L. Poulos, and J. J. Schmidt, *Biointerphases* **3** (2008) FA96.
[119]J. A. Beddow, I. R. Peterson, J. Heptinstall, and D. J. Walton, *Anal. Chem*. **76** (2004) 2261.

[120]R. F. Costello, I. R. Peterson, J. Heptinstall, and D. J. Walton, *Biosens. Bioelectron.* **14** (1999) 265.
[121]X.-F. Kang, S. Cheley, A. C. Rice-Ficht, and H. Bayley, *J. Am. Chem. Soc.* **129** (2007) 4701.
[122]E. Neher, B. Sakmann, and J. H. Steinbach, *Pflügers Arch.* **375** (1978) 219.
[123]J. Teissié, in *Bioelectrochemistry of Membranes*, Ed. by D. Walz, J. Teissié, and G. Milazzo, Birkhäuser Verlag, Basel, Switzerland, 2004, p. 205.
[124]A. A. Brian and H. M. McConnel, *Proc. Natl. Acad. Sci. U.S.A.* **81** (1984) 6159.
[125]K. D. Mossman, G. Campi, J. T. Groves, and M. L. Dustin, *Science* **310** (2005) 1191.
[126]C. Boissiere, J. B. Brubach, A. Mermet, G. de Marzi, C. Bourgaux, E. Prouzet, and P. Roy, *J. Phys. Chem. B* **106** (2002) 1032.
[127]R. J. Mashl, S. Joseph, N. R. Aluru, and E. Jakobsson, *Nano Lett.* **3** (2003) 589.
[128]R. P. Richter, N. Maury, and A. R. Brisson, *Langmuir* **21** (2005) 299.
[129]P. Lenz, C. M. Ajo-Franklin, and S. G. Boxer, *Langmuir* **20** (2004) 11092.
[130]J. Schmitt, B. Danner, and T. M. Bayerl, *Langmuir* **17** (2001) 244.
[131]M. Hetzer, S. Heinz, S. Grage, and T. M. Bayerl, *Langmuir* **14** (1998) 982.
[132]C. E. Dodd, B. R. G. Johnson, L. J. C. Jeuken, T. D. H. Bugg, R. J. Bushby, and S. D. Evans, *Biointerphases* **3** (2008) FA59.
[133]B. L. Jackson, J. A. Nye, and J. T. Groves, *Langmuir* **24** (2008) 6189.
[134]I. Zawisza, A. Lachenwitzer, V. Zamlynny, S. L. Horswell, J. P. Goddard, and J. Lipkowski, *Biophys. J.* **85** (2003) 4055.
[135]L. Burgess, M. Li, S. L. Horswell, G. Szymanski, J. Lipkowski, J. Majewski, and S. Satija, *Biophys. J.* **86** (2004) 1763.
[136]X. Bin, S. L. Horswell, and J. Lipkowski, *Biophys. J.* **89** (2005) 592.
[137]S. Xu, G. Szymanski, and J. Lipkowsky, *J. Am. Chem. Soc.* **126** (2004) 12276.
[138]O. Purrucker, H. Hillebrandt, K. Adlkofer and M. Tanaka, *Electrochim. Acta* **47** (2001) 791.
[139]S. Gritsch, P. Nollert, F. Jähnig, and E. Sackmann, *Langmuir* **14** (1998) 3118.
[140]L-G. Wang, Y-H. Li, and H. T. Tien, *Bioelectrochem. Bioenerg.* **36** (1995) 145.
[141]H. T. Tien, S. H. Wurster, and A. L. Ottova, *Bioelectrochem. Bioenerg.* **42** (1997) 77.
[142]A. Ottova-Leitmannova and H.T. Tien, *Progr. Surf. Sci.* **41** (1992) 337.
[143]Z. Salamon and G. Tollin, *Bioelectrochem. Bioenerg.* **25** (1991) 447.
[144]W. J. Albery, H. A .O. Hill, and A. R. Hillman, *J. Am. Chem. Soc.* **103** (1981) 3904.
[145]H. Gao, G.-A. Luo, J. Feng, A. L. Ottova, and H. T. Tien, *J. Photochem. Photobiol. B: Biology* **59** (2000) 87.
[146]H. T. Tien and J. R. Zon, in *Mechanistic approaches to interactions of electric and electromagnetic fields with living systems*, Ed. by M. Blank and E. Findl, Plenum Press, New York, 1987, p. 301.
[147]Z. Salamon, Y. Wang, G. Tollin, H. A. Macleod, *Biochim. Biophys. Acta* **1195** (1994) 267.
[148]Z. Salamon, G. Lindblom, and G. Tollin, *Biophys. J.* **84** (2003) 1796.
[149]Z. Salamon, Y. Wang, J. L. Soulages, M. F. Brown, and G. Tollin, *Biophys. J.* **71** (1996) 283.
[150]Z. Salamon and G. Tollin, *Biophys. J.* **71** (1996) 848.
[151]Z. Salamon, H. A. Macleod, and G. Tollin, *Biophys. J.* **73** (1997) 2791.
[152]Z. Salamon, D. Huang, W. A. Cramer, and G. Tollin, *Biophys. J.* **75** (1998) 1874.

[153]Z. Salamon, S. Davanathan, I. D. Alves, and G. Tollin, *J. Biol. Chem*. **280** (2005) 11175.
[154]C. Steinem, A. Janshoff, H.-J. Galla, and M. Sieber, *Bioelectr. Bioenerg.* **42** (1997) 213.
[155]A. Michalke, T. Schürholz, H.-J. Galla, and C. Steinem, *Langmuir* **17** (2001) 2251.
[156]L. Becucci, R. Guidelli, Q. Liu, R. J. Bushby, and S. D. Evans, *J. Phys. Chem B* **106** (2002) 10410.
[157]C. Peggion, F. Formaggio, C. Toniolo, L. Becucci, M. R. Moncelli, and R. Guidelli, *Langmuir* **17** (2001) 6585.
[158]H. Lang, C. Duschl, and H. Vogel, *Langmuir* **10** (1994) 197.
[159]H. Lang, C. Duschl, M. Grätzel, and H. Vogel, *Thin Solid Films* **210/211** (1992) 818.
[160]N. Boden, R. J. Bushby, Q. Liu, S. D. Evans, A. T. A Jenkins, P. Knowles, and R. E. Miles, *Tetrahedron* **54** (1998) 11537.
[161]C. Steinem, A. Janshoff, K. von dem Bruch, K. Reihs, J. Goossens, and H-J. Galla, *Bioelectrochem. Bioenerg.* **45** (1998) 17.
[162]J. D. Lear, Z. D. Wassermann, and W. D. De Grado, *Science* **240** (1988) 1179.
[163]N. Bunjes, E. K. Schmidt, A. Jonczyk, F. Rippmann, D. Beyer, H. Ringsdorf, P. Gräber, W. Knoll, and R. Naumann, *Langmuir* **13** (1997) 6188.
[164]R. Naumann, A. Jonczyk, R. Kopp, J. van Esch, H. Ringsdorf, W. Knoll, and P. Gräber, *Angew. Chem. Int. Ed. Engl.* **34** (1995) 2056.
[165]R. Naumann, A. Jonczyk, C. Hampel, H. Ringsdorf, W. Knoll, N. Bunjes, and P. Gräber, *Bioelectrochem. Bioenerg.* **42** (1997) 241.
[166]R. Naumann, E. K. Schmidt, A. Jonczyk, K. Fendler, B. Kadenbach, T. Liebermann, A. Offenhäusser, and W. Knoll, *Biosens. Bioelectron.* **14** (1999) 651.
[167]I. K. Vockenroth, C. Ohm, J. W. F. Robertson, D. J. McGillivray, M. Lösche, and I. Köper, *Biointerphases* **3** (2008) FA68.
[168]J. Leitch, J. Kunze, J. D. Goddard, A. L. Schwan, R. J. Faragher, R. Naumann, W. Knoll, J. R. Dutcher, and J. Lipkowski, *Langmuir* 25 (2009) 10354.
[169]R. Naumann, D. Walz, S. M. Schiller, and W. Knoll, *J. Electroanal. Chem.* **550-551** (2003) 241.
[170] J. W. F. Robertson, M. G. Friedrich, A. Kibrom, W. Knoll, R. L. C. Naumann, and D. Walz, *J. Phys. Chem. B* **112** (2008) 10475.
[171]I. K. Vockenroth, P. P. Atanasova, J. R. Long, A. T. A. Jenkins, W. Knoll, and I. Köper, *Biochim. Biophys. Acta* **1768** (2007)1114.
[172]S. A. Glazier, D. J. Vanderah, A. L. Plant, H. Bayley, G. Valincius, and J. J. Kasianowicz, *Langmuir* **16** (2000) 10428.
[173]I. K. Vockenroth, P. P. Atanasova, A. T. A. Jenkins, and I. Köper, *Langmuir* **24** (2008) 496.
[174]V. Atanasov, N. Knorr, R. S. Duran, S. Ingebrandt, A. Offenhäusser, W. Knoll, and I. Koper, *Biophys. J.* **89** (2005) 1780.
[175]R. F. Roskamp, I. K. Vockenroth, N. Eisenmenger, J. Braunagel, and I. Köper, *ChemPhysChem.* **9** (2008) 1920.
[176]R. Robelek, E. S. Lemker, B. Wiltschi, V. Kirste, R. Naumann, D. Oesterhelt, and E.-K. Sinner, *Angew. Chem. Int. Ed.* **46** (2007) 605.
[177]M. Leutenegger, T. Lasser, E.-K. Sinner, and R. Robelek, *Biointerphases* **3** (2008) FA136.

[178]E. K. Schmidt, T. Liebermann, M. Kreiter, A. Jonczyk, R. Naumann, A. Offenhäusser, E. Neumann, A. Kukol, A. Maelicke, and W. Knoll, *Biosens. Bioelectron.* **13** (1998) 585.
[179]M. Andersson, H. K. Keizer, C. Zhu, D. Fine, A. Dodabalapur, and R. S. Duran, *Langmuir* **23** (2007) 2924.
[180]H. M. Keizer, B. R. Dorvel, M. Andersson, D. Fine, R. B. Price, J. R. Long, A. Dodabalapur, I. Köper, W. Knoll, P. A. V. Anderson, and R. S. Duran, *ChemBioChem* **8** (2007) 1246.
[181]M. Andersson, G. Okeyo, D. Wilson, H. Keizer, P. Moe, P. Blouunt, D. Fine, A. Dodabalapur, and R. S. Duran *Biosen. Bioelectron.* **23** (2008) 919.
[182]I. K. Vockenroth, D. Fine, A. Dodobalapur, A. T. A. Jenkins, and I. Köper, *Electrochem. Commun*. **10** (2008) 323.
[183]L. Becucci, M. R. Moncelli, and R. Guidelli Langmuir **22** (2006) 1341.
[184]L. Becucci, M.V. Carbone, T. Biagiotti, M. D'Amico, M. Olivotto and R. Guidelli, *J. Phys. Chem. B* **112** (2008) 1315.
[185]L. Becucci and R. Guidelli, *Soft Matter* **5** (2009) 2294.
[186]L. Becucci, A. L. Schwan, E. E. Sheepwash and R. Guidelli, *Langmuir* **25** (2009) 1828.
[187]L. Becucci, M. Innocenti, E. Salvietti, A. Rindi, I. Pasquini, M. Vassalli, M. L. Foresti, and R. Guidelli, *Electrochim. Acta* **53** (2008) 6372.
[188] D. C. Grahame, *J. Am. Chem. Soc.* **76** (1954) 4819.
[189]J. Clavilier and C. Nguyen Van Huong, *J. Electroanal. Chem.* **41** (1973) 193.
[190]L. Becucci, R. Romero León, M. R. Moncelli, P. Rovero and R. Guidelli. *Langmuir* **22** (2006) 6644.
[191]L. Becucci and R. Guidelli, *Langmuir* **23** (2007) 5601.
[192]E. Bamberg and R. Benz, *Biochim. Biophys. Acta* **426** (1976) 570.
[193]M. C. Trudeau, J. W. Warmke, B. Ganetzky, and G. A. Robertson, *Science* **269**, (1995) 92; A. Arcangeli, L. Bianchi, A. Becchetti, L. Faravelli, M. Coronnello, E. Mini, M. Olivotto, and E. Wanke, *J. Physiol.* **489** (1995) 455.
[194]L. Becucci, R. Guidelli, C. B. Karim, D. D. Thomas, and G. Veglia, *Biophys. J.* **93** (2007) 1.
[195]L. Becucci, R. Guidelli, C. B. Karim, D. D. Thomas, and G. Veglia, *Biophys. J.* **97** (2009) 2693.
[196]L. Becucci, A. Cembran, C. B. Karim, D. D. Thomas, R. Guidelli, J. Gao and G. Veglia, *Biophys. J.* **96** (2009) L60.
[197]H. I. Stefanova, J. M. East, and A. G. Lee, *Biochim. Biophys. Acta* **1064** (1991) 321; H. I. Stefanova, S. D. Jane, J. M. East, and A. G. Lee, *Biochim. Biophys. Acta* **1064** (1991) 329.
[198]S. L. Robia, K. S. Campbell, E. M. Kelly, Z. Hou, D. L. Winters, and D. D. Thomas, *Circ. Res.* **101** (2007) 1123; Z. Hou, E. M. Kelly, and S. L. Robia, *J. Biol. Chem.* **283** (2008) 28996.
[199]L. Becucci, M. D'Amico, S. Daniele, M. Olivotto, A. Pozzi, and R. Guidelli, Bioelectrochemistry, doi:10.1016/j.bioelechem.2009.08.007.
[200]G. Krishna, J. Schulte, B. A. Cornell, R. Pace, L. Wieczorek, and P. D. Osman, *Langmuir* **17** (2001) 4858.
[201]Y.-S. Shon, S. Lee, S. S. Perry, and T. R. Lee, *J. Am. Chem. Soc.* **122** (2000) 1278.
[202]R. C. Chambers, C. E. Inman, and J. E. Hutchison, *Langmuir* **21** (2005) 4615.
[203]L. J. C. Jeuken, N. N. Daskalakis, X. Han, K. Sheikh, A. Erbe, R. J. Bushby, and S. D. Evans, *Sen. Actuat. B* **124** (2007) 501.

[204]S. Heyse, O. P. Ernst, Z. Dienes, K. P. Hofmann, and H. Vogel, *Biochemistry* **37** (1998) 507.
[205]Y. Cheng, N. Boden, R. J. Bushby, S. Clarkson, S. D. Evans, P. F. Knowles, A. Marsh, and R. E. Miles, *Langmuir* **14** (1998) 839.
[206]S. Heyse, T. Stora, E. Schmid, J. H. Lakey, and H. Vogel, *Biochim. Biophys. Acta* **1376** (1998) 319.
[207]T. Stora, J. H. Lakey, and H. Vogel, *Angew. Chem. Int. Ed.* **38** (1999) 389.
[208]S. Goennenwein, M. Tanaka, B. Hu, L. Moroder, and E. Sackmann, *Biophys. J.* **85** (2003) 646.
[209]O. Purrucker, S. Gonnenwein, A. Fortig, R. Jordan, M. Rusp, M. Bärmann, L. Moroder, E. Sackmann, and M. Tanaka, *Soft Matter* **3** (2007) 333.
[210]M. Tanaka and E. Sackmann, *Nature* **437** (2005) 656; *Phys. Stat. Sol.* **203** (2006) 3452.
[211]M. Kühner and E. Sackmann *Langmuir* **12** (1996) 4866; G. Elender, and E. Sackmann, *J. Phys. II* **4** (1994) 455.
[212]J. Y. Wong, C. K. Park, M. Seitz, and J. N. Israelachvili, *Biophys. J.* **77** (1999) 1458.
[213]C. A. Naumann, O. Prucker, T. Lehmann, J. Ruhe, W. Knoll, and C. W. Frank, *Biomacromolecules* **3** (2002) 27.
[214]M. L. Wagner and L. K. Tamm, *Biophys. J.* **79** (2000) 1400.
[215]M. Tanaka, S. Kaufmann, J. Nissen, and M. Hochrein, *Phys. Chem. Chem. Phys.* **3** (2001) 4091.
[216]M. Tanaka, F. F. Rossetti, and S. Kaufmann, *Biointerphases* **3** (2008) FA12.
[217]E. Sackmann and M. Tanaka, *Trends Biotechnol.* **18** (2000) 58.
[218]M. Kühner, R. Tampé, and E. Sackmann, *Biophys. J.* **67** (1994) 217.
[219]G. Elender, M. Kühner, and E. Sackmann, *Biosens. Bioelectron.* **11** (1996) 565.
[220]F. Rehfeldt and M. Tanaka, *Langmuir* **19** (2003) 1467.
[221]T. Baumgart and A. Offenhäusser, *Langmuir* **19** (2003) 1730.
[222]K. Sengupta, J. Schilling, S. Marx, M. Fischer, A. Bacher, and E. Sackmann, *Langmuir* **19** (2003) 1775.
[223]J. Majewski, J. Y. Wong, C. K. Park, M. Seitz, J. N. Israelachvili, and G. S. Smith, *Biophys. J.* **75** (1998) 2363.
[224]J. Y. Wong, J. Majewski, M. Seitz, C.K. Park, J.N. Israelachvili, and G.S. Smith, *Biophys. J.* **77** (1999) 1445.
[225]C. Dietrich and R. Tampé, *Biochim. Biophys. Acta* **1238** (1995) 183.
[226]D. Beyer, G. Elender, W. Knoll, M. Kühner, S. Maus, H. Ringsdorf, and E. Sackmann, *Angew. Chem. Int. Ed. Engl.* **35** (1996) 1682.
[227]J. Spinke, J. Yang, H. Wolf, M. Liley, H. Ringsdorf, and W. Knoll, *Biophys. J.* **63** (1992) 1667.
[228]C. Erdelen, L. Häussling, R. Naumann, H. Ringdorf, H. Wolf, and J. Yang, *Langmuir* **10** (1994) 1246.
[229]H. Hillebrandt, G. Wiegand, M. Tanaka, and E. Sackmann, *Langmuir* **15** (1999) 8451.
[230]H. Hillebrandt, M. Tanaka, and E. Sackmann, *J. Phys. Chem. B* **106** (2002) 477.
[231]B. Wetzer, D. Pum, and U. B. Sleytr, *J. Struct. Biol.* **119** (1997) 123.
[232]B. Schuster, D. Pum, and U. B. Sleytr, *Biointerphases* **3** (2008) FA3.
[233]W. Knoll, R. Naumann, M. Friedrich, J. W. F. Robertson, M. Lösche, F. Heinrich, D. J. McGillivray, B. Schuster, P. C. Gufler, D. Pum, and U. B. Sleytr, *Biointerphases* **3** (2008) FA125.

[234]P. C. Gufter, D. Pum, U. B. Sleytr, and B. Schuster, *Biochim. Biophys. Acta* **1661** (2004) 154.
[235]B. Schuster, D. Pum, M. Sára, O. Braha, H. Bayley, and U. B. Sleytr, *Langmuir* **17** (2001) 499.
[236]B. Schuster, S. Weigert, D. Pum, M. Sára, and U. B. Sleytr, *Langmuir* **19** (2003) 2392.
[237]K. Ataka, F. Giess, W. Knoll, R. Naumann, S. Haber-Pohlmeier, B. Richter, and J. Heberle, *J. Am. Chem. Soc.* 126 (2004) 16199.
[238]F. Giess, M. G. Friedrich, J. Heberle, R. L. Naumann, and W. Knoll, *Biophys. J.* **87** (2004) 3213.
[239]M. G. Friedrich, J. W. F. Robertson, D. Walz, W. Knoll, and R. L. C. Naumann, *Biophys. J.* **94** (2008) 3698.
[240]R. L. C. Naumann and W. Knoll, *Biointerphases* **3** (2008) FA101.
[241]M. G. Friedrich, F. Giess, R. Naumann, W. Knoll, K. Ataka, J. Heberle, J. Hrabakova, D. H. Murgida, and P. Hildebrandt, *Chem. Commun. (Cambridge)* **21** (2004) 2376.
[242]M. G. Friedrich, V. U. Kirste, J. Zhu, R. B. Gennis, W. Knoll, and R. L. C. Naumann, *J. Phys. Chem. B* **112** (2008) 3193.

Rolando Guidelli

Rolando Guidelli was born in Florence on December 27, 1938. He was promoted to full professor of Electrochemistry at Florence University in 1971. His scientific interests have been focused to electrode kinetics, structure of the metal/water interface and bioelectrochemistry. Professor Guidelli is the recipient of the 2005 "Katsumi Niki" Prize for Bioelectrochemistry of the International Society of Electrochemistry (ISE), of the 2009 "Giulio Milazzo" Prize of the Bioelectrochemical Society, and of the "Sigillo d'oro" of the Italian Chemical Society. He is a fellow of the ISE, honorary member of the Bioelectrochemical Society, and associate editor of the journal *Bioelectrochemistry*.